Structural analysis of a relay ramp affecting Eocene carbonate rocks in the Suez Rift, Egypt

Master of Science thesis

Michael Laukemann

Department of Earth Science

University of Bergen

June 2013

Abstract

Detailed fault zone and relay ramp characterization have only to some extent previously been done in carbonate rocks. This study aims to use field data to contribute a better understanding of the deformation related to normal faults and relay ramps in carbonate rocks. Specifically, the study focuses on characterization of damage zone deformation variations along normal faults, relay ramp complexity and implications for permeability and fluid flow in carbonate reservoirs.

The study area is located within the Hammam Faraun Fault Block of the eastern flank of the Gulf of Suez. Here, a relay ramp, bounded by two overlapping N-S trending faults, comprising mainly Eocene pre-rift carbonate rocks, is presented. Structural data from outcrop studies form the basis of the field data.

The field data display a damage zone deformation asymmetry along the studied faults, where the hanging wall is generally more deformed than the footwall, and show increased fracture frequencies in the proximity to the faults. However, occurrence of shale smear is observed to reduce hanging wall deformation. The asymmetric damage zone deformation pattern may be a result of upward propagation of the faults and because most of the fault movement is represented by downward movement of the hanging wall, while increased fracturing in the proximity of the faults is related to build up of frictional resistance in the fault core, during slip events. Decay of stress away from the faults then leads to decreased fracture frequencies. The deformation reducing effect on the hanging wall, observed by shale smear, is only a minor observation. It is therefore difficult to judge whether this is an isolated occurrence or a recurring pattern. However, the findings do agree well with other studies. The deformation along the studied faults also features mainly fault-parallel fractures with subordinate fault-perpendicular fractures. Fault-parallel fractures are a common feature along normal faults, while fault-perpendicular fractures may have formed as a result of the perturbation effect around growing faults. A fault tip zone and a branching point between two faults have also been studied. The tip zone is characterized by a splay of minor synthetic and antithetic faults which is well supported by other studies, while the branching point displays anomalously high fracture frequencies and may represent a point of single-tip fault interaction. Observations from the relay ramp show the fractures are oriented fault-parallel (N-S), fault-oblique (NE-SW and NW-SE) and fault-transverse (E-W), where cross-cutting relations reveal that the latter are the youngest. The fault-transverse fractures are therefore interpreted to reflect the latest stage of local stress field perturbation during fault propagation and overlap. At this point extreme local stress and rotation of the principal stress axes made it possible for fractures to grow at high angles to fault strike. Finally, the relay ramp is characterized by fracture frequencies only slightly elevated above background fracturing levels, indicating a lower complexity than what is expected in a relay zone based on previous studies. This is interpreted to be a result of: (1) large separation distance between the ramp-bounding faults compared to relay displacement and (2) large separation distance compared to overlapping distance. The relay ramp is therefore interpreted to be a soft-linked relay ramp, or, at the most, a soft-linked relay ramp with incipient breaching.

Acknowledgements

Thanks to the HFF-DOL project by the University of Manchester and the sponsors Total, BG Group, Saudi Aramco and Statoil, for funding this study.

I would like to thank my super supervisors Atle Rotevatn and Eivind Bastesen for an interesting project. They have always been very motivating and encouraging. Thank you for great discussions, both confusing and helpful, mostly the latter, at the university and in the field. I am also grateful for all help from my co-supervisor Rob Gawthorpe.

I would like to thank my field and study companion Anja Eker for great company and for unforgettable memories both in the field, at the university and other trips we have shared.

I would also like to thank Jesal Hirani and Hilary Corlett, from the University of Manchester, for "no probs" times at Moon Beach and for their exceptional Hammam Faraun expertise.

I would like to thank my field assistants Cecilie Tellefsen and Eirik Styve for sunny days with endless fracture counting and good field company. I would also like to thank my field driver "Jan" Zaiem for tasty Bedouin lunches and for teaching us Arabic. *Salam aleikum, shokran*.

A special thanks to Joar and Daniel at "Drivhuset" for healthy distractions and countless laughs, and the rest of my fellow students at the University of Bergen for making my five years as a student the time of my life.

Finally, I would like to thank my family who has been very supportive, both financially and morally, during my years as a student.

Bergen 3rd of June 2013

Michael Laukemann

Table of Contents

1. Introduction

1.1 Background and rationale

Areas undergoing crustal extension are characterized by fault blocks separated by normal faults, resulting in a decrease of fault angle with increasing extension (e.g. Jackson and McKenzie, 1983; McKenzie and Jackson, 1986; Jackson *et al.*, 1988). Such faults evolve from propagation and eventual linkage of *en echelon* arranged fault segments (e.g. Anders and Schlische, 1994; Schlische and Anders, 1996). Eventual linkage can be accommodated by relay ramps, which are a common feature in normal fault systems. Relay ramps were first described in detail by Larsen (1988) as a zone connecting the footwall and the hanging wall of two faults, which transfers strain between them. A relay ramp consists of two parallel overlapping faults with an area of reoriented bedding, developed as a result of the decrease in displacement at the fault tips (Fig. 1.1; Peacock and Sanderson, 1994; Childs *et al.*, 1995).

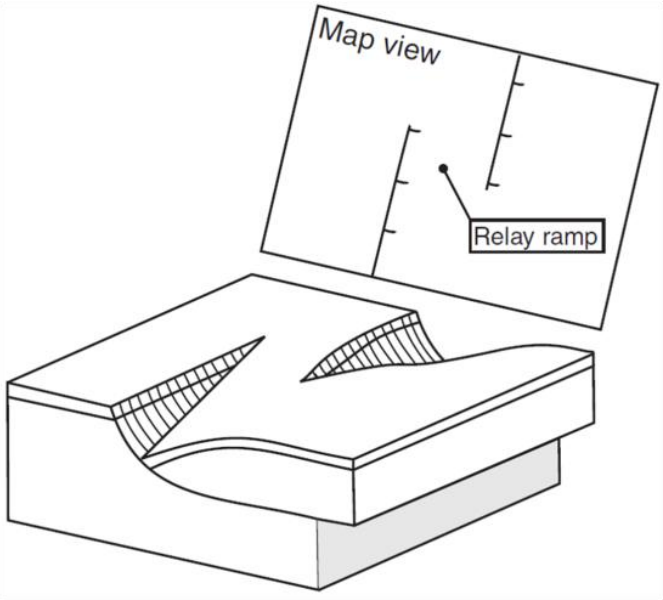

Figure 1.1: Basic model of a relay ramp (Bense and Van Balen, 2004).

Peacock and Sanderson (1994) described the evolution of relay ramps into four stages: (1) the faults are isolated and do not interact, (2) the faults begin to overlap and form a relay ramp with reoriented bedding, (3) fractures connect and start to break the relay ramp, (4) the relay ramp is breached by the connection of the two faults to form a composite fault.

It is important to study relay ramps since they may influence the process of hydrocarbon migration and trapping (Peacock and Sanderson, 1994). Individual faults generally form a barrier to fluid flow, as faults may juxtapose units of low permeability

towards units of high permeability or fault core itself that may act as a seal (Yielding *et al.*, 1997), whereas relay ramps can act as a cross-fault fluid conduit (Bense and Van Balen, 2004). This is mainly a result of bed continuity through unbreached, folded relay beds (Rotevatn *et al.*, 2009) or juxtaposition of several reservoir units at different stratigraphic levels because of high fault displacement gradients (Manzocchi *et al.*, 2010). In the first stages of relay ramp evolution presented by Peacock and Sanderson (1994), the footwall and hanging wall are connected, offering connectivity across the ramp, while in the later stages fractures develop in the ramp, progressively connecting the fault segments making a barrier for cross-fault fluid flows (Morley *et al.*, 1990). Fractures transferring displacement between the two fault segments are a common feature of relay ramps. The connecting fractures are generally oriented oblique to the segments they connect (Peacock and Sanderson, 1994) and affect the properties of a reservoir; increased orientation variability and fracture frequency of relay ramps lead to a higher permeability (Berkowitz, 1995), where fractures oriented at intermediate to high angles relative to fault strike, may increase the cross-fault permeability (Rotevatn and Bastesen, 2012).

1.2 Aims and objectives

This study forms part of the Hammam Faraun Dolomites project by the University of Manchester.

The overall aim of this study is to attempt to improve the understanding of deformation systems along normal faults and in relay ramps, in carbonate rocks. Field data is used to characterize and quantify the deformation, which is important since internal fault zone and relay ramp characteristics are well below seismic resolution. Specifically, this study aims to establish damage zone deformation variations along normal faults and relay ramp complexity with emphasis on fracture systems complexity, and its implications for permeability and fluid flow in carbonate reservoirs.

1.3 Study area

The study area comprising the current study is located within the Hammam Faraun Fault Block (HFFB) of the eastern flank of the Gulf of Suez (Fig. 1.2). The fault block is bounded to the west by the NW-SE trending Hammam Faraun Fault that defines the coastline. The fault has a throw of c. 5 km, juxtaposing syn- and post-rift sediments with Eocene pre-rift carbonate rocks. The fault block is bounded to the east by the Thal Fault and to the south by

the Baba-Markha Fault, while the northern boundary lies close to a change in dip regime. The area is characterized by a desert climate and cross-cutting wadi systems (dry riverbeds) that exposure the studied rocks.

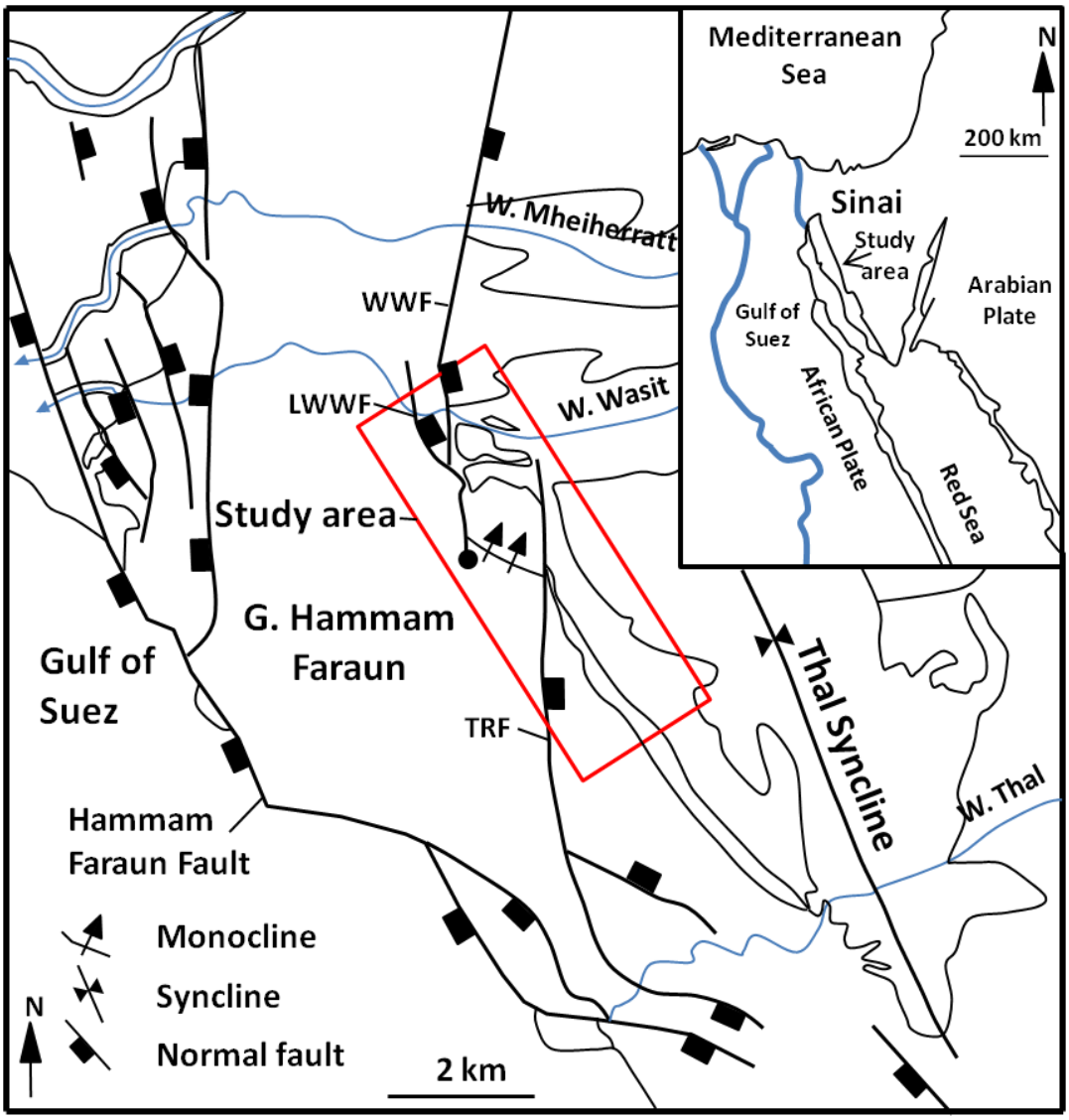

Figure 1.2: The study area. Redrawn from Armstrong (1997).

The study area features two overlapping N-S trending, antithetic faults that are located c. 5.5 km inland from the Hammam Faraun Fault (Fig. 1.2). Between the two faults, is a relay ramp featuring beds that are folded into a monocline (Fig. 1.3). The westernmost of the two faults bounding the relay ramp is referred to as the Wadi Wasit Fault (WWF) and has a maximum throw of c. 250 m (Armstrong, 1997; Sharp *et al.*, 2000a), decreasing in a southward direction into the ramp. The northern segment of the WWF includes a splay forming an unnamed N-S trending antithetic fault, hereby referred to as the Little Wadi Wasit

Fault (LWWF), with a maximum throw of c. 150 m (Armstrong, 1997; Sharp *et al.*, 2000a). The easternmost bounding fault is termed the Thal Ridge Fault (TRF), featuring a maximum throw of c. 450 m (Armstrong, 1997; Sharp *et al.*, 2000a), decreasing northward into the ramp. This means that the WWF and the TRF increase in throw in opposite directions. Armstrong (1997) and Sharp *et al.* (2000a) suggest that the northern end of the TRF is connected with the WWF by an unexposed fault, and have interpreted it as a *hanging wall breached relay zone* (*sensu* Trudgill and Cartwright, 1994; Cartwright *et al.*, 1996). This statement will be further addressed in the discussion.

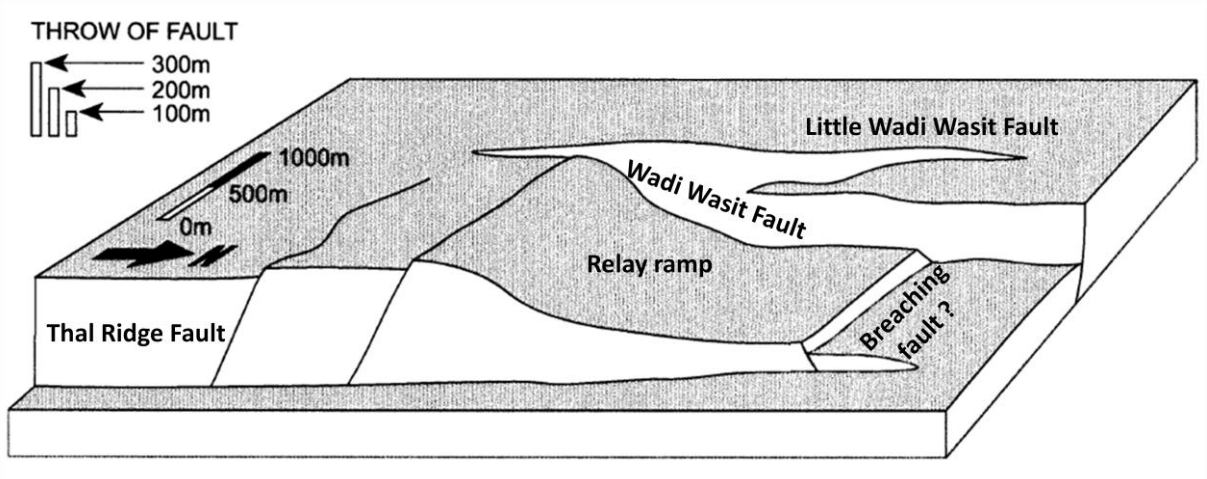

Figure 1.3: Conceptual figure illustrating the relay zone and the throw distribution along the faults. Modified from Sharp *et al.* (2000a).

1.5 Methodology

Data was collected during two field seasons in November 2011 and November 2012 in Sinai, Egypt. The field methods include fault mapping, recording of fracture frequencies and orientations as well as mapping of lithology.

Maps from Google Earth were used in the mapping of lithological boundaries and faults. Also maps with fault throw made by Armstrong (1997) and Sharp *et al.* (2000b) were studied to get an overview of the faults and later quality controlled in the field.

Several locations along the faults and in the ramp were chosen to make fracture frequency profiles (scanlines) to assess the fracture distribution, where a scanline involves recording of fracture frequencies per meter. The scanlines along faults were done sub-perpendicular to fault strike; most of them were collected in hanging wall because of bad exposures in footwall. Several scanlines were collected in the ramp, which together comprise a complete scanline transect from the WWF to the TRF. At all locations additional data, such as fracture, fault plane and bedding orientations were recorded.

The lithology was described and mapped in the entire field area with focus on characterizing the mechanical properties between different formations.

2. Geological setting

2.1 Introduction

The aim of this chapter is to give an overview of the regional geology in the studied area. Part 2.2 deals with the temporal evolution of the Suez Rift from late Precambrian to present, while part 2.3 focuses on the structure of the rift with emphasis on the major fault populations. Parts 2.4 and 2.5 outline the structural geology and a stratigraphic framework of Hammam Faraun.

2.2 Temporal evolution of the Suez Rift

The Suez Rift is representing the aborted NW - SE trending extension of the Red Sea Rift system which developed in the late Oligocene - Miocene times (c. 24 - 15.5 Ma), as a result of a change in relative plate motions between the African and Arabian plates (e.g. Robson, 1971; Patton *et al.*, 1994; Khalil and McClay, 2001; Bosworth *et al.*, 2005). The termination of the Suez rifting coincides with the initiation of the Dead Sea - Aquaba transform, which accommodated further extension in the Red Sea Rift (Cochran, 1983). The rift is up to c. 300 km long and 80 km wide, and displays half-grabens and rotated normal fault blocks (Moustafa and Abdeen, 1992; Patton *et al.*, 1994; Bosworth, 1995; Jackson *et al.*, 2006).

2.2.1 Rift phases

In *Oligocene*, right-lateral wrenching in the northern part of the Gulf of Suez occurred, which led to deposition of continental sands and conglomerates (Patton *et al.*, 1994). Continental rifting began in the southeastern part of the Red Sea area (Bayer *et al.*, 1988) and propagated north during the period (Fig. 2.1a; Patton *et al.*, 1994). In the *Aquitanian - Burdigalian (23 - 16 Ma)*, fluvial and shallow marine sediments were deposited in the rift (Patton *et al.*, 1994) and the development of the rift-basin was dominated by slow rates of subsidence (Fig. 2.1b; Moretti and Colletta, 1987; Richardson and Arthur, 1988). In the *Burdigalian (20,4 - 16 Ma)*, subsidence rates accelerated and remained high throughout the rest of the period (Moretti and Colletta, 1987; Richardson and Arthur, 1988), while deep-marine sediments were deposited (Patton *et al.*, 1994). This was the time of maximum structural development and a large amount of extension of the basin, widening the rift to near present day width, occurred during this period (Patton *et al.*, 1994). At the end of this phase the subsidence rates became variable and showed a general trend towards slowing (Moretti and Colletta, 1987; Richardson and Arthur, 1988). This happened roughly simultaneously with the increasing activity on the Dead

Sea Transform, and is thought to have replaced the Gulf of Suez as the site of rifting (Fig. 2.1c; Patton *et al.*, 1994). In the *Langhian - Serravallian (16 - 11,6 Ma)*, the rift basement along the rift shoulders is recorded to be unroofed (Evans, 1990). As subsidence decreased, the basin began to fill and a large part of the deformation that the Gulf of Suez had experienced were accommodated by the Dead Sea Transform (Fig. 2.1d; Patton *et al.*, 1994). In the *Serravallian - Messinian (13,7 - 5,3 Ma)*, the Gulf of Suez and the Red Sea were isolated due to possible basin restrictions in the north, and the Dead Sea Transform experienced a relatively inactive period (Fig. 2.1d; Patton *et al.*, 1994). In the *Pliocene (5,3 - 2,6 Ma)*, the activity along the Dead Sea Transform rose (Garfunkel, 1981). This happened at the same time as renewed subsidence occurred in the central and southern offshore parts of the gulf (Moretti and Colletta, 1987; Richardson and Arthur, 1988). Both this and the present day subsidence in the area are likely a response of continued motion of the Dead Sea Transform (Fig. 2.1d; Patton *et al.*, 1994).

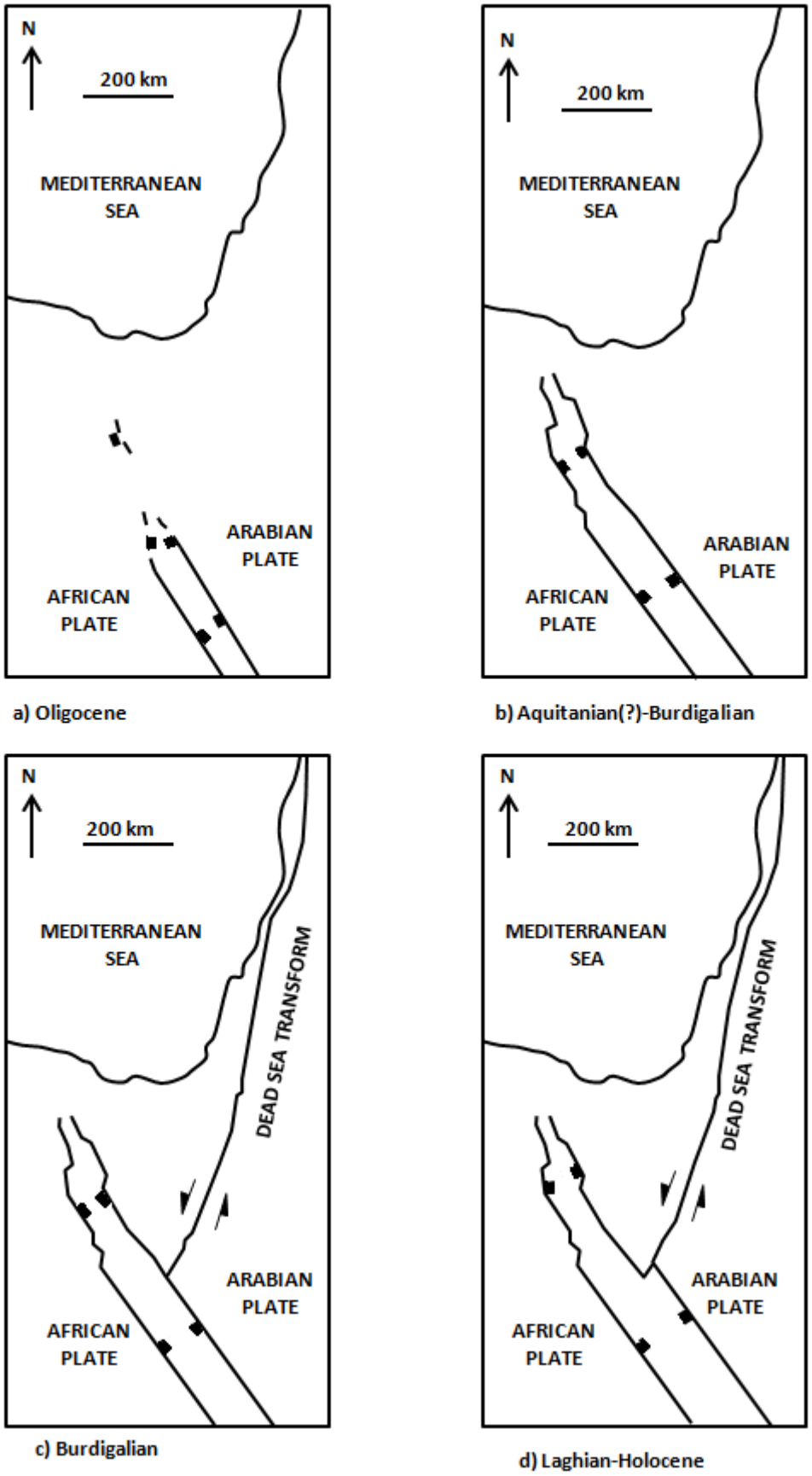

Figure 2.1: Sequential development of the Gulf of Suez from Oligocene to present. Redrawn from Armstrong (1997).

2.3 Rift structure

Patton *et al.* (1994) grouped the faults that determine the shapes of the rotated fault blocks into four major populations on the basis of orientation:

(1) The statistically most significant trend is the rift-parallel trend called the *clysmic trend*, with fault strike between 310 and 340° (NW-SE and NNW-SSE). The clysmic trend is found throughout the gulf and has been active during the entire phase of rift development (Lyberis, 1988). The clysmic faults represents both dip-slip (Angelier, 1985) and oblique-slip (Lyberis, 1988) motion. In the northern part of the Gulf, a subpopulation with strike between 310 and 315° (NW-SE) is present (Robson, 1971; Moustafa and El Shaarawy, 1987); oriented parallel to the coastline at eastern Sinai, for example along the southwestern side of Gebel Hammam Faraun and the northeastern edge of the North Galala Plateau. These faults are also aligned with major basement lineaments, and may have exploited preexisting basement structures during the rifting (Moustafa and El Shaarawy, 1987).

(2) The second most significant trend, the *North-oblique trend*, is oblique to the clysmic trend with fault strike between 350 and 30° (N-S and NNE-SSW). These faults were active during the initial stages of rifting and do not occur uniformly throughout the gulf, but are mostly expressed on the surface at the terminations of major rift blocks (Montenat *et al.*, 1988). The faults are dominated by dip-slip motion, but also frequently represented by sinistral, strike-slip motion (Lyberis, 1988; Montenat *et al.*, 1988; Moustafa and Abdeen, 1992) and infrequently by dextral, strike slip motion (Moustafa and Abdeen, 1992).

(3) The third trend is the *Northwest-oblique trend*, with fault strike between 280 and 310° (E-W and NW-SE). This trend is weakly expressed relative to the two previously described trends, and the faults show a preference for dextral strike-slip motion (Angelier, 1985; Lyberis, 1988; Montenat *et al.*, 1988), like the Baba-Markha Fault that bounds the Hammam Faraun Fault block to the south.

(4) The fourth trend is the *cross trend*, and is relatively infrequently observed with a distinctive fault strike between 50 and 75° (NE-SE and ENE-WSW). These faults are oriented near-orthogonal to the clysmic trend, and show significantly less throw relative to the other trends (Montenat *et al.*, 1988). The cross trend lies parallel to the most defined preexisting basement fabrics.

The interaction of the four fault populations defines the shapes of the rotated fault blocks in the Gulf of Suez. It is assumed that the principal direction of extension has been nearly perpendicular to the major axis of the rift (Angelier, 1985) or slightly oblique to this direction (Lyberis, 1988) throughout the rifting.

The rotated fault blocks have been divided into three dip provinces based on along-strike change of dip of the block-bounding faults (Fig. 2.2; Colletta *et al.*, 1988; Patton *et al.*, 1994): The northern and southern faults of the rift are predominantly dipping to the NE while the central is predominantly dipping to the SW. The dip provinces are thought to be a result of large transverse faults trending approximately perpendicular to the axis of the Gulf of Suez (Abdine, 1981).

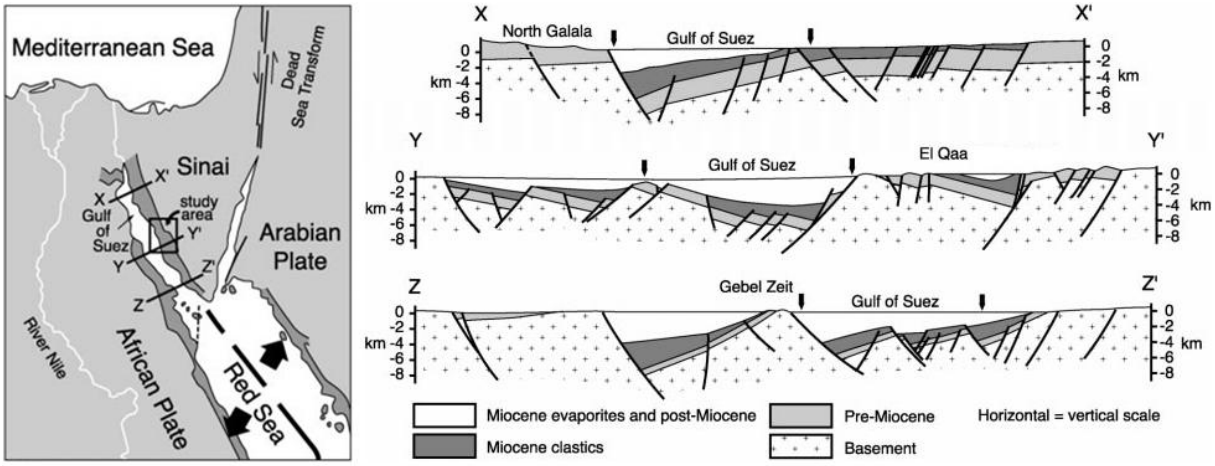

Figure 2.2: Cross sections of the Suez Rift displaying the three dip provinces. X being the northern, Y the central and Z the southern. The arrows represent the present coastlines. Modified from Sharp *et al.* (2000b).

2.4 Hammam Faraun Fault Block

The Hammam Faraun Fault Block (HFFB) (Fig. 2.3) is a rotated fault block (Moustafa and Abdeen, 1992), elongated in a NW-SE direction, c. 20 km wide and c. 40 km long, and is located within the central dip province (Moustafa, 1996; Jackson *et al.*, 2006). The fault block is dipping moderately to the east (12 - 15°) and is controlled to the east and west by block-bounding faults; the Thal and Hammam Faraun Fault, respectively (Moustafa and Abdeen, 1992; Gawthorpe *et al.*, 2003; Jackson *et al.*, 2006). These two faults are more than 25 km long and dip steeply (60 - 80°) to the SW (Gawthorpe *et al.*, 2003; Jackson *et al.*, 2006). The Thal Fault and the Hammam Faraun Fault have up to c. 2 km and c. 5 km displacements, respectively (Moustafa, 1996; Young *et al.*, 2003). The dominant strike for both faults is NW-SE, with subordinate N-S, NNE-SSW and E-W trending segments, creating a zigzag pattern in map view (Gawthorpe *et al.*, 2003). The southern margin of the HFFB is bounded by the E-

W trending, south dipping, Baba - Markha Transfer Fault with a throw of c. 3.5 km, while the northern boundary lies close to the northern dip province and are bounded by a N-S trending fault system (Moustafa and Abdeen, 1992; Moustafa, 1996; Jackson *et al.*, 2006). The HFFB is internally dissected by several short (4-10 km) faults, synthetic and antithetic to the east and west block-bounding faults, displaying an *en echelon* fault array with displacements less than 1 km (Sharp *et al.*, 2000a; Gawthorpe *et al.*, 2003; Jackson *et al.*, 2006). According to Gawthorpe *et al.* (2003) these faults started out as isolated segments and grew by linkage during the rift initiation phase. The relay ramp in focus for this study may likely be formed due to a similar growth process.

The rotation and faulting of the HFFB are not totally rigid and folding and flexuring are observed many places, including several synclines, anticlines and monoclines that are related to the rift tectonics. The monoclines are composed of footwall anticline and hanging wall syncline pairs, oriented parallel to the faults as a response to fault propagation folding and fault drag (Sharp *et al.*, 2000b). Fault perpendicular folds are also observed close to faults as a result of displacement variations along strike (Gawthorpe *et al.*, 2003; Jackson *et al.*, 2006).

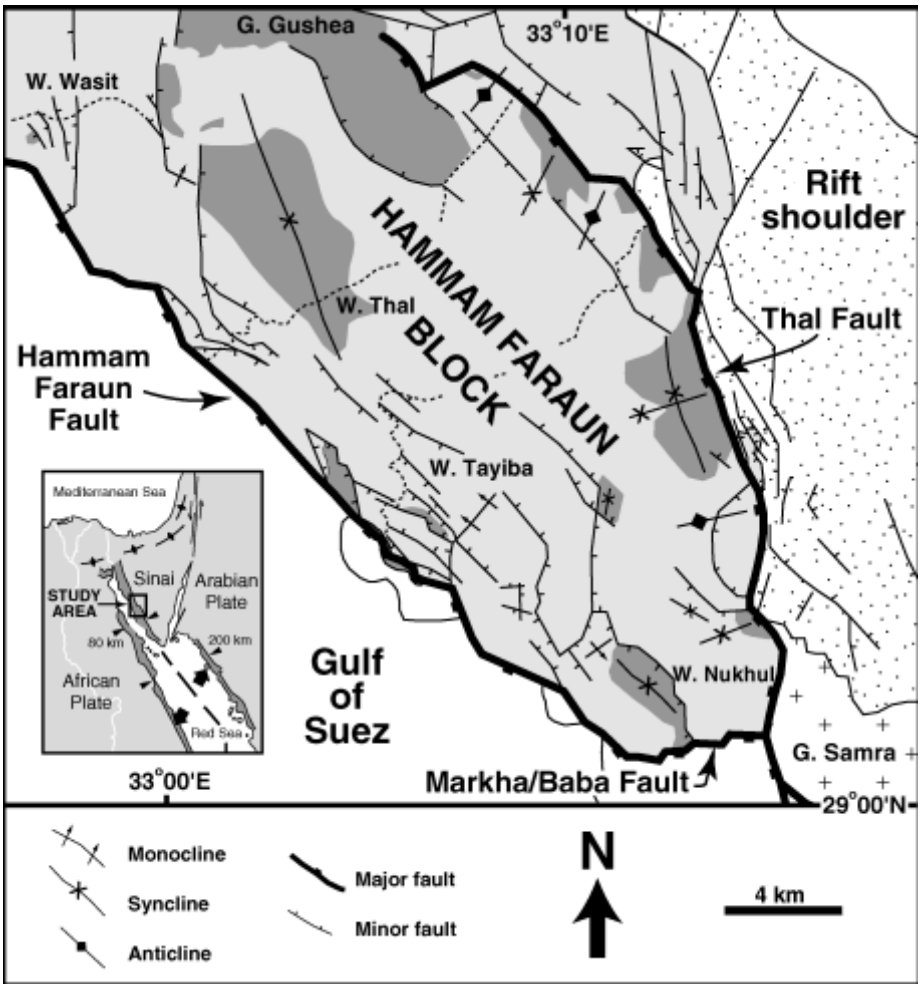

Figure 2.3: Map of the Hammam Faraun Fault Block, showing the main structural features. From Young *et al.* (2003).

2.5 Stratigraphic framework

The stratigraphy of the study area can be subdivided into pre-rift (Cambrian to Eocene), syn-rift (Oligocene to Miocene) and post-rift (Pliocene to Quaternary) deposits (Sharp *et al.*, 2000b) that overlie the Precambrian metamorphic and crystalline basement rocks (Fig. 2.4; Schütz, 1994).

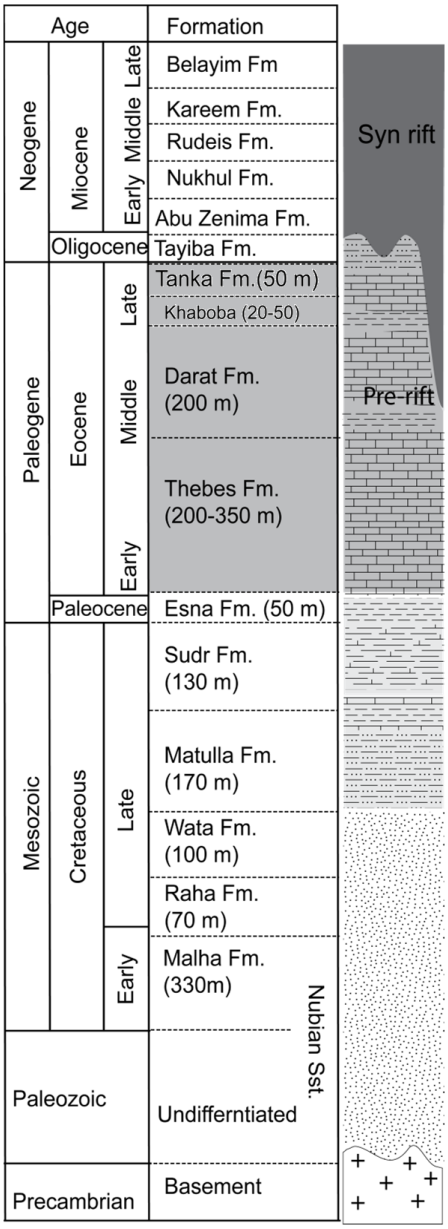

Figure 2.4: Stratigraphy of the Hammam Faraun Fault Block. Rocks of the field area are shaded grey. Modified from Bastesen and Rotevatn (2012).

Pre-rift

The lower part of the pre-rift deposits comprises the continental Nubian sandstones of Cambrian to early Cretaceous age. The sandstones can further be subdivided into siliciclastic Cambrian to Permian age continental deposits and an overlying succession of aeolian and fluvial sandstones of the Malha Formation, of Cretaceous age (Bosworth, 1995; Gupta *et al.*, 1999). The depositional environment during the Cretaceous gradually changed to marine conditions and mixed siliciclastic and carbonate sediments of the Raha, Wata and Matulla formations were deposited (Moustafa, 2003). In late Cretaceous to Eocene, a succession of

deep to shallow marine carbonates, shales and siltstones were deposited as a result of a marine transgression (Abul-Nasr and Thunell, 1987; Kuss *et al.*, 2000). This indicates the establishment of a carbonate platform and the succession includes the Sudr, Esna, Thebes, Darat, Khaboba and Tanka formations:

- The Sudr Formation (upper Campanian - Maastrichtian) consists of uniform, massive white chalk beds, with a thickness of 100-130 m (Schütz, 1994). It contains abundant planctonic foraminifera and was deposited in a deep marine environment (Samuel *et al.*, 2009).
- The Esna Formation (Paleocene) is a relatively thin shale unit (15-50 m) with interbedded chalky limestone (Robson, 1971; Schütz, 1994). It decreases in thickness towards the north, explained by tectonic movement of the Syrian Arc deformation (Patton *et al.*, 1994), which happened in the late Cretaceous (Moustafa, 1993).
- The Thebes Formation (early Eocene) is a deep-water micritic deposit with abundant chert bands, deposited in a basin deepening towards the south (Kuss *et al.*, 2000). Moustafa and Abdeen (1992) classified the Thebes Formation into three units: (1) a lower unit of limestone with chert bands, (2) a middle unit of hard chalky limestone and (3) an upper unit of chalky limestone with chert bands and a marly top. The formation was most likely partly exposed, eroded and redeposited, because of syndepositional slumping in north and phosphatic layers in the southern part of the HFFB (Abul-Nasr and Thunell, 1987; Kuss *et al.*, 2000).
- The Darat Formation (middle Eocene) consists of alternating layers of brown shales and white marls, and some limestone (Schütz, 1994). It is relatively rich in molluscs and the depositional environment is considered to be lower shelf (Abul-Nasr and Thunell, 1987).
- The Khaboba Formation (upper middle Eocene) is made of shale and marls, interbedded with chalky limestone with some flint bands (Schütz, 1994). Some parts of the Khaboba Formation is also rich in molluscs and contains some coral heads, and a carbonate platform is considered to be the depositional environment (Abul-Nasr and Thunell, 1987).
- The Tanka Formation (upper Eocene) consists of thin interbedded chalky limestone and claystone (Moustafa and Abdeen, 1992). The depositional environment is considered to be an intertidal carbonate platform (Abul-Nasr and Thunell, 1987).

Syn-rift

The onset of rifting is marked by the presence of basaltic flows, dikes and sills of early Miocene age (Moustafa, 1993), restricted to the HFFB (Moustafa and Abdeen, 1992). The Miocene syn-rift sediments unconformably overlie the early Miocene rift volcanics (Moustafa, 1993). The syn-rift sediments include several units: the Abu Zenima Formation, the Nukhul Formation, the Rudeis Formation and the Kareem Formation:

- The Abu Zenima Formation, of Oligo- Miocene age, consists of non-marine mud-, silt- and sandstones with some conglomerate beds (Moustafa and Abdeen, 1992; Sharp *et al.*, 2000a), and has been interpreted to be deposited during the rift initiation (Patton *et al.*, 1994).
- The Nukhul Formation is a fluvial to shallow marine clastic deposit (Schütz, 1994) characterized by calcareous sandstones and marls (Scott and Govean, 1985). As the Abu Zenima formation, the Nukhul Formation has also been interpreted to be deposited during the rift initiation (Patton *et al.*, 1994).
- The Rudeis Formation consists of shales and marls from an open marine environment, and are the thickest (average of 500 m) and most widespread of the Miocene formations (Schütz, 1994). The sedimentation occurred as the basin were quickly subsiding, which made huge thickness variations (Schütz, 1994), and has been interpreted to be deposited during the rift climax (Patton *et al.*, 1994).
- The Kareem Formation (Langhian) is an up to 500 m thick marine succession of interbedded sandstones, shales and carbonates with some anhydrites in the lower part (Evans, 1988; Salah and Alsharhan, 1997). It was deposited in deltaic and submarine fans, while the anhydrites were precipitated in local lagoons (Salah and Alsharhan, 1997).

Post-rift

The post-rift exposures are mainly Quaternary sediments, which include deposits in the wadi floors and gravel terraces in the troughs of the large synclines and other topographical low areas, as well as offshore (Moustafa, 1993).

3. Theoretical background

3.1 Introduction

The aim of this chapter is to give an overview of the theoretical background needed to understand the data, discussion and conclusions of the study. Part 3.2 deals with the current theories of faulting, part 3.3 on the damage zones related to fault, while part 3.4 and 3.5 focus on the development of fractures. Lastly, part 3.6 gives a basic overview of the effects of shale smear.

3.2 Faulting and fault evolution

3.2.1 Single faults

It is important to understand the temporal and spatial evolution of single fault segments. By studying the geometry of the fault planes, coal mine studies of fault throw revealed that the fault planes are elliptical with maximum throw at the centre and decreasing towards the edges (Rippon, 1984). The outer limit of the ellipse is called the tip-line, where the shortest axis of the ellipse is parallel to the direction of displacement (Barnett *et al.*, 1987). The displacement is greatest near the centre of the fault and decreases towards the tips (Fig. 3.1).

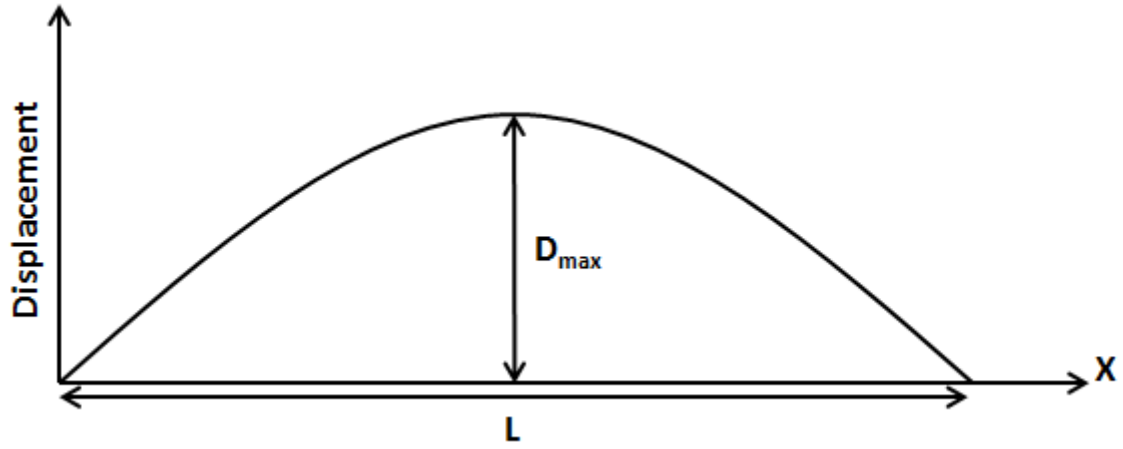

Figure 3.1: Illustration of the displacement distribution of an idealized fault intersecting the surface. D_{max} is the maximum displacement and L is the length of the fault, and X is distance.

A scale invariant power law of how the displacement (D) and length (L) of faults are related was developed: $D=cL^n$, where c is a constant related to material properties of which shear modulus is the most important (e.g. Watterson, 1986; Walsh and Watterson, 1988; Cartwright *et al.*, 1996). There is no exact value of the exponent n, but based on publications it varies from 1.0 (Cowie and Scholz, 1992b) to 2.0 (Watterson, 1986; Walsh and Watterson,

1988). This model is however only applicable to growing faults in which the entire fault surface is involved in each slip event (Watterson, 1986). Later studies of D and L data have been used to modify the power law which gives a linear relationship: D=cL, where c is critical shear strain (Cowie and Scholz, 1992a; Dawers *et al.*, 1993; Scholz *et al.*, 1993).

3.2.2 Interacting faults

There are postulated two general models of how normal faults grow: (Model 1) isolated faults growing by radial propagation (Fig. 3.2) and eventual linkage (e.g. Watterson, 1986; Walsh and Watterson, 1988; Cowie and Scholz, 1992a; Cartwright *et al.*, 1995); known as the "isolated fault model" (*sensu* Walsh *et al.*, 2003) or "fault growth by segment linkage" (*sensu* Cartwright *et al.*, 1995); or (Model 2) the "alternative growth model" (*sensu* Walsh *et al.*, 2002) or the "coherent fault model" (*sensu* Walsh *et al.*, 2003) where the fault segments appear isolated in map-view but, in three dimensions, are components of a single structure (Childs *et al.*, 1995; Walsh *et al.*, 2002; Walsh *et al.*, 2003). The fundamental difference between the two models is that; (In model 1) each fault is initially isolated and is mechanically unrelated to the fault array it will be a component of, while (model 2) suggests that each fault segment initially is a part of a mechanically related array (Walsh *et al.*, 2003). In the latter model fault lengths are rapidly established and further growth is ceased as faults interact, meaning that the faults have essentially constant lengths during most of the growth evolution (Walsh *et al.*, 2002). The isolated fault segments observed in map-view of the coherent fault model is typically a result of upward or lateral splaying of a single fault (Jackson and Rotevatn, in press) and are most applicable where the faults have been reactivated (Walsh *et al.*, 2002; Walsh *et al.*, 2003).

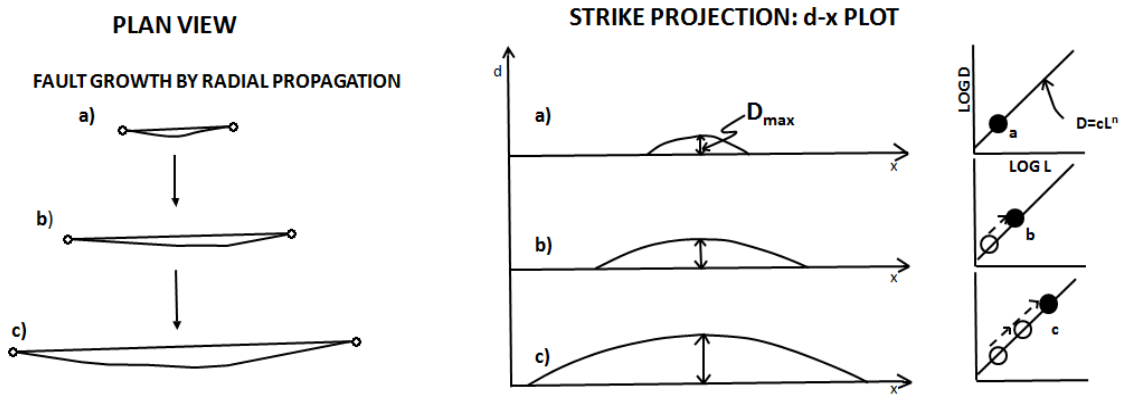

Figure 3.2: Fault growth by radial propagation through three stages of growth are compared for both models in plane view, on a displacement (d) against distance (x) plot, and on a log displacement (D) vs. log length (L) plot. A fault growing by radial propagation follows a growth low, as shown earlier. If the material properties are assumed to be constant, the increase in length and displacement will follow a linear path in a log D vs. log L plot throughout the growth of the fault. Redrawn from Cartwright *et al.* (1995).

Interacting faults create zones or relays where strain is transferred between the faults. Such relay structures where first described by Goguel (1965) and have since been described in several tectonic settings all over the world, but it was Larsen (1988) that began to study the structures in detail. Morley *et al.* (1990) were the first to make a classification of transfer zones (Fig. 3.3). The transfer zones are divided into pairs of faults that have a common footwall or hanging wall, called conjugate transfer zones, and pairs where the hanging wall of one fault is the footwall of the other, called synthetic transfer zones. The transfer zone studied in the current study is synthetic overlapping, and will hereinafter be described as a relay ramp.

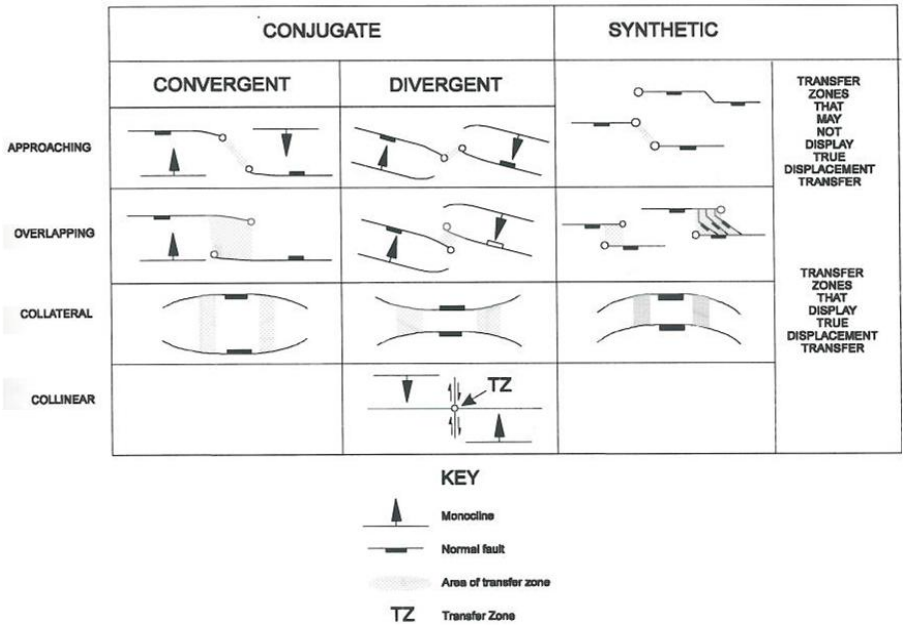

Figure 3.3: Classification of transfer zones after Morley *et al.* (1990). The transfer zone in the current study is synthetic overlapping.

A relay ramp is defined by Larsen (1988) as transfer zones that occur between normal fault having the same dip direction (Fig. 3.4). The bedding between the fault segments is reoriented, maintaining the continuity between the hanging wall and footwall of the fault zone (Peacock and Sanderson, 1994). Thus, the ramp dip is defined by the displacement gradient of the two overlapping faults. The ramp is often dissected by fractures that transfers displacement between the two fault segments (Peacock and Sanderson, 1994), and is also often breached by minor faults that connect the two fault segments, called oblique- or lateral-transfer faults (Larsen, 1988). The ramp is i.e. eventually thought to be breached and create a single fault (Peacock and Sanderson, 1994). The closer the spacing between the two overlapping fault segments the higher the strain concentration in the ramp is, while with increased spacing the strain is distributed larger a greater area (Trudgill and Cartwright, 1994).

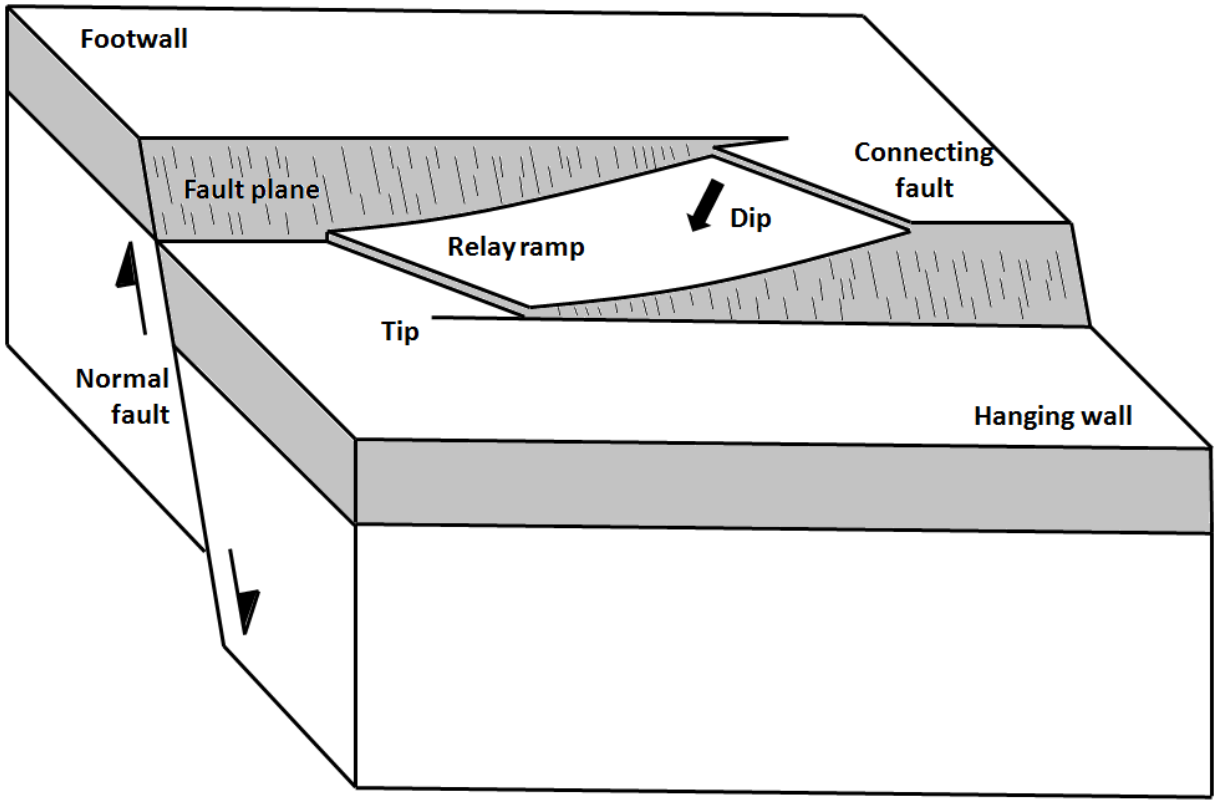

Figure 3.4: Block diagram showing the main features of a relay ramp. The bedding of the relay ramp is reoriented to accommodate strain between the two faults. The folding of the bedding leads to formation of faults and fractures. The ramp illustrated has been breached at both ends by connecting faults. Redrawn from Peacock and Sanderson (1994).

Peacock and Sanderson (1994) constructed a theoretical model to describe how a pair of normal faults evolve from two isolated faults to one single fault. The model describes the displacement evolution of the fault and the topographical changes:

1. *Isolated faults* (Fig. 3.5a): The faults are isolated and do not overlap. The d-x profiles are normal.

2. *Early relay ramp development* (Fig. 3.5b): The faults overlap and topographical changes induced by the interaction of the faults develop a relay ramp. The hanging wall of one fault is connected with the footwall of the other. The bedding of the ramp is rotated about an axis sub-perpendicular to the fault plane. The ramp has a tendency to rotate towards the hanging wall. The interaction of the faults change the scaling relationship of individual faults as the D/L increases (Cartwright *et al.*, 1995). The d-x profile also changes, becoming steepened towards the fault tips related to the portion nearest the point of maximum displacement. This is because the displacement transfer between the two fault segments is accommodated by rotation of the relay ramp. The total fault displacement of the two overlapping segments if added is often at minima in the overlap zone. This is mainly a response caused by the hanging wall directed rotation of the relay ramp. Increased amount of overlap decreases the amount of dip towards the hanging wall.

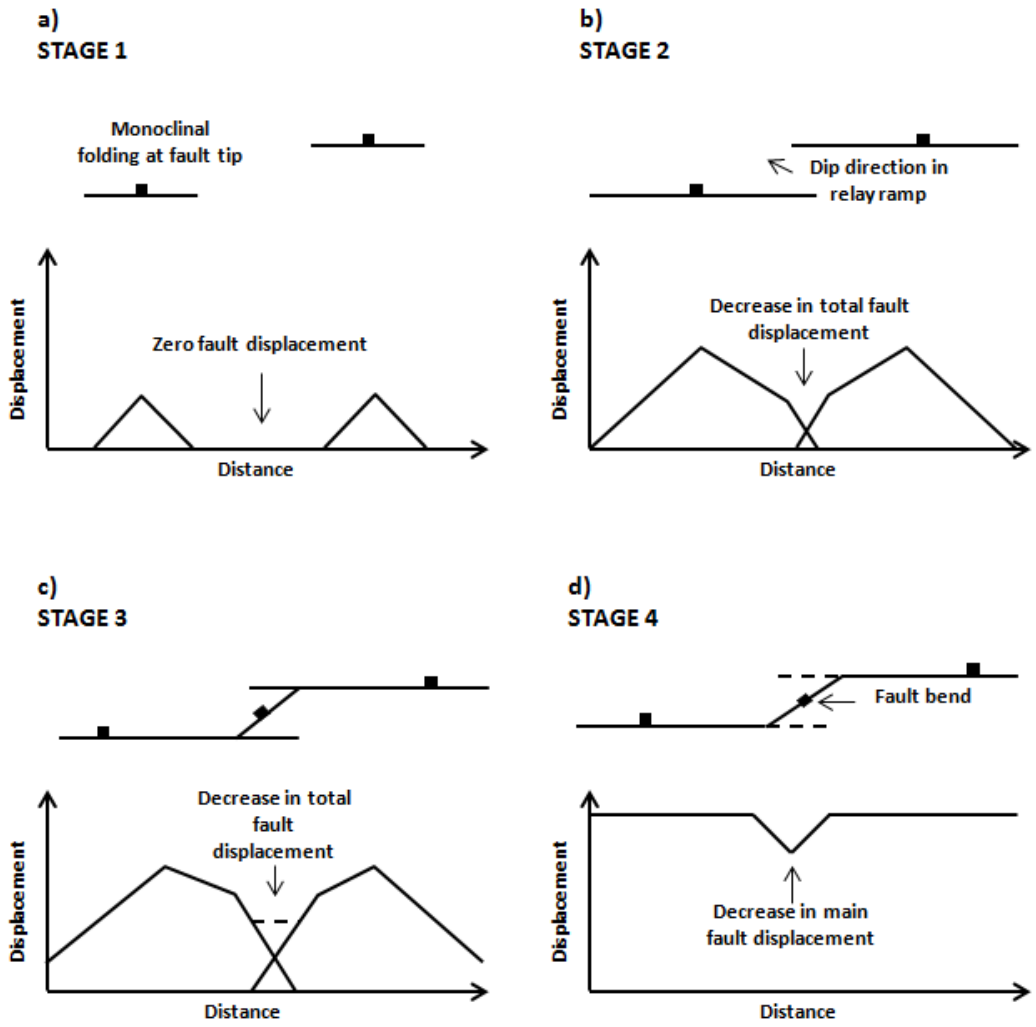

Figure 3.5: Displacement development and corresponding d-x profiles for each stage of the model. **(a)** The faults are isolated and do not overlap. **(b)** Interaction of the two faults and a relay ramp begins to develop. The displacement is transferred between the faults by rotation. **(c)** A fully relay ramp is developed. **(d)** Breaching of the relay ramp, and further strain is accommodated by the fault. Redrawn from Peacock and Sanderson (1991).

3. *Late relay ramp development* (Fig. 3.5c): The dip of the relay ramp continues to increase until the ramp has rotated to its limit and begins to break up. The limit is determined by the rheology and bed thickness. This stage is also characterized by fractures cutting across the ramp trying to connect the two faults. The highest stress concentrations and therefore also the amount of connecting fractures occur near the tips of the overlapping fault segments. These fractures connect the two fault segments and eventually break the ramp. The orientations of the fractures are strongly controlled by the rotational stress. This may be a result of the rotation of the ramp towards the hanging wall, from the closure of folds at the fault tips and from small-scale connecting faults accommodating displacement.

4. *Breaching of the ramp* (Fig. 3.5d): As the faults grow and displacement increases the relay ramp becomes gradually more deformed and rotated. Displacement is transferred between the faults until the ramp no longer can accommodate strain by further deformation (Childs *et al.*, 1995), and it becomes hard linked (Imber *et al.*, 2004) to form a single composite fault. The linkage point is marked by a kink/jog in the fault trace. The ramp is now redundant and is preserved at approximately the same angle it was breached. If one of end of the ramp breach, the area around the other end will be preserved as normal drag. If the ramp breach at both ends, it will be preserved as a fault-bound horse. There are three ways of breaching the ramp (Fig. 3.6; Childs *et al.*, 1995). The linkage zone is at this point the place of displacement minima along-strike of the segmented fault (Dawers and Anders, 1995), but as the composite fault grows and displacement accumulates, the displacement minima will eventually diminish as well as the kink/jog in the fault trace (Rotevatn and Bastesen, 2012).

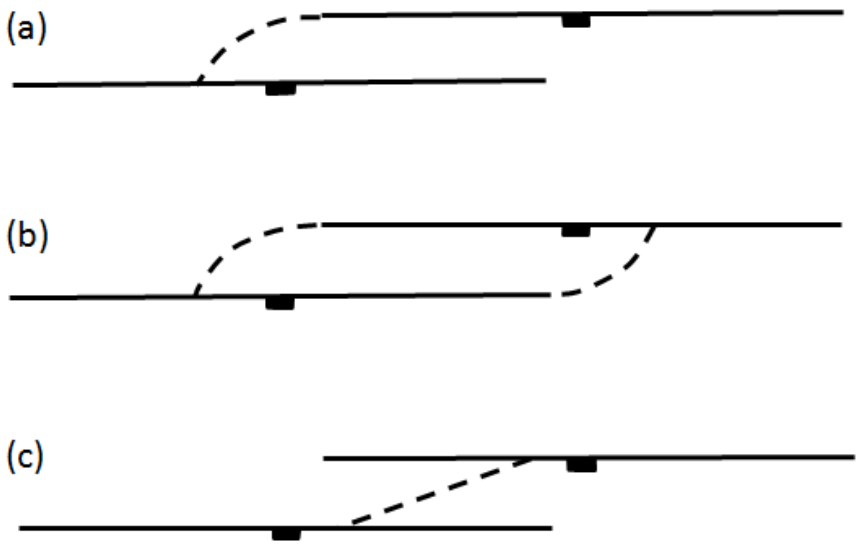

Figure 3.6: Three possible ways in which the relay ramp may be breached. **(a)** Propagation of either the hanging wall (shown) or the footwall fault. **(b)** Propagation of both the hanging wall and the footwall. **(c)** Secondary linking fault. Redrawn from Childs *et al.* (1995).

Cartwright *et al.* (1995) made a model for fault linkage with emphasis on the variation of the D/L values throughout the linkage process. The model consists of three fault segments propagating towards each other (Fig. 3.7). When the segments propagate independently, the D/L ratio is constant and will follow the equilibrium line (Fig. 3.7a). Once the stress fields at the tips of the segments begin to interact, the faults begin to overlap. At this point the D/L value for each individual fault will increase and plot as a point over the equilibrium line.

Plotting all the faults together as one composite fault would make L the distance along all the faults and D the greatest value of throw on any of the faults. This value would plot as a point below the equilibrium line. As long as they propagate as individual segments the point of the D/L value will continue to move away from the equilibrium line (Fig. 3.7b). At the final stage the relay ramps breach and the three faults link up. This results in an increase of the D value, while the value of L remains nearly constant. The new point of the D/L plot will therefore move back on the equilibrium line as the scaling relationship is back to normal (Fig. 3.7c).

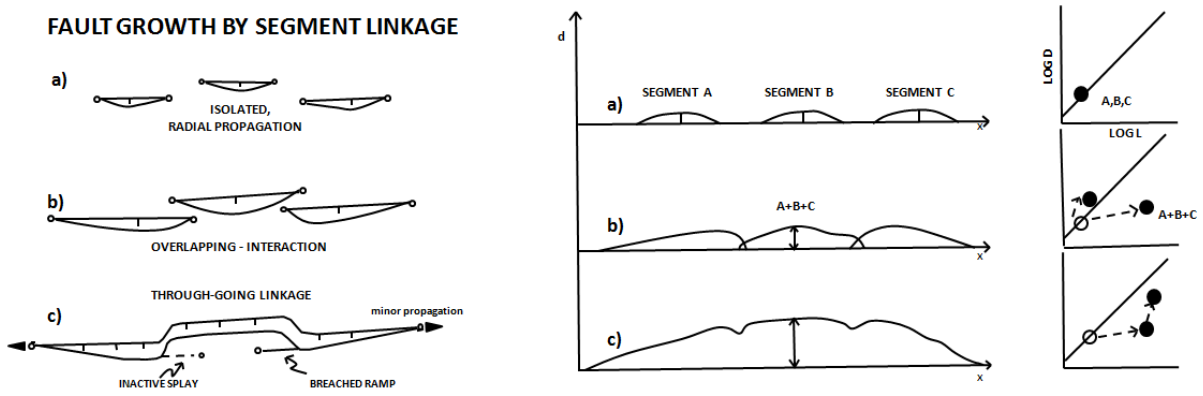

Figure 3.7: Schematic evolution of three faults. They are compared for both models in plane view, on a displacement (d) against distance (x) plot, and on a log displacement (D) vs. log length (L) plot. Redrawn after Cartwright *et al.* (1995).

3.3 Fault damage zones

Architecturally faults are divided into a fault core and a damage zone (Caine *et al.*, 1996). Both are surrounded by the host rock which has a background value of deformation frequency (Agosta and Aydin, 2006). The fault core is where the displacement is accommodated at most, characterized as a high-stain zone composed of slip surfaces and comminuted rock (Micarelli *et al.*, 2003; Bastesen and Braathen, 2010), while a damage zone is defined as the volume of deformed rock surrounding the fault core (e.g. McGrath and Davison, 1995; Kim *et al.*, 2004). The featured structures within this zone can provide information of fault propagation and growth (e.g. McGrath and Davison, 1995; Vermilye and Scholz, 1998, 1999) and fluid flow (e.g. Sibson, 1996; Martel and Boger, 1998). The permeability properties differ from fault core to damage zone; fault cores have generally low permeability and may therefore act as seals, but not always (Billi *et al.*, 2003; Agosta and Aydin, 2006; Micarelli *et al.*, 2006; Bastesen *et al.*, 2009); while the damage zones generally have higher permeability featuring highly conducting fracture networks (Billi *et al.*, 2003; Rotevatn and Bastesen, 2012). Kim *et*

al. (2004) categorized damage zones into: linking damage zone, tip damage zone and wall damage zone (Fig. 3.8).

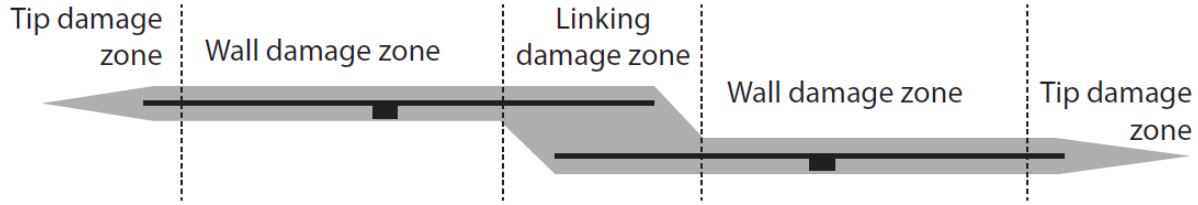

Figure 3.8: Damage zone terminology. The linking damage zone represents where the faults overlap; the wall damage zone, the footwall and hanging wall damage zone beyond the overlap zone; tip damage zone, the extension of the fault tip (Rotevatn and Bastesen, 2012).

3.4 Fracture development

A fracture is a surface where the material continuity has been lost (van der Pluijm and Marshak, 2004). Fractures can be divided into several types (Fossen, 2010): (1) A *shear fracture* is a slip surface with fracture-parallel movement, and is used for mm- to dm-scale displacements. (2) A *joint* is an extension fracture with extension perpendicular to the walls and very little displacement. (3) A *fissure* is an extension fracture filled with air or fluids. (4) A *vein* is an extension fracture filled with minerals. (5) A *dike* is an extension fracture filled with magma.

In fracture mechanics is common to classify fractures into three modes based on the displacement field (Fig. 3.9): Mode I is extension with displacement perpendicular to the walls of the fracture. Mode II is represented by shear movement parallel to the fracture. Mode III is tearing that involves slip parallel to the edge of the fracture (Fossen, 2010).

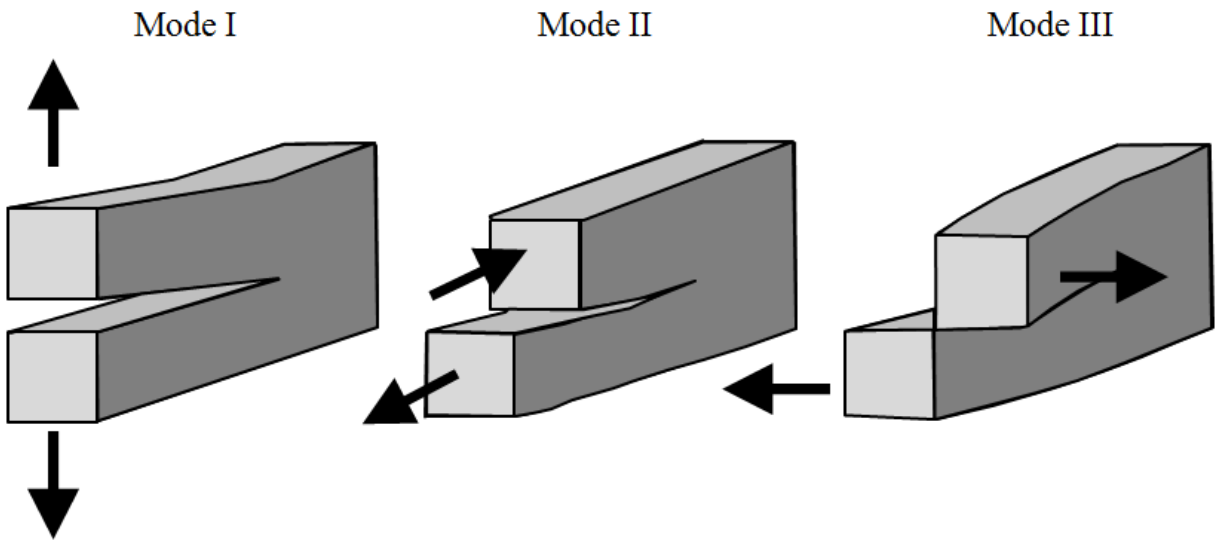

Figure 3.9: Modes of fracture. Mode I: opening, Mode II: sliding, Mode III: tearing.

Peacock and Mann (2005) described the factors controlling the geometry, frequency and distribution of fractures in reservoir rocks. They divided the factors into three main parts:

(1) Rock characteristics and diagenetic factors

Rock characteristics and diagenetic factors are the primary controls on fracturing. *Lithology* is an important factor, where brittle beds tend to be more fractured compared to more ductile beds (Ladeira and Price, 1981). *Sedimentary structures* such as bedding-plane irregularities and fossils can initiate fractures (McConaughy and Engelder, 1999). The *bed thickness* is commonly proportional to the mean spacing of joints that from a joint set (Narr and Suppe, 1991; Gross *et al.*, 1995; Shaocheng *et al.*, 1998). The joint frequencies also tend to be higher in thinner beds (Ladeira and Price, 1981). *Mechanical stratigraphy* is another important control. Joints can be inhibited to connect between two brittle beds if the beds are relatively thick and less brittle (Helgeson and Aydin, 1991). Fractures can also develop throughout two beds, by acting as a single mechanical unit (Finn *et al.*, 2003). Fracture propagation can be controlled by the mechanical behavior of the *bedding planes* (Renshaw and Pollard, 1995). Fractures tend, for example, to terminate at bedding-planes that are boundaries between beds of very different competence.

(2) Structural factors

The style and geometry of fractures can be controlled by the *tectonic setting*, where the fracture orientations are controlled by the stress regime. Extension fractures tend to form

perpendicular to the least compressive stress (σ_3) (Pollard and Aydin, 1988). The geometry of fracture networks is controlled by the *palaeostress* history, which control the sequence of fracture development (Rawnsley *et al.*, 1998; Eyal *et al.*, 2001). An important aspect of the palaeostress history is *subsidence and uplift* (Bahat, 1999). Fractures close to the earth's surface are commonly caused by stress relief induced by uplift (Rawnsley *et al.*, 1998). The fractures formed by tectonics are by Rawnsley *et al.* (1998) thought to be more systematic and form distinct sets, while the fractures formed by uplift are nonsystematic. Today it is well known that the fracture frequency is increasing in the *proximity to faults* (Pohn, 1981), and that the fracture orientation can change towards a fault because of perturbation of stresses (Rives *et al.*, 1992; Petit and Mattauer, 1995; Kattenhorn *et al.*, 2000). By analyzing fracture frequencies and orientations one can determine the relationship between the faults and fractures, which is an important part of this study. It is also assumed that the fracture frequency and complexity are related to curvature and strain in folds (Casey and Butler, 2004). The *timing of structural events* is an important control on the fracture distribution. Peacock (2001) showed that pre- and post-fault fracture frequencies don't tend to increase towards the fault zone, while syn-fault fracture frequency tend to increase significantly near the fault. He also stated that the pre-fault fractures in the fault zone could be opened to form veins. Mineralization and diagenesis influence fractures (Laubach, 1988). Pre- and syn-mineralized fractures are closed or partly closed veins, while post mineralized fractures tend to be open. The *angle between bedding and fractures* are commonly approximately 90° (Helgeson and Aydin, 1991), and therefore the dip of the bedding often control the dip of the fractures.

(3) Present-day factors

The *orientations of in situ stresses* commonly influence the apertures of open fractures. Fractures that are perpendicular to the maximum compressive stress (σ_1) tend to be closed, while fractures that are perpendicular to σ_3 tend to be open. *Fluid pressure* and in situ stresses varies with *depth* (Sepúlvda and Zack, 1991) and can control the initiation of fractures, and which that are open (Secor, 1965).

These three factors show how geometries, orientations and distributions of fractures are controlled. This is important to understand in order to improve predictions and modeling (Peacock and Mann, 2005).

3.5 Fractures around normal faults and in relay ramps

Fracture orientations around normal faults were studied by Anderson (1951) who indicates that mode I, opening fractures (Fig. 3.9) generally forms perpendicular to the least compressive stress (i.e. parallel to the fault strike) (Fig. 3.10a). This theory is based on predictions in an extensional regime, but does not consider fracture growth related to stress perturbation induced by growing faults (Fig. 3.10b; Kattenhorn *et al.*, 2000). The perturbation effect of propagating faults has been documented (e.g. Barton and Zoback, 1994; Maerten *et al.*, 2002) to affect orientations of secondary structures such as minor faults and fractures. Kattenhorn *et al.* (2000) argue that fractures propagating across a relay ramp, under conditions of remote tectonic tension and lithostatic stress, may be oriented with an oblique angle relative to fault strike, but not larger than 30°. They further argue that the relationship between fault-parallel and fault-perpendicular remote stresses affect the fracture orientations in relay ramps; as the remote fault-parallel stress increases relative to the fault-perpendicular stress the relative angle between fractures and faults also increases.

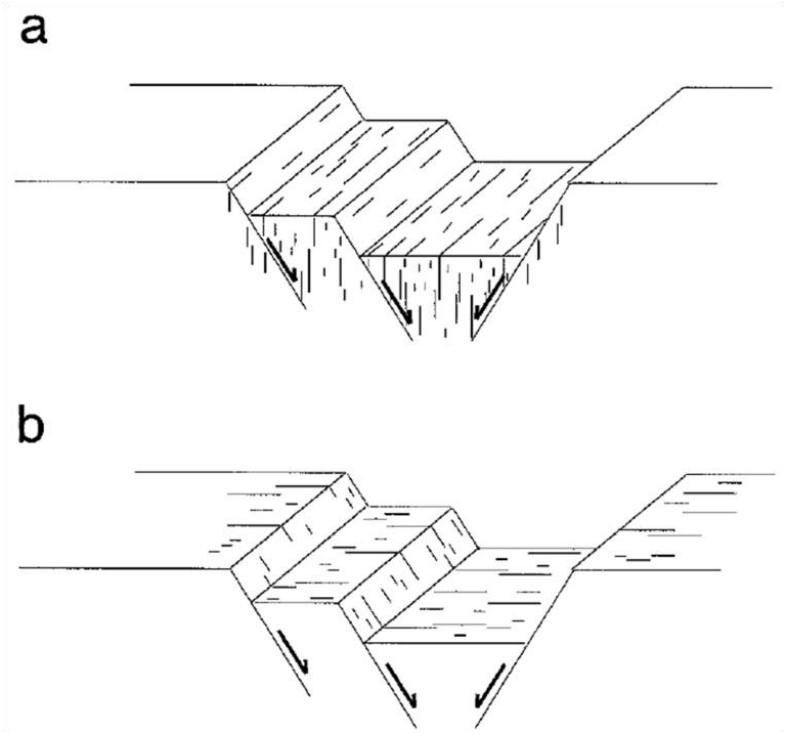

Figure 3.10: Prediction of fracture orientations in proximity to normal faults. **(a)** Fractures oriented parallel to the fault strike of normal faults (Anderson, 1951). **(b)** Fractures oriented at high angles to the fault strike of normal faults (Kattenhorn *et al.*, 2000).

3.6 Shale smear

Shale smear if defined as a more or less continuous shale membrane entrained in the fault core during fault movement (Fig. 3.11), and was originally used for sandstone-shale sequences by (Lindsay *et al.*, 1993), but can be applied in other scenarios like a carbonate-shale sequence. Core data has shown that continuous shale smear may act as a barrier to fluid flow (e.g. Gibson, 1994; Færseth, 2006), and it is therefore important to be able to predict the smearing in fault zones.

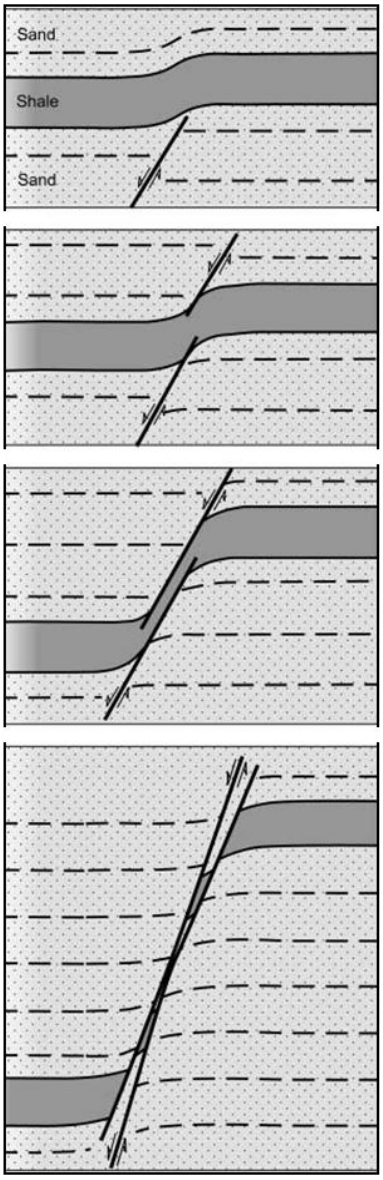

Figure 3.11: Conceptual model of the evolution of shale smear in a fault zone, modified from (Færseth, 2006). As the fault grow the shale smear gets more and more thinned out until it eventually gets discontinuous.

4. Field data

4.1 Introduction

The purpose of this chapter is to give a detailed description of the studied localities with emphasis on fracture frequencies, orientations, lithologies and throw. This was done in order to get an overview of the deformation along the faults and in the ramp. Part 4.2 and 4.3 describe the localities along the faults and in the ramp, while part 4.4 describes hanging wall maximum and mean fracture frequency vs. fault throw along WWF and TRF. All localities can be seen in Figure 4.1.

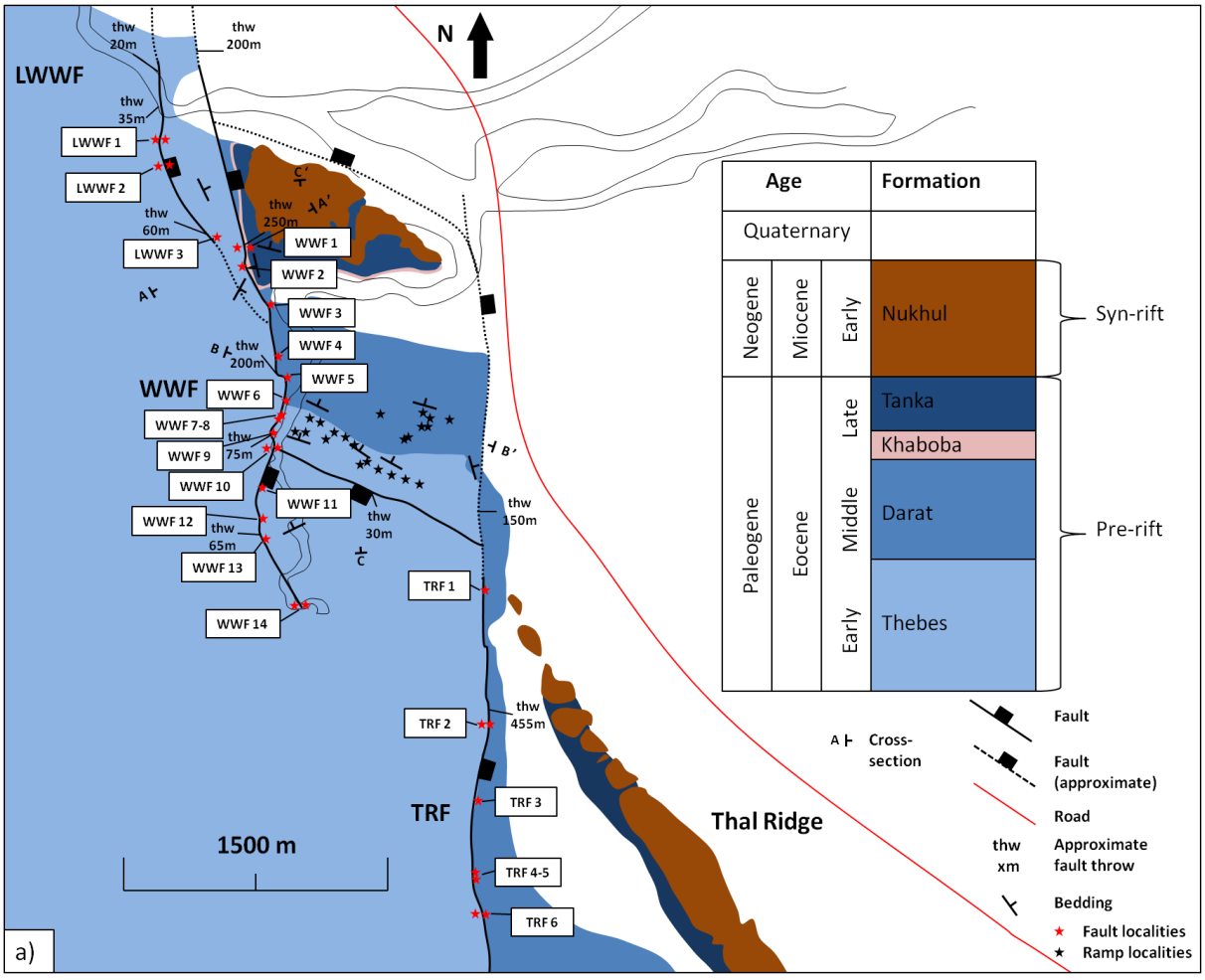

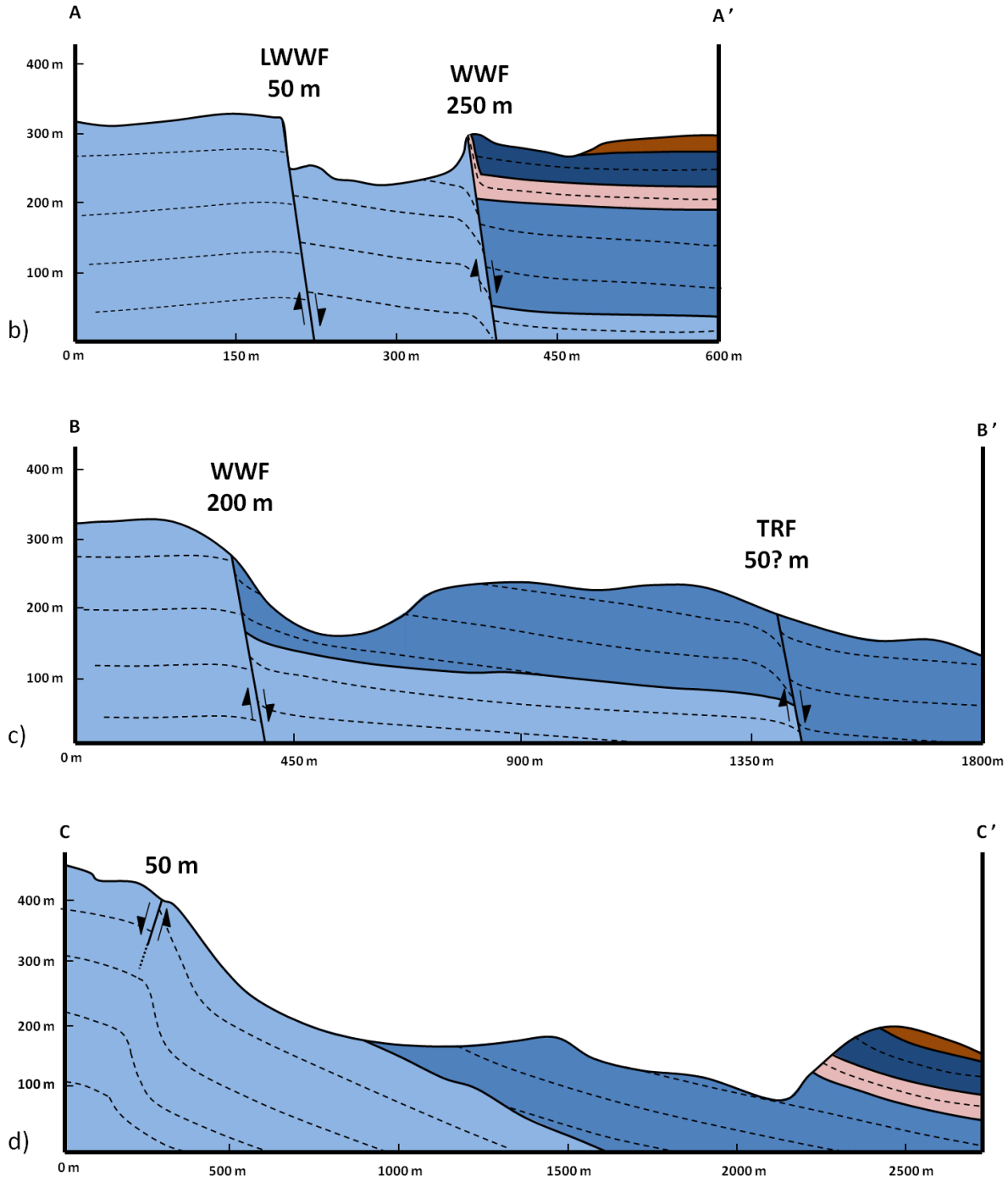

Figure 4.1: Geological map and cross-sections of the study area based on field work, supplemented by Armstrong (1997). **(a)** Map showing the studied localities. Cross-section markers can be seen on this map **(b)** NE-SW cross-section in the northern part of the study area. **(c)** NW-SE cross-section through the relay ramp. **(d)** N-S cross-section through the ramp.

4.2 Description of studied localities along faults

The localities chosen for this study are located along the LWWF, WWF, TRF and in the relay ramp. A total of 58 localities were studied (APPENDIX). Each locality involved measurement of fracture frequencies and orientations and description of lithology and fault core. All throw

values are based on previous work done by Armstrong (1997) and Sharp *et al.* (2000), and has been quality controlled in the field.

The inner damage zone is in this thesis defined as the first meters of the scanline with fracture frequencies above c. 30 fractures per meter (fpm), while the outer damage zone represents the remaining frequencies below c. 30 fpm (i.e. the rest of the scanline). However, some places the mean outer damage zone frequency is above 30, which is a result of local high fracture frequencies in the outer part of the scanlines.

4.2.1 Background fracturing

Background fracturing levels in the Thebes Fm. was assessed in Wadi Dolly and Wadi Tayeba, at areas that are unaffected by faults (Fig. 4.2). These frequencies were assed in order to compare with the frequencies along the LWWF, WWF, TRF and in the relay ramp.

- In Wadi Dolly both of the grainstones have the lowest fracture frequencies with a mean of 4.4 and 4.1 fpm. The packstone and mudstone have higher frequencies with a mean of 7.6 and 8.7, respectively. In Wadi Tayeba the grainstone has the lowest frequencies with an even distribution of fractures and a mean of 3.4 fpm, while the mudstone has higher frequencies with a more irregular distribution and a mean of 8.2 fpm.
- At both localities grainstone is observed to have the lowest fracture frequencies, while mudstone has the highest. Packstone has values slightly lower than the mudstone.

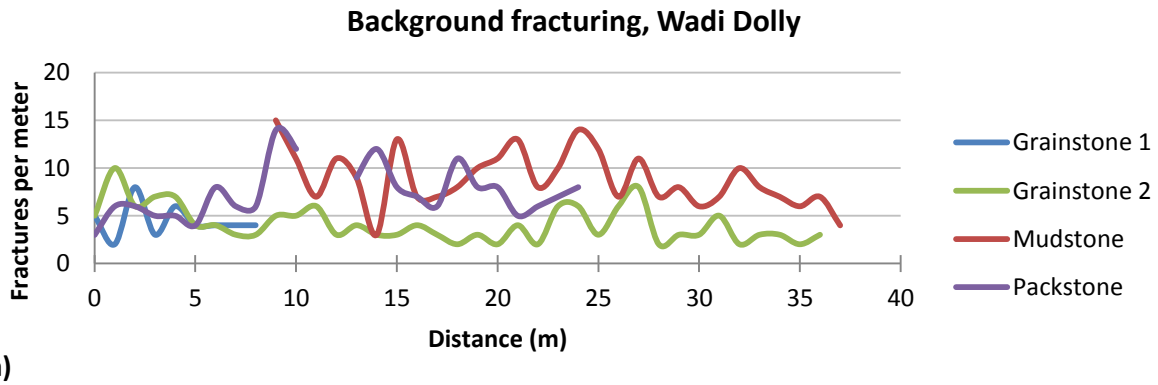

a)

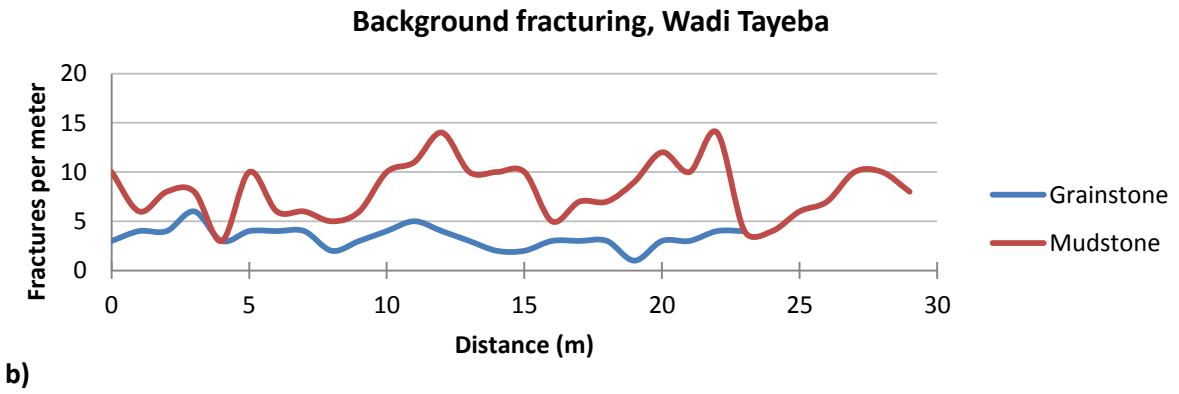

b)

Figure 4.2: Background fracture frequencies from Wadi Dolly **(a)** and Wadi Tayeba **(b)**.

Table 4.1: *Key data from background fractures.*

Locality	Mean fracture frequency	Formation
Wadi Dolly grainstone 1	4,4	Thebes
Wadi Dolly mudstone	8,7	Thebes
Wadi Dolly grainstone 2	4,1	Thebes
Wadi Dolly packstone	7,6	Thebes
Wadi Tayeba grainstone	3,4	Thebes
Wadi Tayeba mudstone	8,2	Thebes
All background localities	6,1	

Table 4.1 shows that the mean background fracture frequency for the Thebes Fm. is 6.1 fpm. Since the rest of the thesis does not differentiate the lithology of the Thebes Fm., this value will be used for comparison. Background fracturing in the Darat Fm. were not assed in the current study but work by Bosworth *et al.* (2012) show a mean background fracturing of 3.5 fpm. The overall background fracture frequency is therefore assumed to be 3-9 fpm.

4.2.2 Little Wadi Wasit Fault

The LWWF is a fault splay of the WWF in the northwestern part of the study area. Three localities were chosen along the fault: LWWF 1, 2 and 3 (Fig. 4.3a). Both the footwall and the hanging wall of the fault consist of the Thebes Fm. and the throw is increasing southwards.

- LWWF 1 has an even distribution of fractures with a mean of 16 fpm for both the footwall and the hanging wall (Fig. 4.3b). LWWF 2 (Fig. 4.4a) has a similar trend for

the footwall, but increased fracture frequency close to the fault (Fig. 4.3c). The first meters of the scanline involve frequencies up to 69 fpm that decrease away from the fault. The first 30 meters of LWWF 3 (Fig. 4.4d) were not assessed due to bad exposure. The remaining part of the scanline displays an uneven fracture distribution with a peak of 78 fpm, 44 meters away from the fault (Fig. 4.3d). This area is characterized as stockwork fractures (4.4b).

- The main fracture orientation for the LWWF localities is sub-parallel to the fault, with subordinate N-S trending and fault sub-perpendicular fractures (Fig. 4.4c).
- The fractures are mainly characterized as hairline fractures (sub-mm wide) and calcite-filled fractures (< 1 cm wide), and the fault sub-parallel fractures are generally long (> 10 m). No shale smear or fault rock lenses are observed and the fault core is characterized as a relatively discrete slip surface.

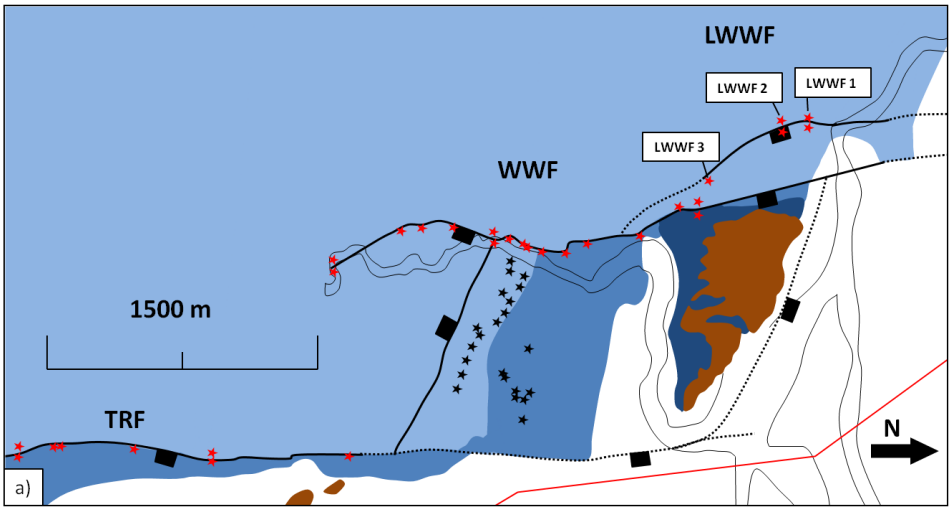

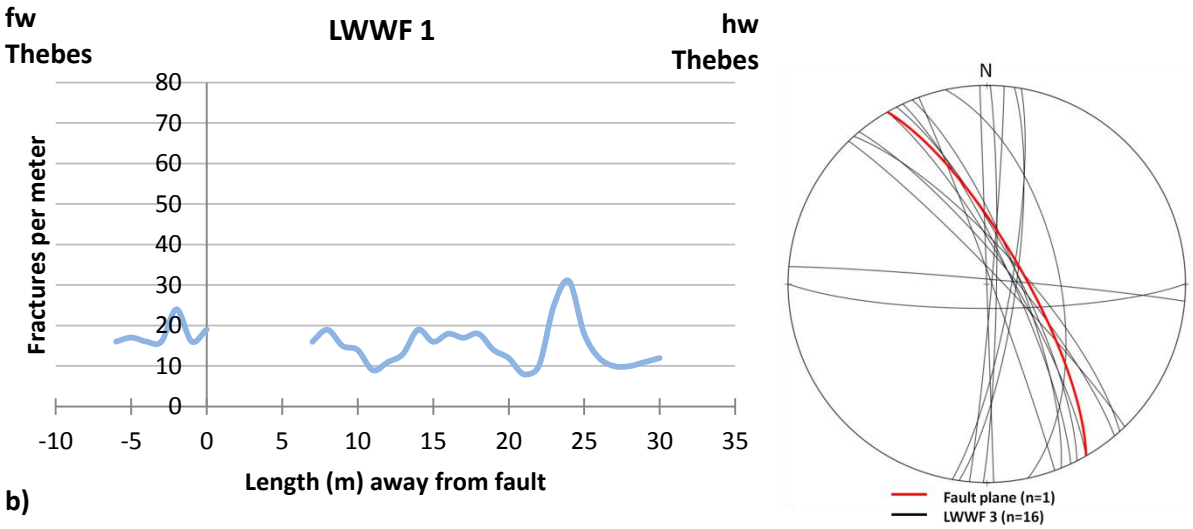

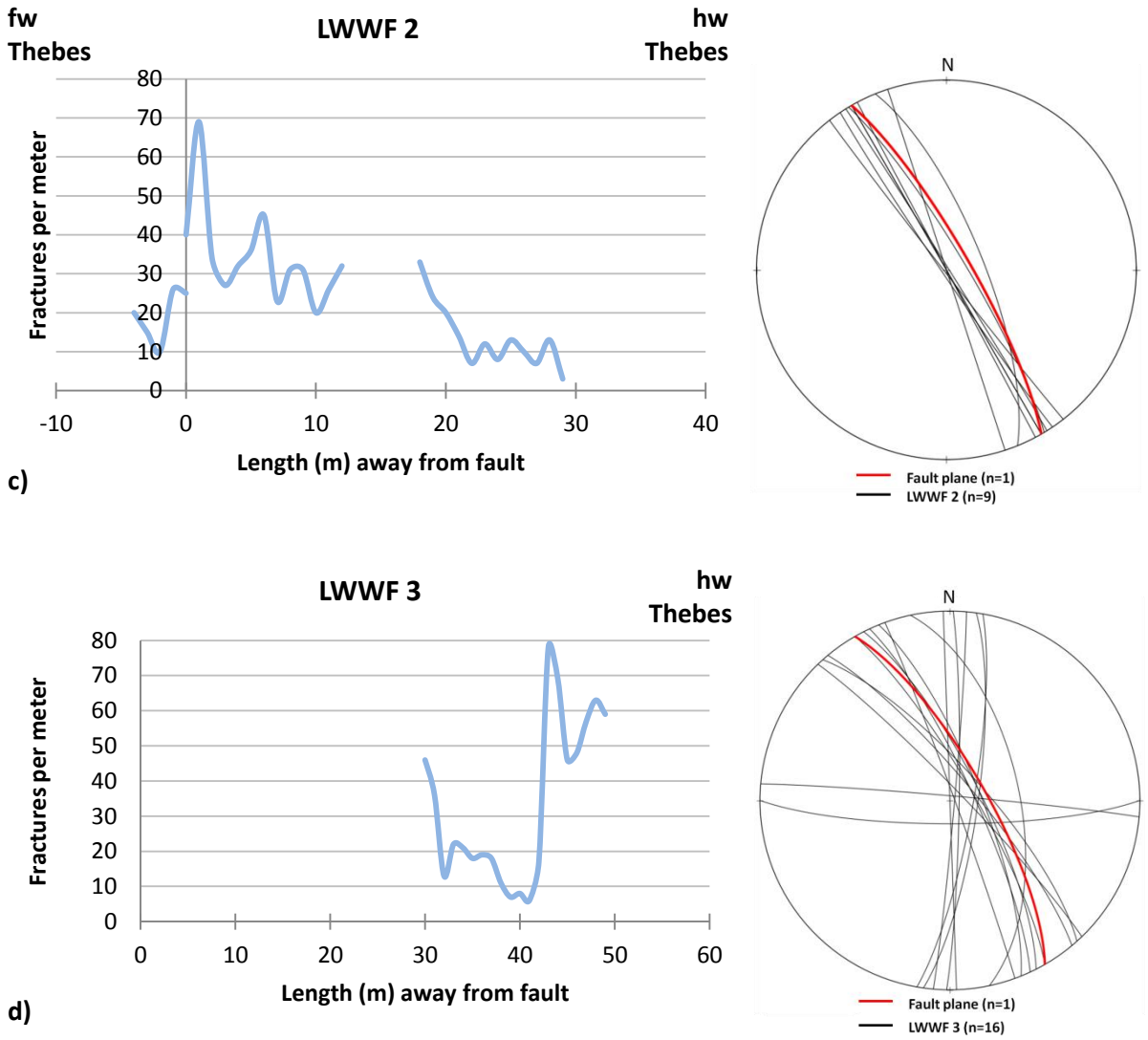

Figure 4.3: (a) Map showing the localities. Legend is shown in Fig. 4.1a. Fracture frequencies for localities LWWF 1 **(b)**, LWWF 2 **(c)** and LWWF 3 **(d)**. Fracture orientations are shown as equal area lower hemisphere stereonets, showing both the fault plane and fractures along the scanlines. The distance is displayed as negative values for the footwall in the graphs, which had to be done in order to put the footwall and hanging wall in the same graph.

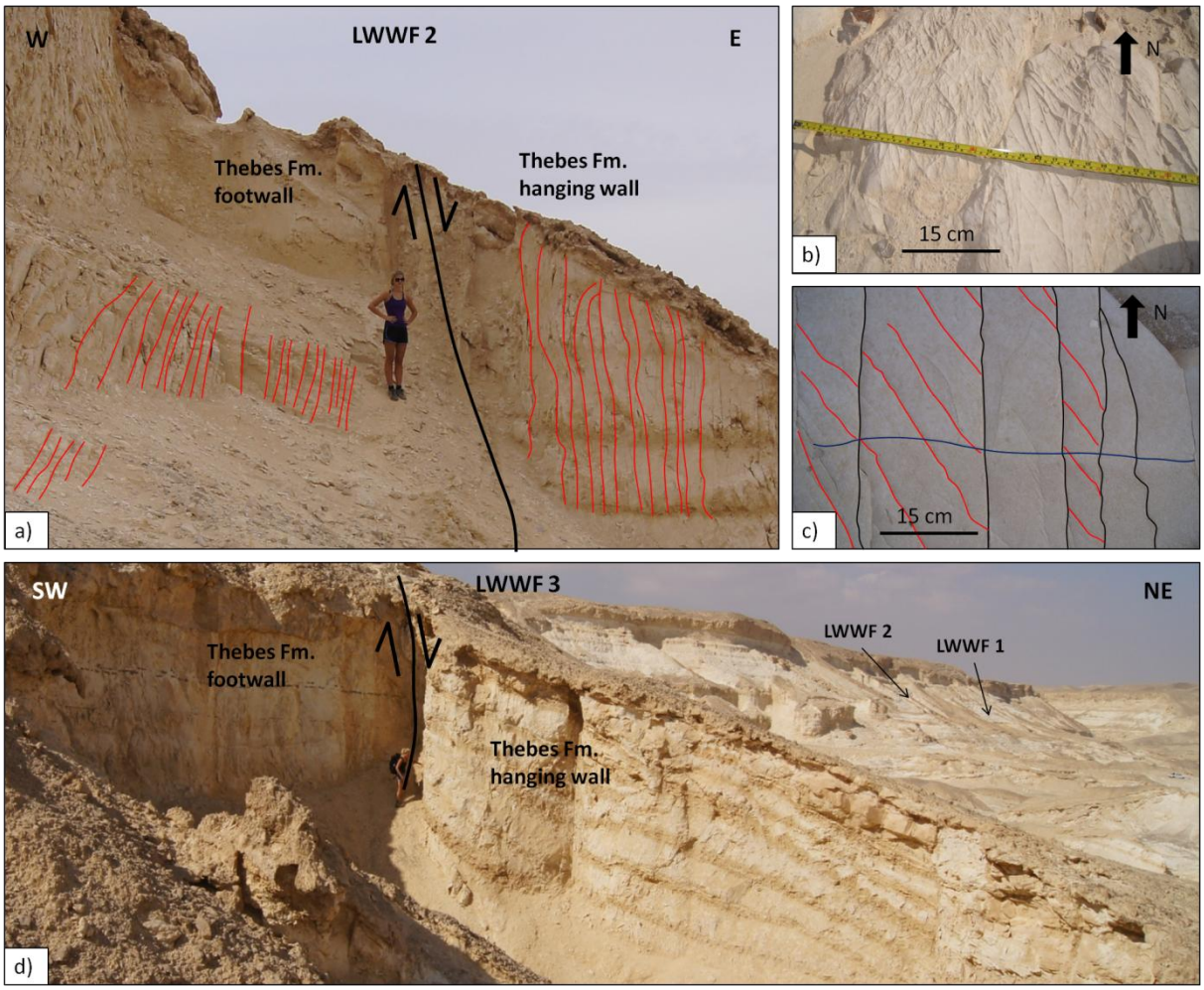

Figure 4.4: (a) Picture of the LWWF at LWWF 2. The most prominent fractures are drawn as red lines. **(b)** Example of stockwork fractures at LWWF 3. See camera cover for scale **(c)** Three main fracture orientations at LWWF 3: fault sub-parallel (red), N-S (black) and fault sub-perpendicular (blue). Note the number of fault sub-parallel fractures. **(d)** Picture of LWWF at LWWF 3. The localities of LWWF 1 and 2 can be seen in the background.

Table 4.2: *Key data from LWWF.*

Locality N → S	**Throw**	**Max fracture frequency**	**Mean fracture frequency**	**Inner damage zone, mean fracture frequency**	**Outer damage zone, mean fracture frequency**	**Formation**	**Fault plane**
LWWF 1 fw	c. 40 m	24	17,7	-	17,7	Thebes	340/87
LWWF 1 hw		31	14,9	-	14,9	Thebes	
LWWF 2 fw		25	19,2	-	19,2	Thebes	330/80
LWWF 2 hw		69	24,4	40,4	18,2	Thebes	
LWWF 3 hw	c. 60 m	78	33,1	-	18,6 (33,1)	Thebes	320/75

Table 4.2 shows that both max and mean fracture frequency is increasing southwards as the throw also is increasing, and that the fracture frequencies are higher in the hanging wall than in the footwall. The fault is slightly turning from N-S to NW-SE, while there are no

prominent changes in the outer damage zone value along the fault. The high mean fracture frequency (33.1) of the outer damage zone at LWWF 3 hanging wall is the frequency if the fracture peak in Figure 4.3d is added to the mean value.

Summary of the Little Wadi Wasit Fault

- Higher fracture frequencies in the hanging wall than in the footwall
- Higher fracture frequencies in the proximity to the fault
- Fracture frequency is increasing as fault throw is increasing
- Three fracture orientations (ranged after frequency): fault sub-parallel, N-S trending and fault sub-perpendicular
- Fault core is characterized as a relatively discrete slip surface

4.2.3 Wadi Wasit Fault (north)

The WWF is the western ramp-bounding fault, and has been divided into four sub-areas based on hanging wall lithology, in order to best present along-strike variations. The northern part of the WWF comprises two localities: WWF 1 and 2 (Fig. 4.5). The footwall of WWF 1 and 2 is of the Thebes Fm., while the hanging wall of both localities is of the Tanka Fm. (Fig. 4.6). Only the footwall is exposed at WWF 2. The throw is c. 250 at WWF 1 and slightly decreasing towards WWF 2.

- The highest number of fractures is observed close to the fault for both localities, except for the first meter that have relatively low fpm values. The first ten meters of the WWF 1 footwall have fracture frequencies in excess of 100 fpm that decrease to c. 20 fpm 50 meters away from the fault. The first ten meters of the hanging wall of WWF 1 have values up to 60 fpm that decrease to c. 20 fpm 20 meters away from the fault (Fig. 4.5b). The footwall of WWF 2 has a trend where the first 5 meters have fpm values up to 80 fpm that rapidly even out at c. 20 fpm for the rest of the scanline (Fig. 4.5c).
- The main fracture orientation for both localities is sub-parallel to the fault, with a minor trend sub-perpendicular to the fault. There are in addition small fractures oriented in all various directions.
- The fractures in the hanging wall, of the Tanka Fm., are characterized as hairline fractures and hematite- and calcite-filled fractures. The hematite-filled fractures are mainly located close to the fault, while calcite-filled fractures occur throughout the

scanline. The thickness of the Tanka-beds varies from 90-35 cm and consists mostly of bed-bound fractures. The non-bed-bound fractures are generally vertical, fault sub-parallel oriented. In the footwall of WWF 1 and 2, the fractures are mainly characterized as hairline fractures and calcite-filled fractures. Here the fault sub-perpendicular fractures are the most thoroughgoing (Fig. 4.6b), longer than 10 meters.

- Shale smear occurs at both localities represented by the Khaboba Fm. shales in the fault core (Fig. 4.6a). The Khaboba Fm. is observed to be thinnest at WWF 1 and widening out both north and south of the locality (Fig. 4.6d). These were the only two localities along the WWF with shale smear.

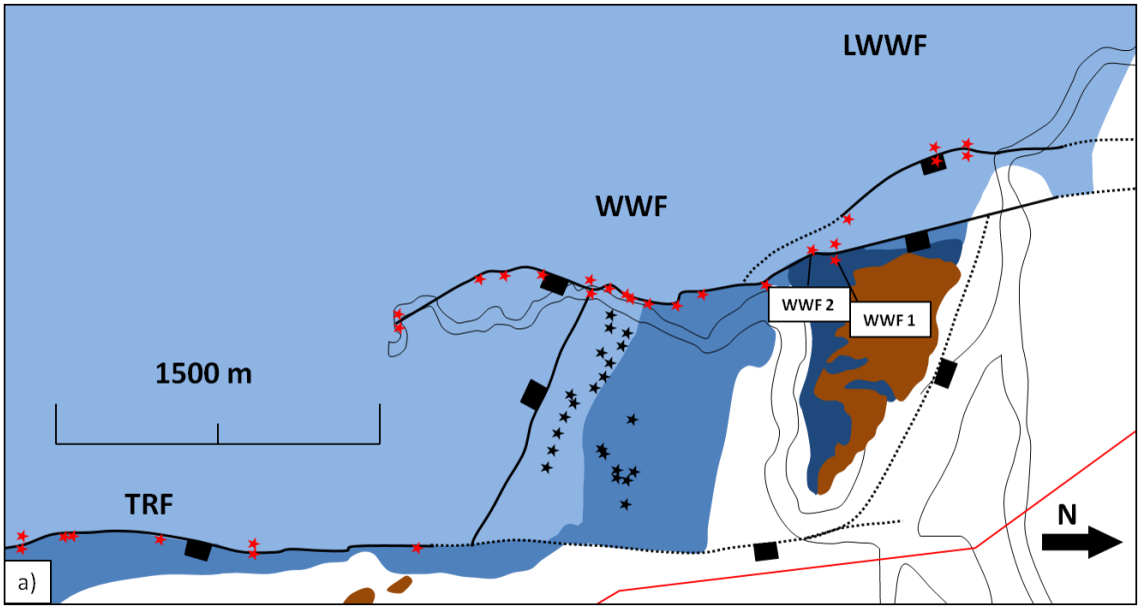

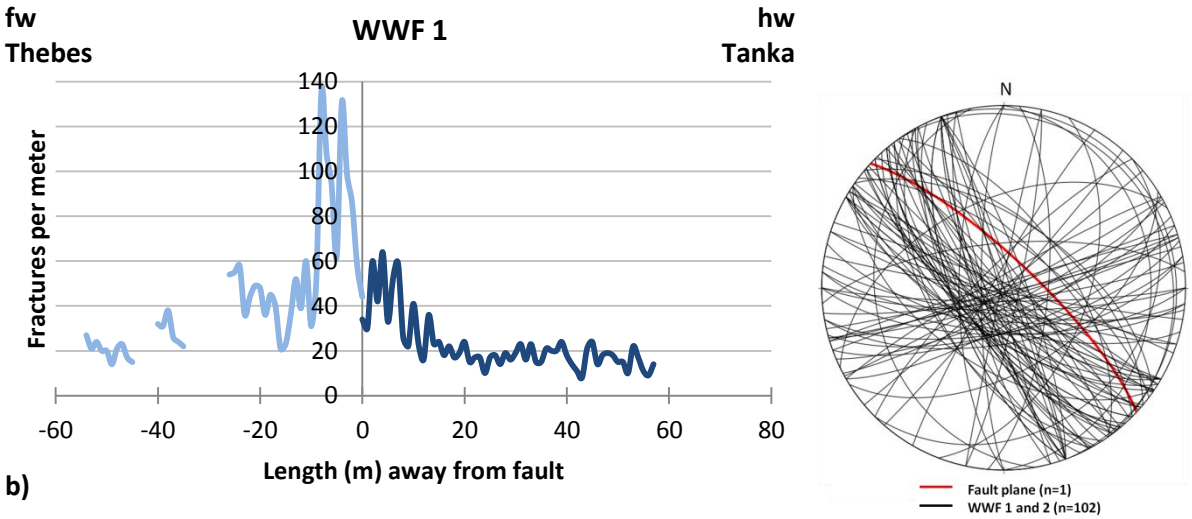

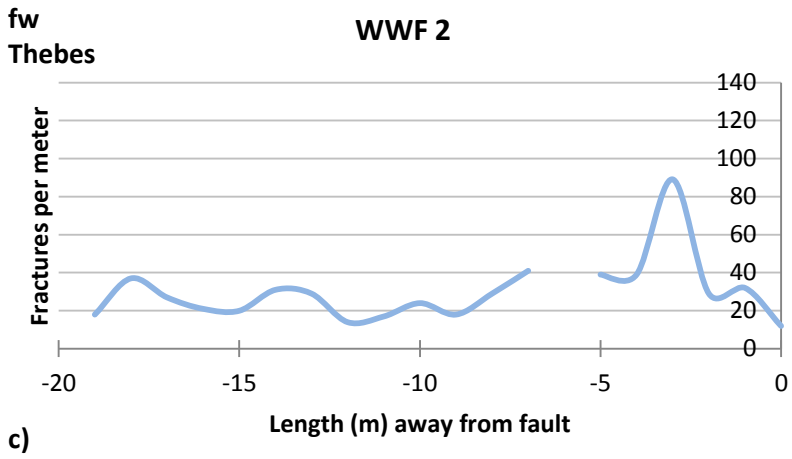

Figure 4.5: (a) Map showing the localities. Legend is shown in Fig. 4.1a. Fracture frequencies for localities WWF 1 **(b)** and WWF 2 **(c)**. Fracture orientations are shown as equal area lower hemisphere stereonets, showing both the fault plane and fractures along both scanlines.

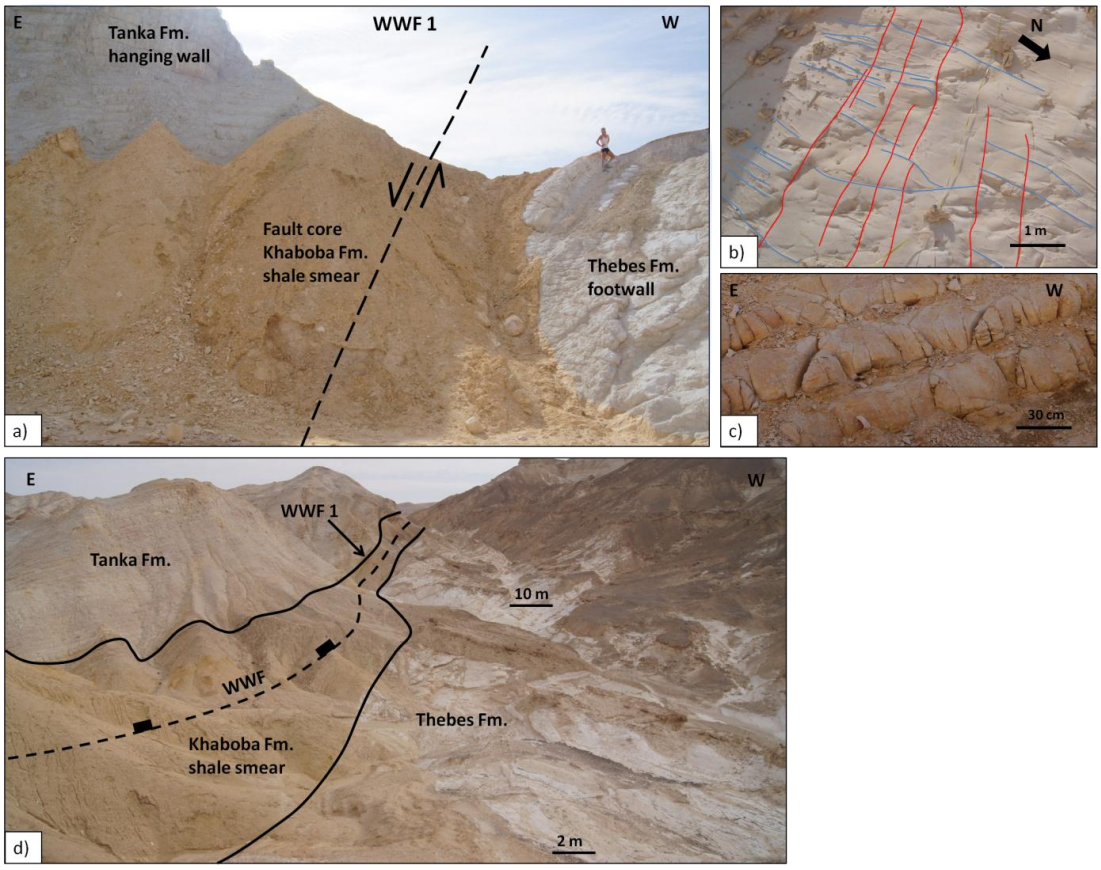

Figure 4.6: (a) Locality WWF 1, showing the fault core with Tanka Fm. in the hanging wall and Thebes Fm. in the footwall and the Khaboba Fm. as shale smear. The Tanka-beds are sub-horizontal close to the core while dipping c. 20-40° further away. The Thebes-beds are steeply dipping close to the fault and evens out at c. 20° away from the fault. **(b)** Thoroughgoing fractures, sub-perpendicular to the fault (red) and fractures sub-parallel to the fault (blue) in the Thebes Fm. at WWF 1 footwall. **(c)** Tanka-beds at WWF 1 hanging wall. **(d)** The Khaboba Fm. shale smear is thinning out at WWF 1. Note that there are two scales because of the perspective of the picture.

Table 4.3: *Key data from WWF (north).*

Locality N → S	Throw	Max fracture frequency	Mean fracture frequency	Inner damage zone, mean fracture frequency	Outer damage zone, mean fracture frequency	Formation	Fault plane
WWF 1 fw		131	45,8	59,1	23,4	Thebes	
WWF 1 hw	c. 250 m	64	22,4	46,7	18,7	Tanka	
WWF 2 fw	< c. 250 m	89	29,8	38,8	23,3	Thebes	313/77

Table 4.3 shows that there are higher max fracture and damage zone frequencies in the footwall than in the hanging wall. Both max and mean fracture frequency are decreasing towards south as the throw also is decreasing.

Summary of the Wadi Wasit Fault (north)

- Higher fracture frequencies in the footwall than in the hanging wall
- Higher fracture frequencies in the proximity to the fault
- Fractures are oriented in all various directions but mainly fault sub-parallel with subordinate fault sub-perpendicular fractures
- Fault core is characterized by shale smear

4.2.4 Wadi Wasit Fault (upper central)

The upper central part of the Wadi Wasit Fault includes the localities: WWF 3, 4, 5 and 6 (Fig. 4.7). The footwall is of Thebes Fm., while the hanging wall is of Darat Fm. for all localities. The Darat Fm. is characterized as alternating layers of mudstone and wacke/packstone, while the Thebes Fm. is mainly packstone. Only the hanging wall had exposures that were measurable in this part. The throw is less than c. 250 m at WWF 3 and decreasing to less than c. 200 m towards WWF 6.

- WWF 3 and 4 show high fracture frequencies close to the fault, while the first meters of WWF 5 and 6 were not measured. The fracture frequency stabilizes around 20 fpm at WWF 4 and 6, while it is more varied at WWF 3 and 5. Both latter localities have small peaks around 13 meter away from the fault of respectiviely 53 and 54 fpm. These are characterized as stockwork fractures.
- The fracture orientation at WWF 3 is mainly fault sub-parallel, while at WWF 4, 5 and 6 the main orientation is fault sub-perpendicular.
- The most thoroughgoing/longest fractures are oriented N-S. WWF 3 is just below where LWWF and WWF connect. All the fractures are mainly characterized as

hairline fractures and calcite-filled fractures, and the fault core is observed as a relatively discrete slip surface.

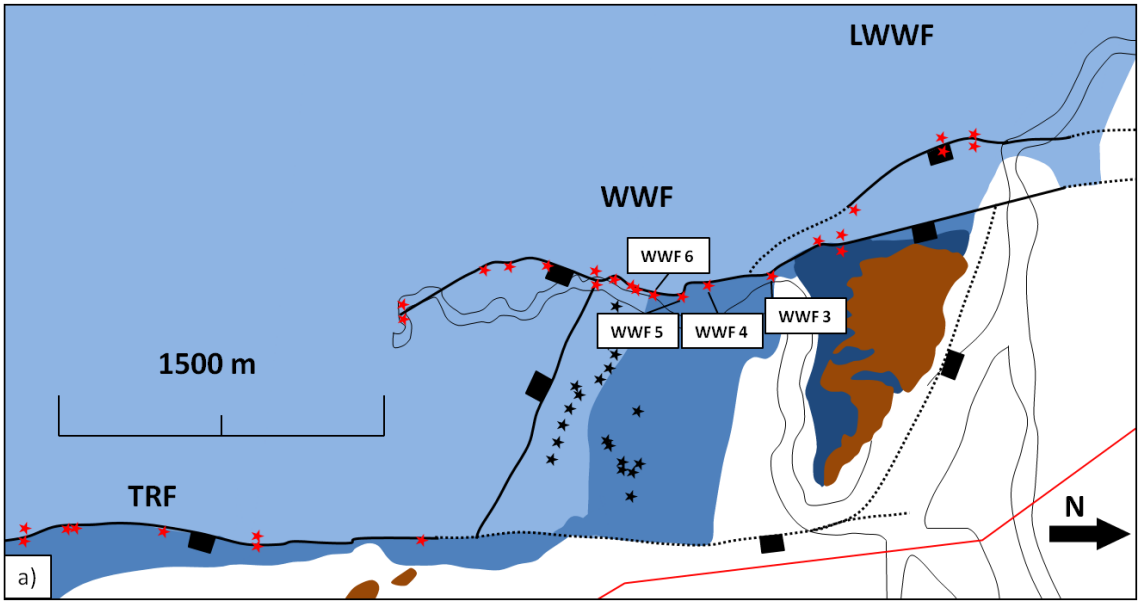

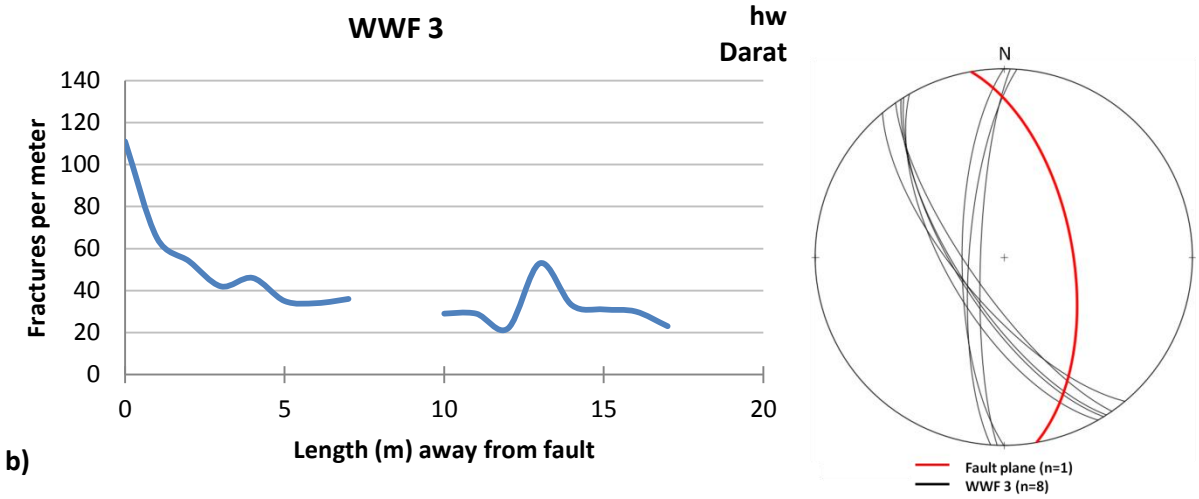

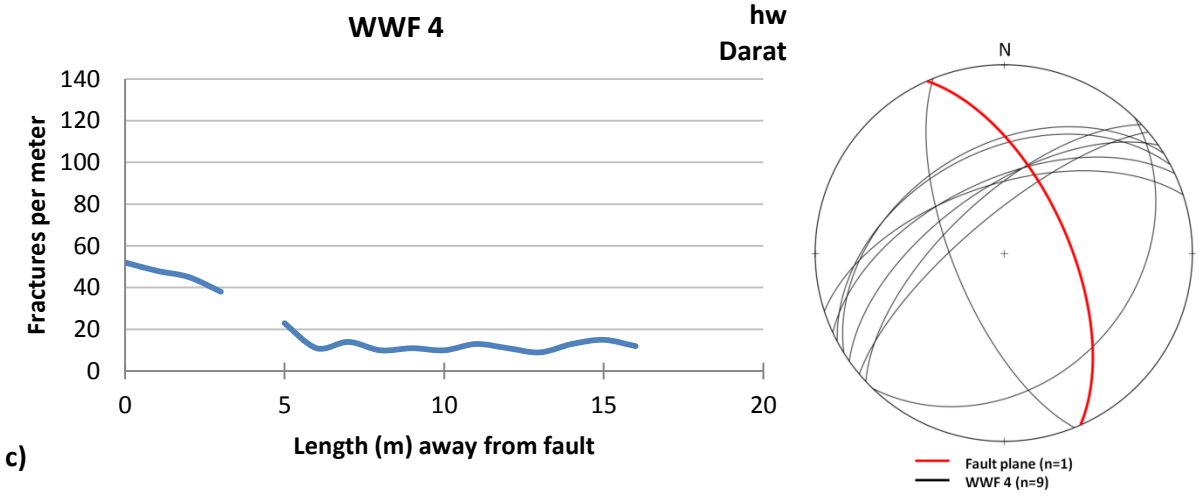

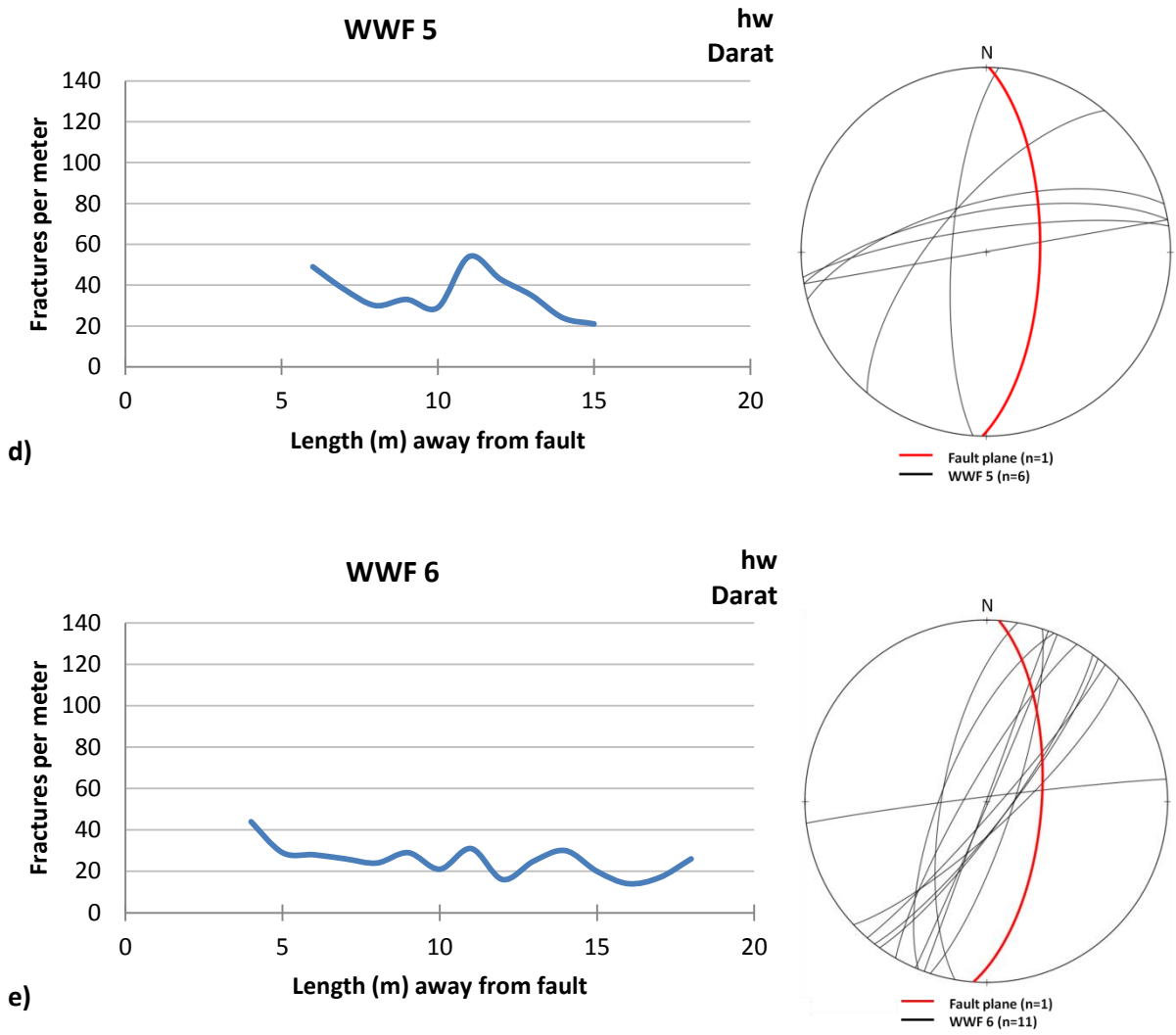

Figure 4.7: (a) Map showing the localities. Legend is shown in Fig. 4.1a. Fracture frequencies for localities WWF 3 **(b)**, WWF 4 **(c)**, WWF 5 **(d)** and WWF 6 **(e)**. Fracture orientations are shown as equal area lower hemisphere stereonets, showing both the fault plane and fractures along the scanlines.

Table 4.4: *Key data from WWF (upper central).*

Locality N → S	**Throw**	**Max fracture frequency**	**Mean fracture frequency**	**Inner damage zone, mean fracture frequency**	**Outer damage zone, mean fracture frequency**	**Formation**	**Fault plane**
WWF 3 hw	< c. 250 m	111	42,1	58,8	32,0	Darat	350/60
WWF 4 hw	< c. 250 m	52	20,9	45,8	12,7	Darat	336/62
WWF 5 hw	c. 200 m	49	35,6	-	34,1	Darat	011/66
WWF 6 hw	< c. 200 m	44	25,3	-	24,0	Darat	004/65

Table 4.4 shows that WWF 3 has the highest fracture frequency and most fractured damage zone. The max and mean fracture frequency at WWF 4 and 5 are naturally lower because of

no data from the closest meters to the fault. As the throw is decreasing southwards, the max fracture frequency is also decreasing.

Summary of the Wadi Wasit Fault (upper central)

- Higher fracture frequencies in the proximity of the fault
- Max and mean fracture frequency is decreasing as the fault throw is decreasing
- Fractures are mainly oriented sub-perpendicular to the fault with subordinate fault sub-parallel fractures
- Fault core is characterized as a relatively discrete slip surface

4.2.5 Wadi Wasit Fault (lower central):

The lower central part of the Wadi Wasit Fault includes the localities: WWF 7, 8, 9 and 10 (Fig. 4.8). Both the footwall and hanging wall of all localities are of the Thebes Fm. WWF 7, 8 and 9 comprise scanline of the hanging wall, while WWF 10 comprises scanline of both the footwall and the hanging wall. The throw is between c. 200-150 m at WWF 7 and is decreasing below 75 m at WWF 10.

- The fracture frequency at WWF 7 and 8 stabilizes at c. 20 fpm ten meter away from the fault, while it is higher and more varied at WWF 9 and 10. At WWF 8, 9 and 10 higher fracture frequencies close to the fault are observed, where the first meters of WWF 9 have frequencies over 100 fpm (Fig. 4.9a). The hanging wall of WWF 10 (Fig. 4.9b) has a higher fracture frequency than the footwall.
- At all localities the fractures are mainly oriented sub-parallel to the fault and are generally characterized as hairline fractures and calcite-filled fractures. The fault core is characterized as both a relatively discrete slip surface (Fig. 4.9a) and fault rock lenses (Fig. 4.9b).

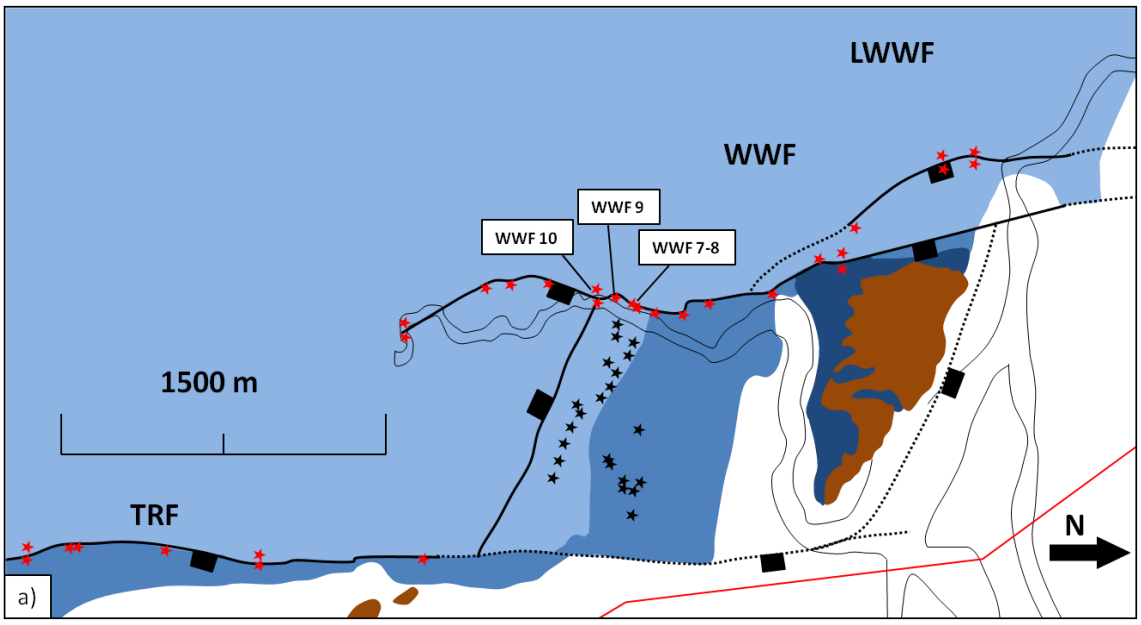
LWWF
WWF
WWF 9
WWF 10
WWF 7-8
1500 m
TRF
N
a)

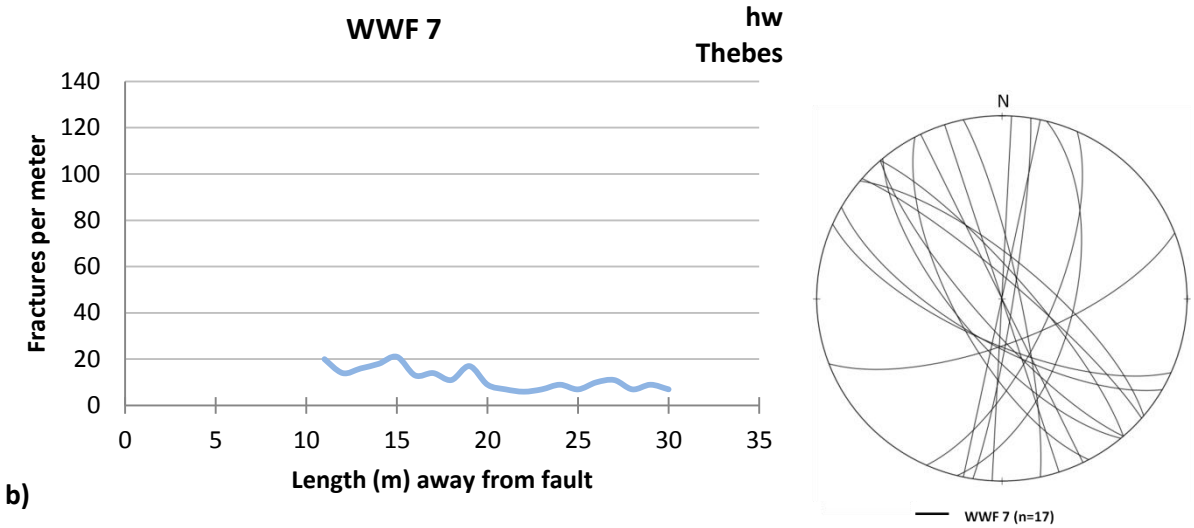
WWF 7
hw
Thebes
Fractures per meter
0
20
40
60
80
100
120
140
0
5
10
15
20
25
30
35
Length (m) away from fault
N
WWF 7 (n=17)

b)

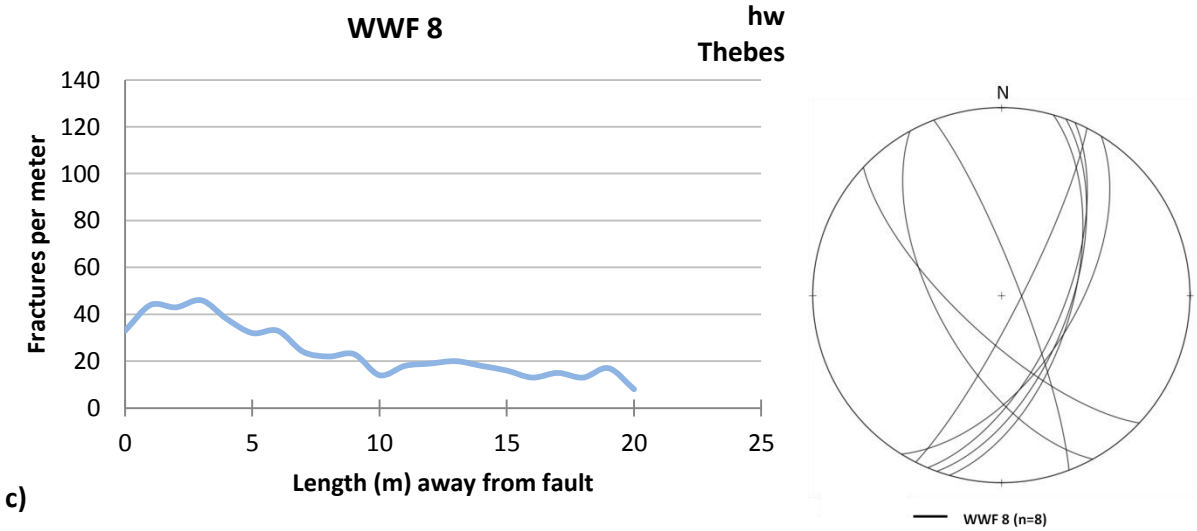
WWF 8
hw
Thebes
Fractures per meter
0
20
40
60
80
100
120
140
0
5
10
15
20
25
Length (m) away from fault
N
WWF 8 (n=8)

c)

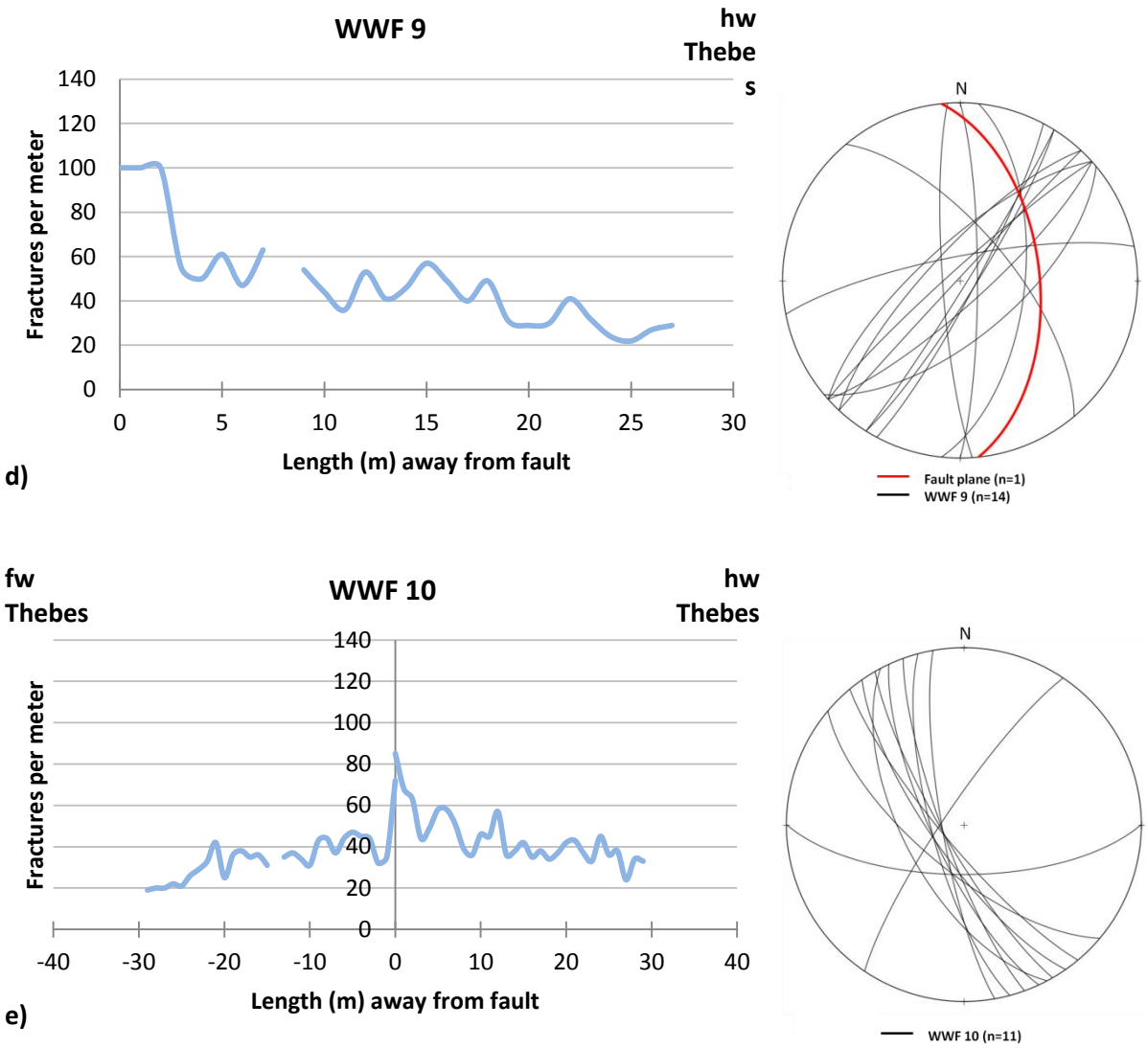

Figure 4.8: (a) Map showing the localities. Legend is shown in Fig. 4.1a. Fracture frequencies for WWF 7 **(b)**, WWF 8 **(c)**, WWF 9 **(d)** and WWF 10 **(e)**. Fracture orientations are shown as equal area lower hemisphere stereonets, showing both the fault plane and fractures along the scanlines.

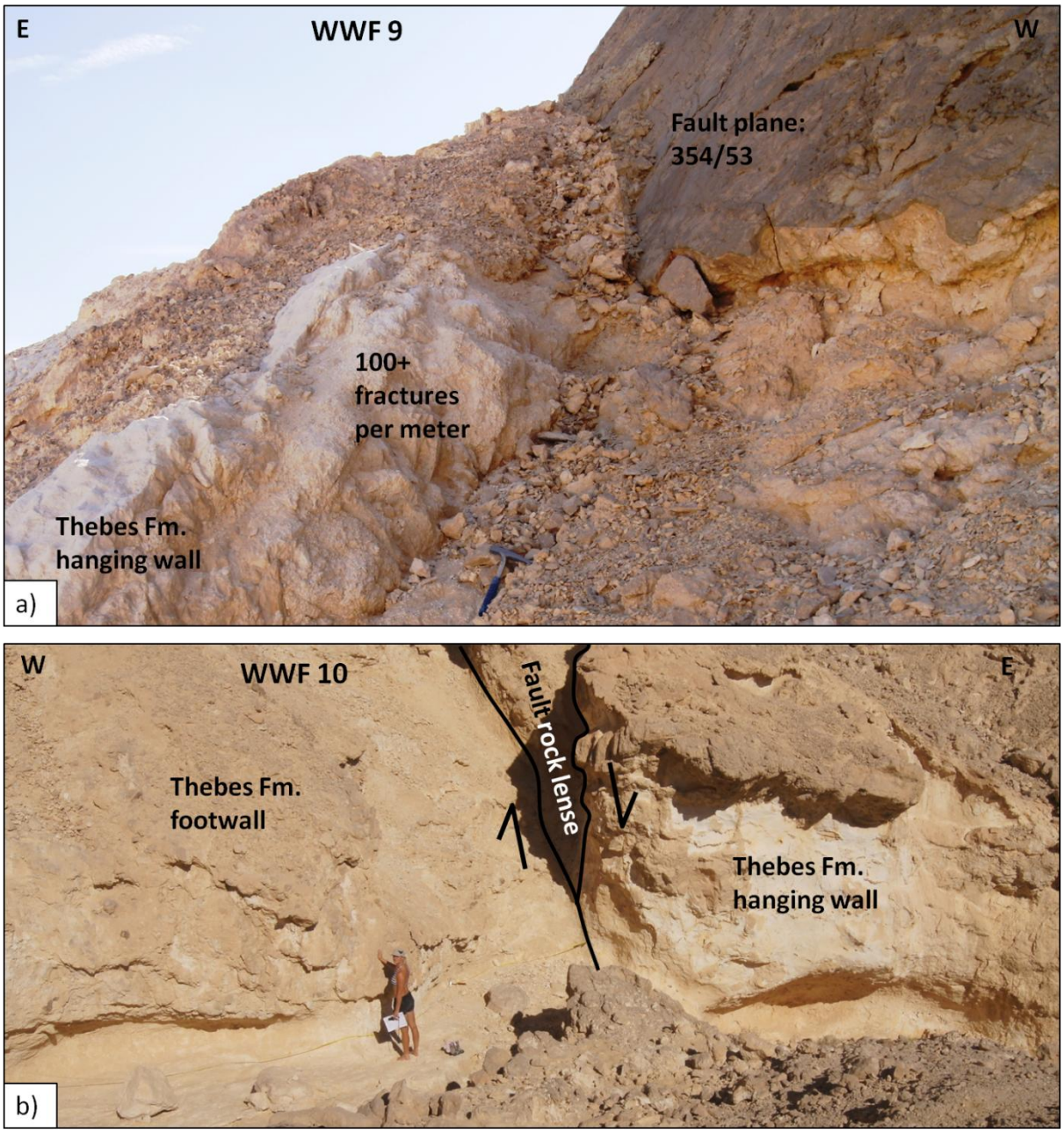

Figure 4.9: (a) WWF 9 showing the fault plane (relatively discrete slip surface) and the highly fractured Thebes Fm. hanging wall. Note the hammer for scale. **(b)** WWF 10 footwall to the left and hanging wall to the right. The fault core is characterized as a fault rock lense.

Table 4.5: *Key data from WWF (lower central)*

Locality N → S	**Throw**	**Max fracture frequency**	**Mean fracture frequency**	**Inner damage zone, mean fracture frequency**	**Outer damage zone, mean fracture frequency**	**Formation**	**Fault plane**
WWF 7 hw	c. 200 - 75 m	21	11,7	-	11,7	Thebes	
WWF 8 hw	c. 200 - 75 m	46	24,2	38,4	17,1	Thebes	
WWF 9 hw	c. 75 m	100+	48,5	72,0	38,6	Thebes	354/53
WWF 10 fw		72	34,9	53,5	33,5	Thebes	
WWF 10 hw	< c. 75 m	85	44,1	65,0	40,9	Thebes	

Table 4.5 shows that both max and mean fracture frequency at WWF 7 (no data from the eleven closest meters to the fault) and 8 are relatively low, while the frequencies are increased at WWF 9 and 10. The mean fracture frequency for both the inner and outer damage zone at WWF 9 and 10 hanging wall are quite similar, while the footwall of WWF 10 has slightly lower values. In this part of the fault the fracture frequency is increasing southwards as the fault throw is decreasing, in contrast to the rest of the localities along the WWF.

Summary of the Wadi Wasit Fault (lower central)

- Higher fracture frequency in the hanging wall than in the footwall
- Higher fracture frequency in the proximity of the fault
- Max and mean fracture frequency is increasing as the fault throw is decreasing
- Fractures are oriented both fault sub-parallel and sub-perpendicular
- Fault core is characterized as both a relatively discrete slip surface and fault rock lenses

4.2.6 Wadi Wasit Fault (south)

The southern part of the Wadi Wasit Fault includes the localities: WWF 11-14 (Fig. 4.10). Both the footwall and hanging wall of all localities are of the Thebes Fm. WWF 14 includes scanline of the footwall and hanging wall, while the rest only comprise the hanging wall. WWF 14 is the southernmost locality where the Wadi Wasit Fault is observed (4.11b). At WWF 11 the throw is c. 75 m, decreasing to less than c. 65 m at WWF 14.

- WWF 11 has no data from the first 27 meters of the scanline and does only measure fractures from the outer damage zone. WWF 12 and 13 show high fracture frequencies close to the fault that even out around 20 fpm, respectively 3 and 10 m away from the fault (Fig. 4.11a). At the footwall of WWF 14 the fracture frequency is slightly higher

close to the fault and even out below 20 fpm, except for a peak of 44 fpm 14 meters away from the fault where the scanline interfere with a minor fault or a fracture corridor. The hanging wall of WWF 14 has also a slightly higher fracture frequency close to the fault that even out below 20 fpm 8 meters away from the fault.

- At WWF 11 the fault is oriented approximately N-S, based on observations from map. This means that the main fracture orientation at WWF 11, 12, 13 and 14 is fault sub-parallel, while there also is a minor trend of fault sub-perpendicular fractures at the three latter localities.
- All fractures are generally characterized as hairline fractures and calcite-filled fractures. At WWF 14 no main fault is observed, but rather a splay of minor faults as the locality is in the southern tip area of the WWF (Fig. 4.11b). The fault core is characterized as a relatively discrete slip surface (Fig. 4.11a).

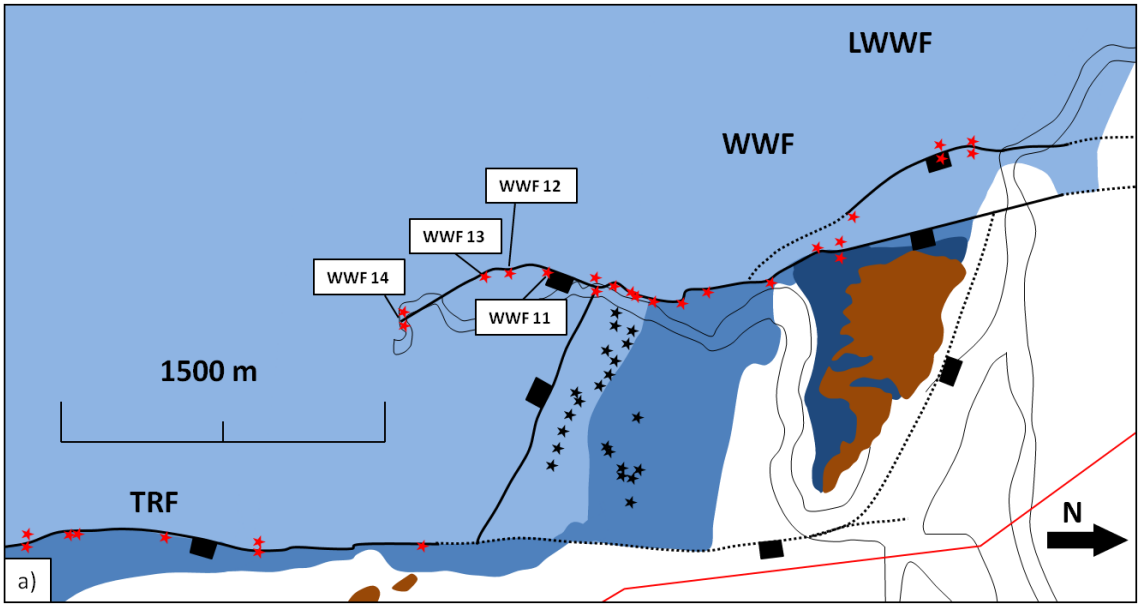

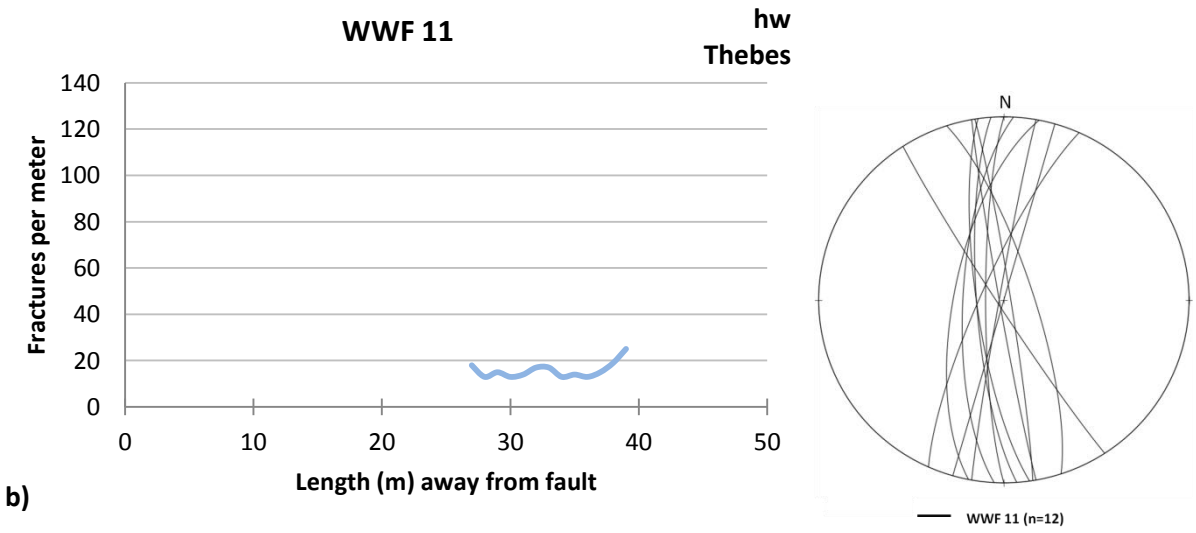

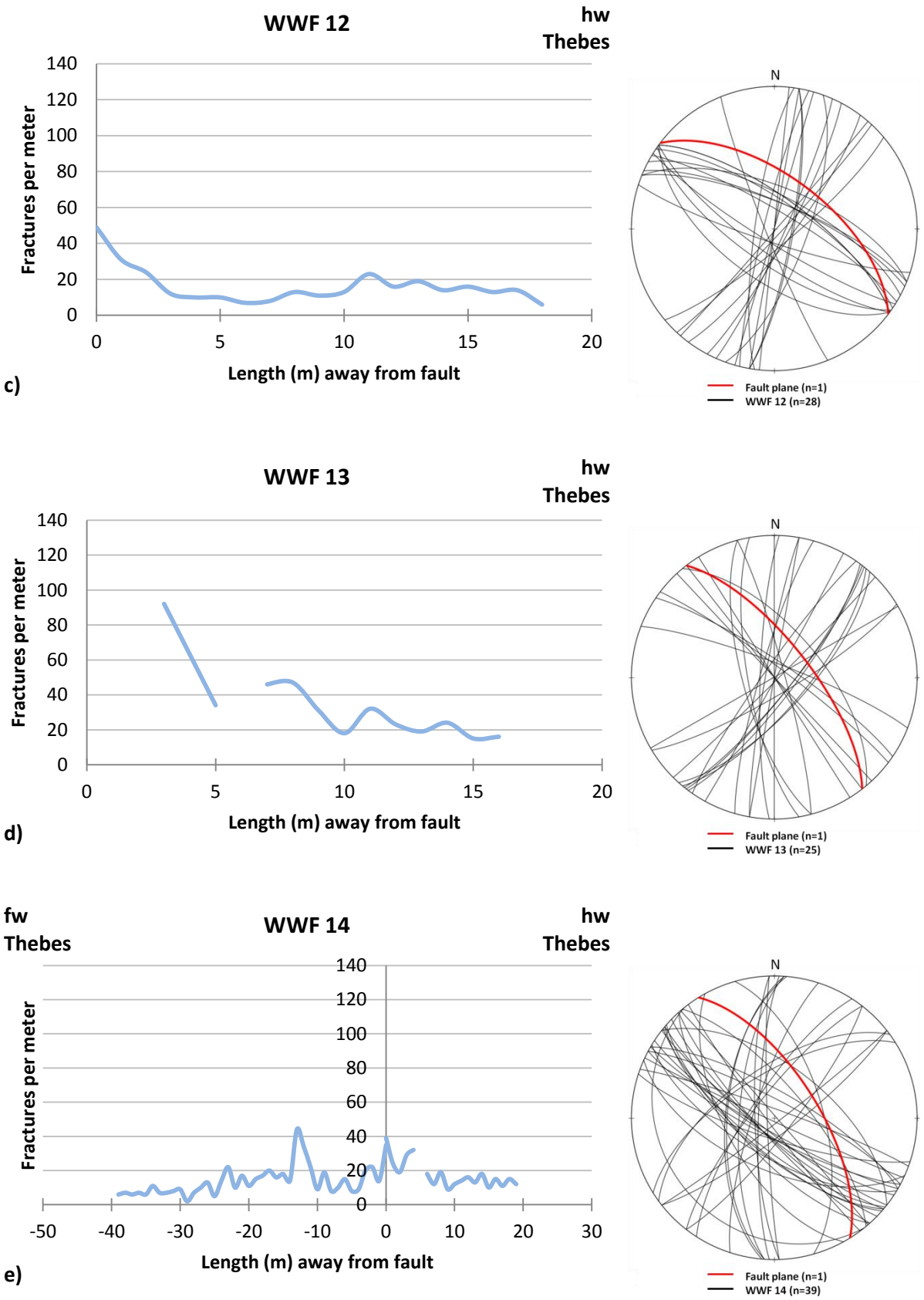

Figure 4.10: (a) Map showing the localities. Legend is shown in Fig. 4.1a. Fracture frequencies for localities WWF 11 **(b)**, WWF 12 **(c)**, WWF 13 **(d)** and WWF 14 **(e)**. Fracture orientations are shown as equal area lower hemisphere stereonets, showing both the fault plane and fractures along the scanlines.

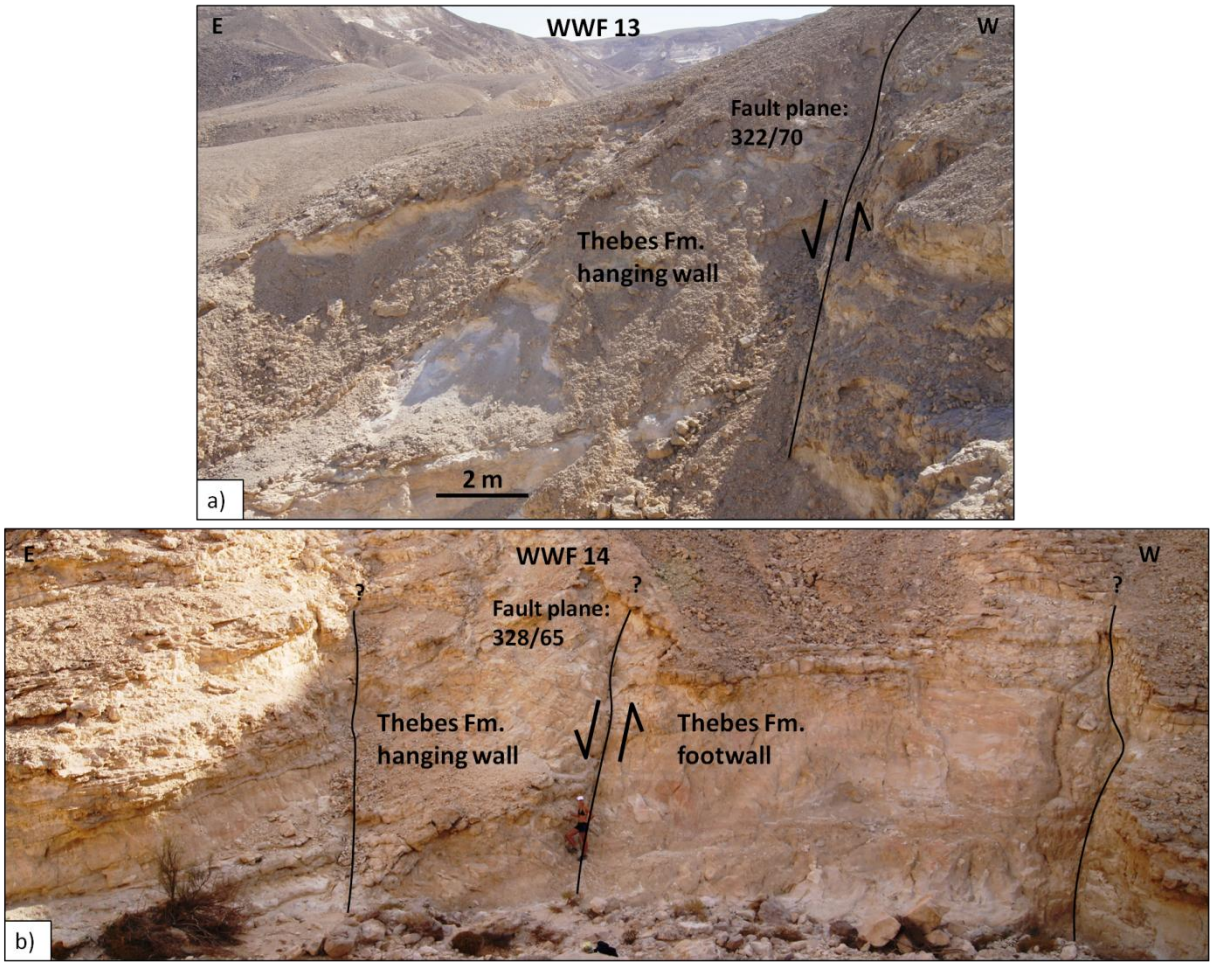

Figure 4.11: (a) WWF 13 displaying a relatively discrete slip surface. **(b)** WWF 14 with several small synthetic and possibly antithetic faults. The one in the middle has been used as the main fault in the scanline. The fault to the right interferes with the peak in WWF 14 footwall scanline.

Table 4.6: *Key data from WWF (south).*

Locality N → S	**Throw**	**Max fracture frequency**	**Mean fracture frequency**	**Inner damage zone, mean fracture frequency**	**Outer damage zone, mean fracture frequency**	**Formation**	**Fault plane**
WWF 11 hw	< c. 75 m	25	15,8	-	15,8	Thebes	
WWF 12 hw	c. 65 m	49	16,3	34,7	12,8	Thebes	307/60
WWF 13 hw	c. 65 m	92	35,4	52,2	21,0	Thebes	322/70
WWF 14 fw		44	13,9	24,5	13,3	Thebes	
WWF 14 hw	< c. 65m	39	17,7	28,6	13,9	Thebes	328/65

Table 4.6 shows that the max, mean and mean damage zone frequencies are increasing from WWF 11-13, but decreasing from WWF 13-14. The footwall and hanging wall of WWF 14 have quite similar fracture frequencies.

Summary of the Wadi Wasit Fault (south)

- Higher fracture frequency in the proximity to the fault
- Fractures are mainly oriented both fault sub-parallel and sub-perpendicular
- Fault core is characterized as a relatively discrete slip surface
- Fault tip zone is characterized as a splay of small faults and fractures oriented fault sub-parallel, sub-perpendicular and N-S

Summary of the entire Wadi Wasit Fault

As a general trend along the Wadi Wasit Fault the fracture frequencies are decreasing towards south as the fault throw is decreasing, and higher fracture frequencies are observed in the hanging wall than in the footwall, except for localities where shale smear is present. The fractures are mainly oriented sub-parallel to the fault, but a fault sub-perpendicular trend becomes stronger in the overlapping part of the fault. The fault core is characterized as shale smear in the northern part of the fault, while as relatively discrete slip surfaces and fault rock lenses from WWF 3 and southwards.

4.2.7 Thal Ridge Fault (north)

The Thal Ridge Fault is the eastern ramp-bounding fault. The localities along the fault have been divided into two sub-areas in order to best present along-strike variations. All localities along the TRF have a footwall of the Thebes Fm. and a hanging wall of the Darat Fm. The northern part of the Thal Ridge Fault includes the localities TRF 1, 2 and 3 (Fig. 4.12). TRF 2 includes scanline of the footwall and hanging wall, while the rest only comprise the hanging wall. The throw at TRF 1 is c. 250 and is increasing towards TRF 3 where it is more than c. 455 m.

- TRF 1 and 2 have a higher fracture frequency close to the fault, while TRF 3 has a more even fracture distribution. The hanging wall of TRF 2 is a very complex locality a will be given a further description (Fig. 4.13): The first 17 meter of the scanline comprises the upper part of the Darat Fm. Then there is a 13 meter thick sequence of clay with gypsum-filled stockwork fractures and a thin layer of glauconitic sand that marks the boundary between the upper and lower Darat Fm. This sequence also contains a minor fault about 30 meters away from the main fault. The rest of the scanline consists of the lower Darat Fm.

- The fractures at all localities are mainly oriented sub-parallel to the fault, while at TRF 2 there is a minor trend oriented sub-perpendicular to the fault. There are in addition small fractures oriented in all various directions.
- The fractures are generally characterized as anastomosing hairline fractures and calcite- and some gypsum-filled fractures located in the muddier units. The fault core is characterized by fault rock lenses. At TRF 3 the surface is very weathered which add an uncertainty to the measured frequency. The exact number of fractures may therefore be higher than observed.

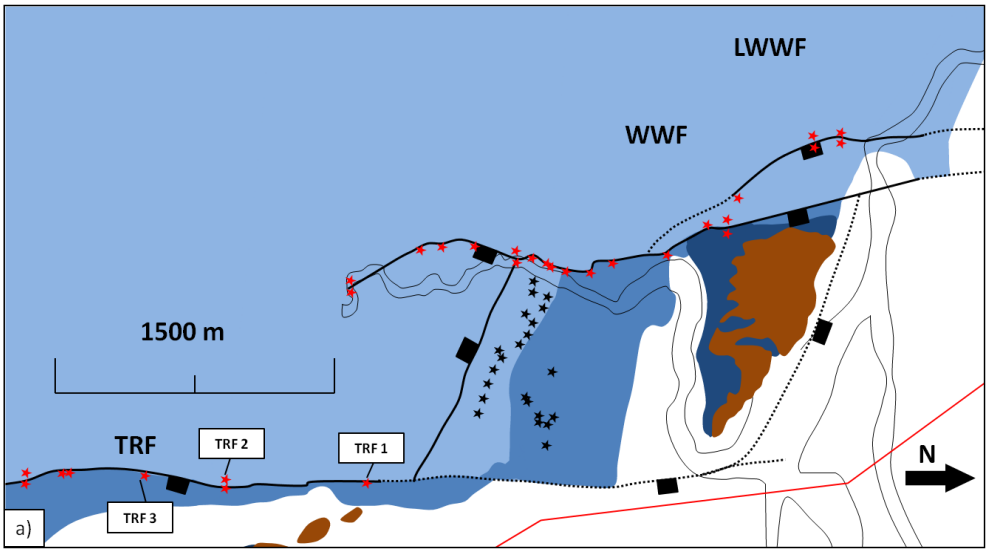

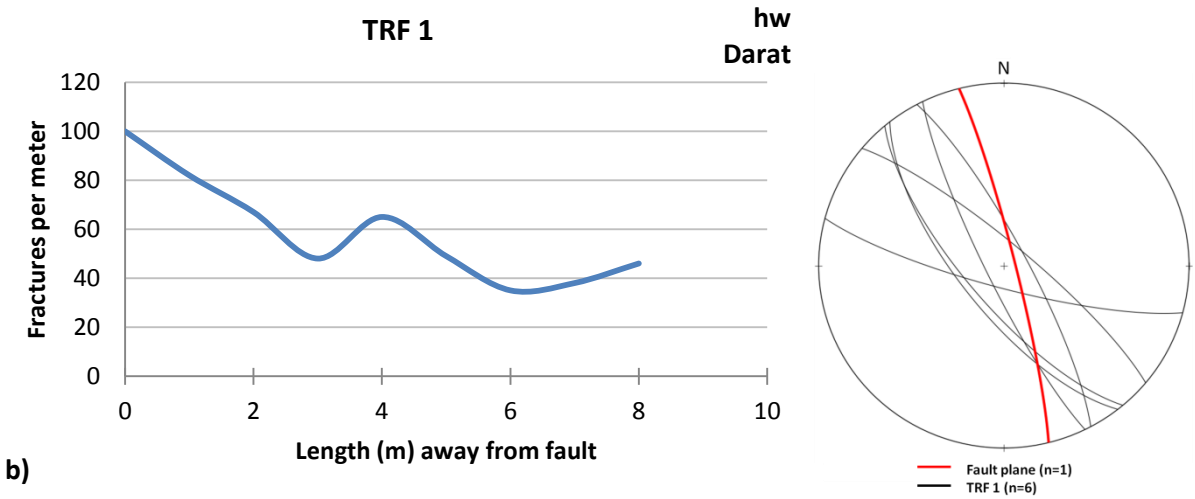

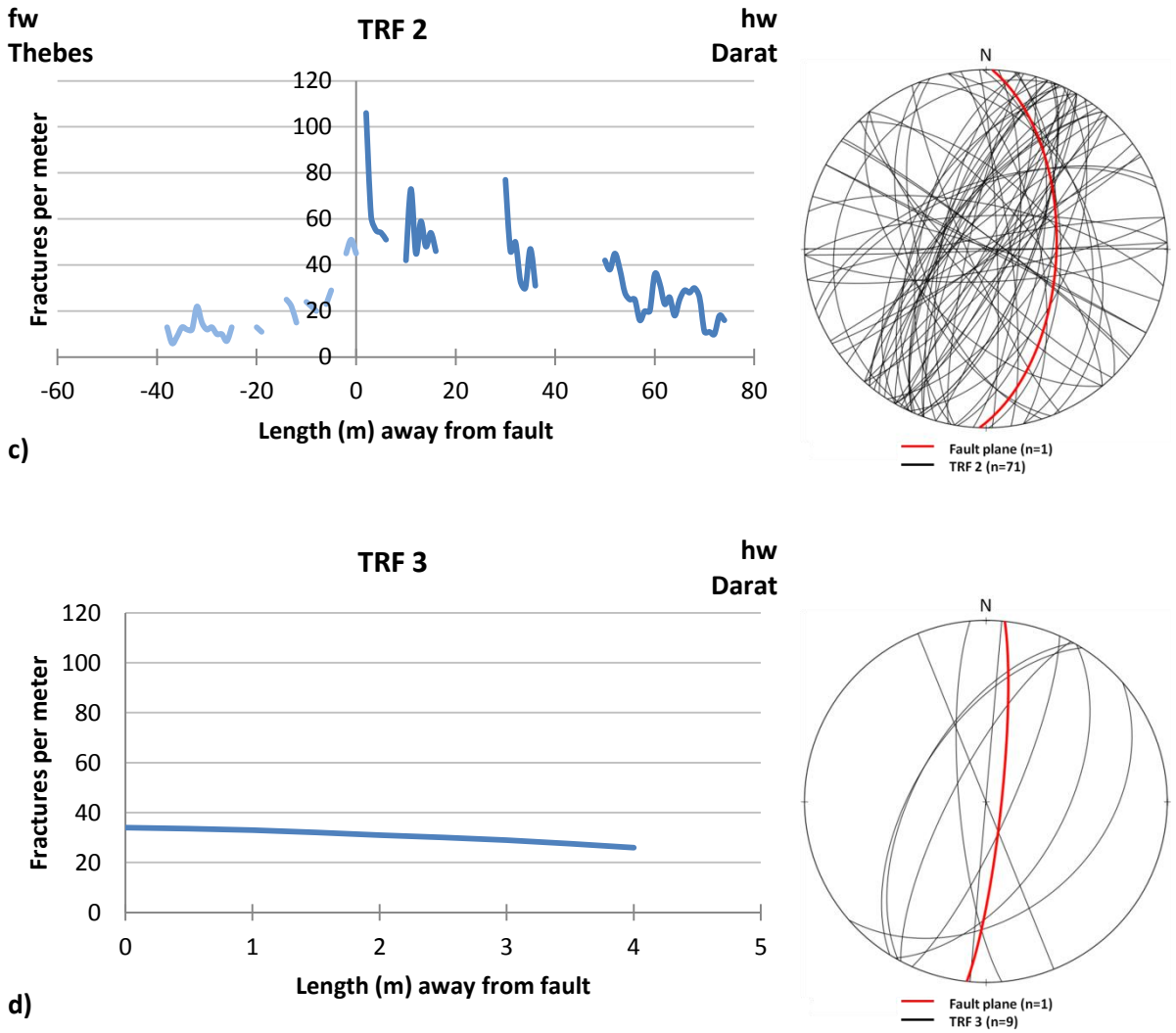

Figure 4.12: (a) Map showing the localities. Legend is shown in Fig. 4.1a. Fracture frequencies for localities TRF 1 **(b)**, TRF 2 **(c)** and TRF 3 **(d)**. Fracture orientations are shown as equal area lower hemisphere stereonets, showing both the fault plane and fractures along the scanlines**.**

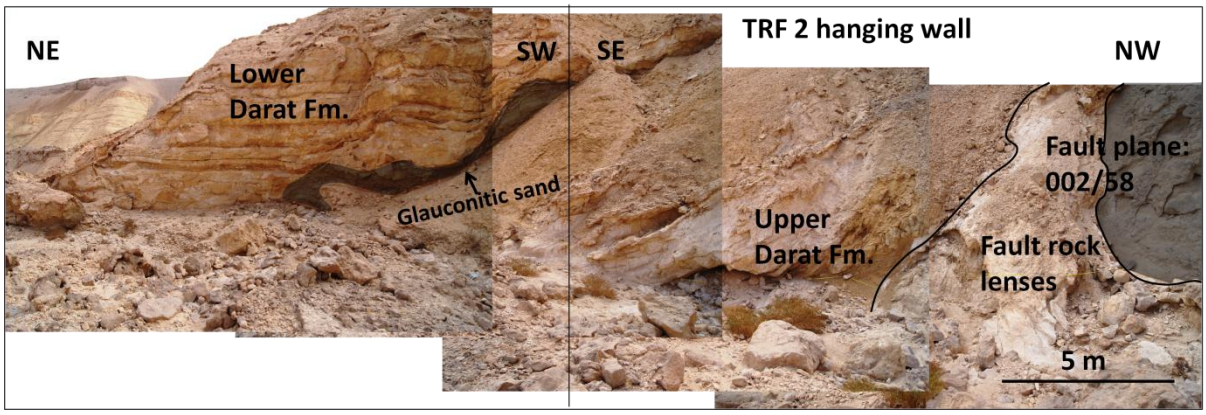

Figure 4.13: TRF 2 hanging wall where the grey area to the right is the fault plane. The figure is composed of several pictures where the black line marks a change in profile orientation. The black unit is the glauconitic sand that marks the boundary between upper and lower Darat Fm.

Table 4.7: *Key data from TRF (north).*

Locality N → S	Throw	Max fracture frequency	Mean fracture frequency	Inner damage zone, mean fracture frequency	Outer damage zone, mean fracture frequency	Formation	Fault plane
TRF 1 hw	c. 410 m	100+	58,9	58,9	-	Darat	346/85
TRF 2 fw		51	18,7	29,2	12,3	Thebes	
TRF 2 hw	c. 455 m	106	37,4	53,1	25,4	Darat	002/58
TRF 3 hw	> c. 455 m	34	30,6	30,6	-	Darat	006/83

Table 4.7 shows that the hanging wall of TRF 1 and 2 has similar values both for max fracture frequency and for the damage zone frequencies, while TRF 3 has relatively very low fracture frequencies. The fracture frequencies therefore decrease to the south as the throw is increasing.

Summary of the Thal Ridge Fault (north)

- Higher fracture frequencies in the hanging wall than in the footwall
- Higher fracture frequencies in the proximity to the fault
- Fractures are mainly oriented fault sub-parallel, but are oriented in all various directions
- Fault core is characterized by fault rock lenses

4.2.8 Thal Ridge Fault (south)

The southern part of the Thal Ridge Fault includes the localities: TRF 4, 5 and 6 (Fig. 4.14, 4.15). TRF 6 includes scanline of the footwall and hanging wall, while the rest only comprise the hanging wall. The throw is relatively stable and is expected to be above 400 m.

- TRF 4, 5 and 6 footwall have fracture frequencies slightly higher close to the fault and stabilize around 20 fpm away from the fault. TRF 6 hanging wall has a very high fracture frequency (100+ fpm) close to the fault that is decreasing away from the fault.
- The main fracture orientation at all localities are fault sub-parallel, with a minor trend of fault sub-perpendicular fractures.
- The fractures close to the fault are commonly anastomosing hairline fractures, while the rest is characterized as distributed calcite-filled fractures. It is uncertain whether the start of the TRF 4 scanline is adjacent to the fault, and may therefore instead start some meters away from the fault. At TRF 5 the surface is very weathered as at TRF 3 and there may therefore be more fractures than what was observed.

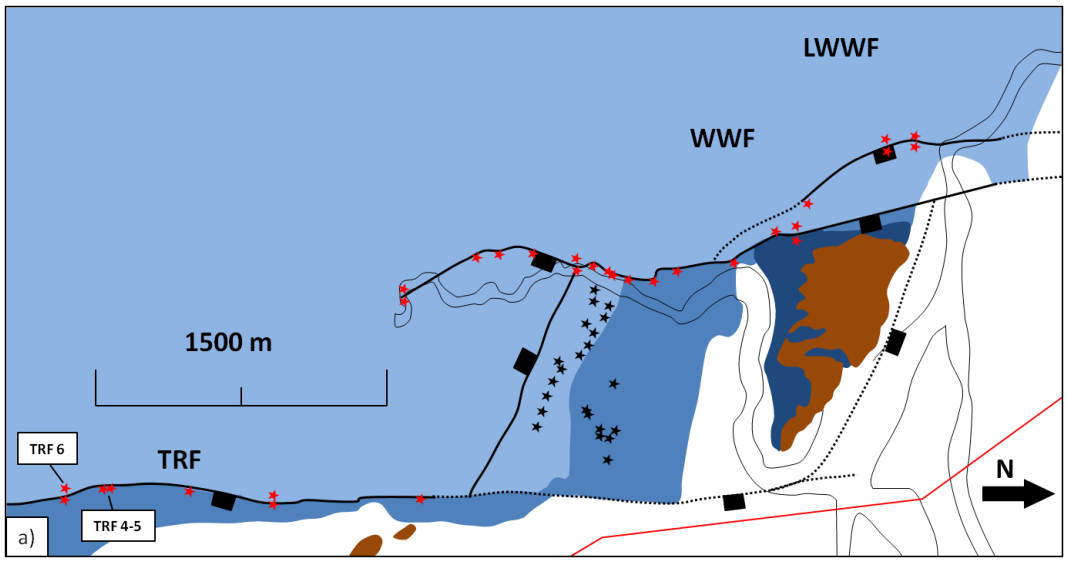
LWWF
WWF
1500 m
TRF 6
TRF
TRF 4-5
a)
N

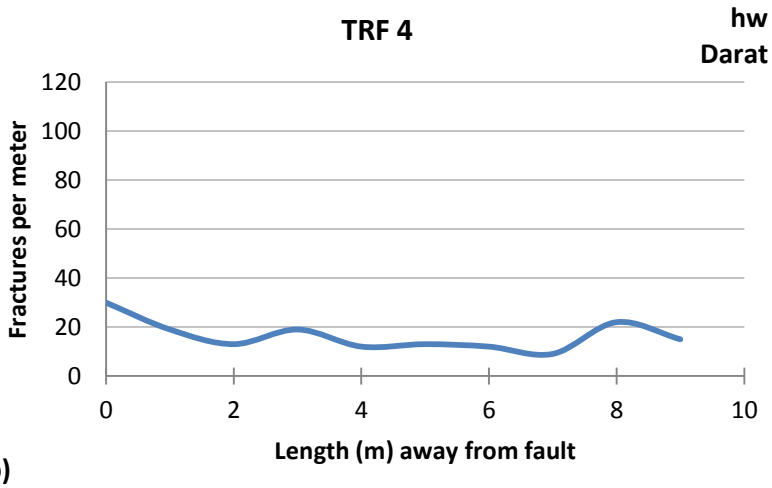
TRF 4
hw
Darat
Fractures per meter
120
100
80
60
40
20
0
0
2
4
6
8
10
Length (m) away from fault

b)

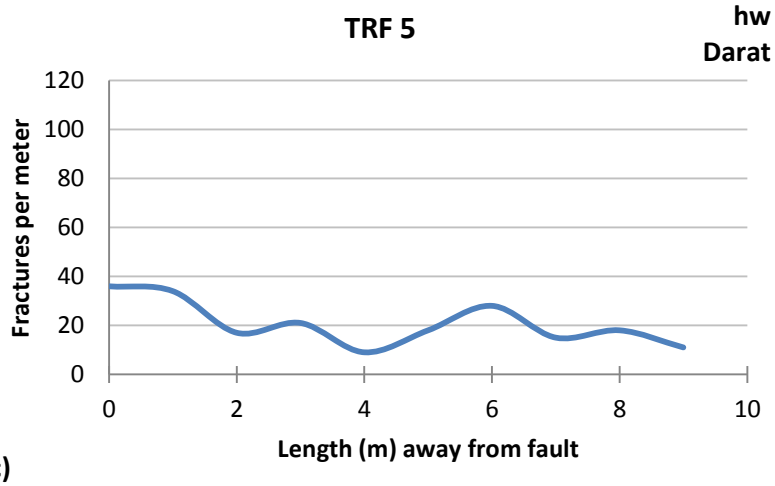
TRF 5
hw
Darat
Fractures per meter
120
100
80
60
40
20
0
0
2
4
6
8
10
Length (m) away from fault

c)

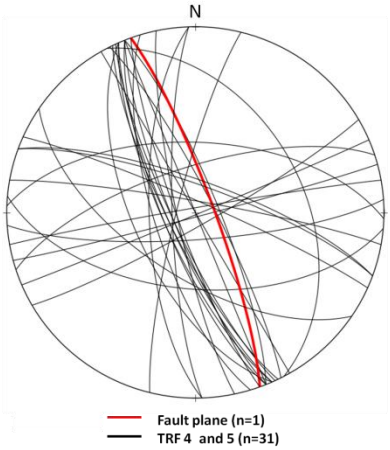
N
Fault plane (n=1)
TRF 4 and 5 (n=31)

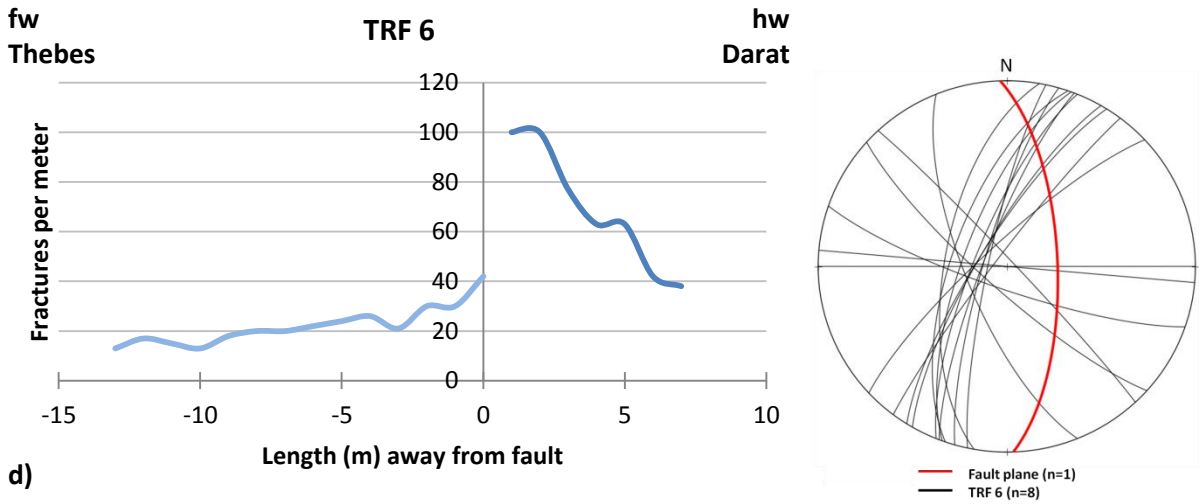

Figure 4.14: (a) Map showing the localities. Legend is shown in Fig. 4.1a. Fracture frequencies for localities TRF 4 **(b)**, TRF 5 **(c)** and TRF 6 **(d)**. Fracture orientations are shown as equal area lower hemisphere stereonets, showing both the fault plane and fractures along the scanlines.

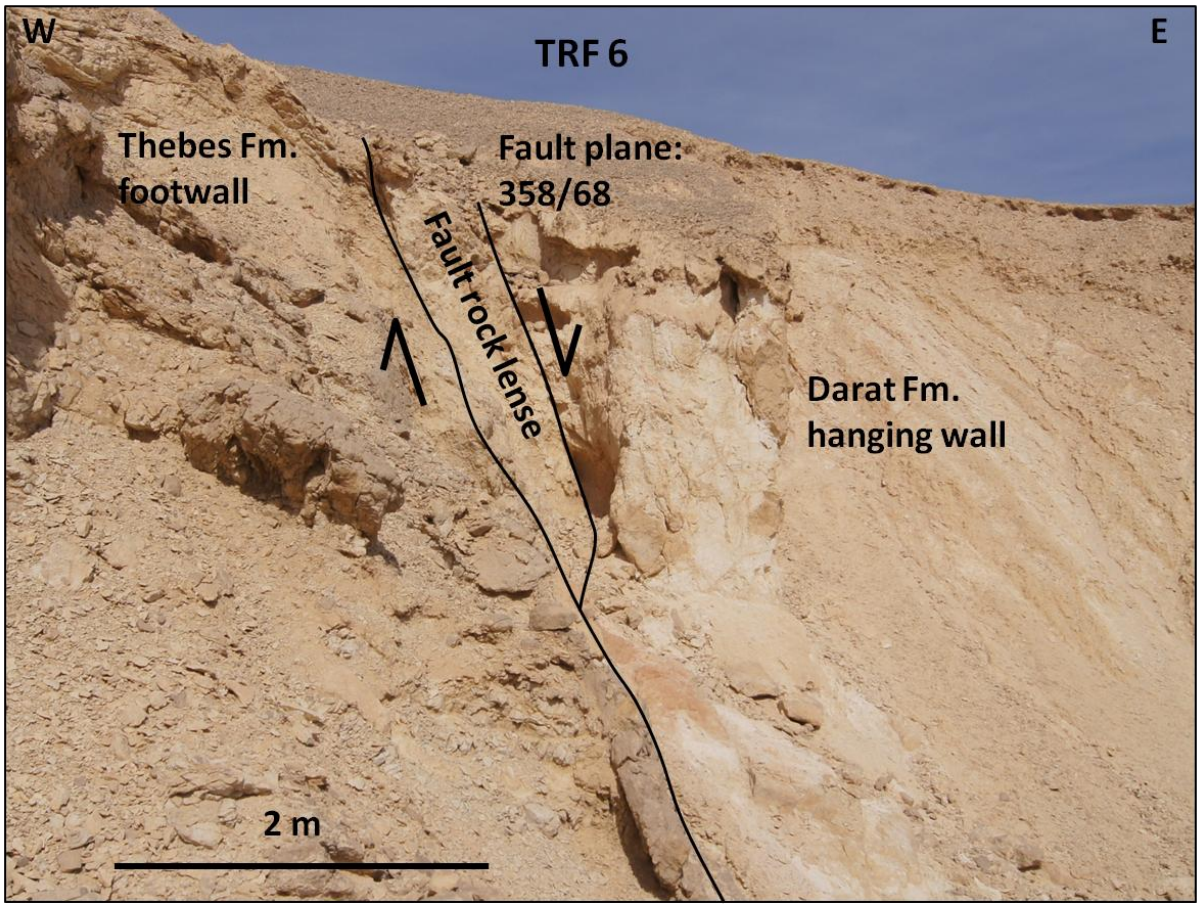

Figure 4.15: Locality TRF 6. Thebes Fm. in the footwall and the Darat Fm. in the hanging wall. The fault core is characterized as a fault rock lense.

Table 4.8: *Key data from TRF (south).*

Locality N → S	Throw	Max fracture frequency	Mean fracture frequency	Inner damage zone, mean fracture frequency	Outer damage zone, mean fracture frequency	Formation	Fault plane
TRF 4 hw	> c. 400 m	30	16,4	24,5	14,4	Darat	
TRF 5 hw	> c. 400 m	36	20,7	29,0	17,1	Darat	340/82
TRF 6 fw		42	22,2	34,0	19,0	Thebes	
TRF 6 hw	> c. 400 m	100+	69,0	69,0	-	Darat	358/68

Table 4.8 shows that the fracture frequencies are increasing towards the south from TRF 4-6, as the fault throw is increasing. A higher fracture frequency is also observed in the hanging wall than in the footwall of locality TRF 6.

Summary of the Thal Ridge Fault (south)

- Higher fracture frequencies in the hanging wall than in the footwall
- Higher fracture frequencies in the proximity to the fault
- Max fracture frequency is increasing as the fault throw is increasing
- Fractures are mainly oriented sub-parallel to the fault with subordinate fault sub-perpendicular fractures

Summary of the entire Thal Ridge Fault

The general trend along the Thal Ridge Fault is a high fracture frequency, except for locality 3, 4 and 5 were low frequencies may be a result of measurement errors. This will be further addressed in the discussion. The fractures are generally oriented sub-parallel to the fault with subordinate sub-perpendicular fractures. Rock lenses and relatively discrete slip surfaces characterize the fault core.

4.3 Description of the ramp

The ramp (Fig. 4.16) is constrained by the Wadi Wasit Fault to the west and the Thal Ridge Fault to the east and consists mainly of the Thebes and Darat Fm., depending on the northern extent of the Thal Ridge Fault. The spacing between the two faults is 1.2 km in the ramp and the overlapping distance is maximum 2.4 km and minimum 1.2. The overlapping distance is uncertain because of bad exposures of the northern part of the TRF. To the south the ramp starts as the top of a monocline, in the Thebes Fm., with beds dipping c. 10° to the north. In this area the ramp is cut by a minor fault (c. 30 m throw) trending NW-SE. Further north the

monocline dips steeply to the north (up to 60°) until it evens out to around 20° to the north where the Darat Fm. is present. In the easternmost part of the ramp the beds are slightly turning, dipping 30-50° to the NE.

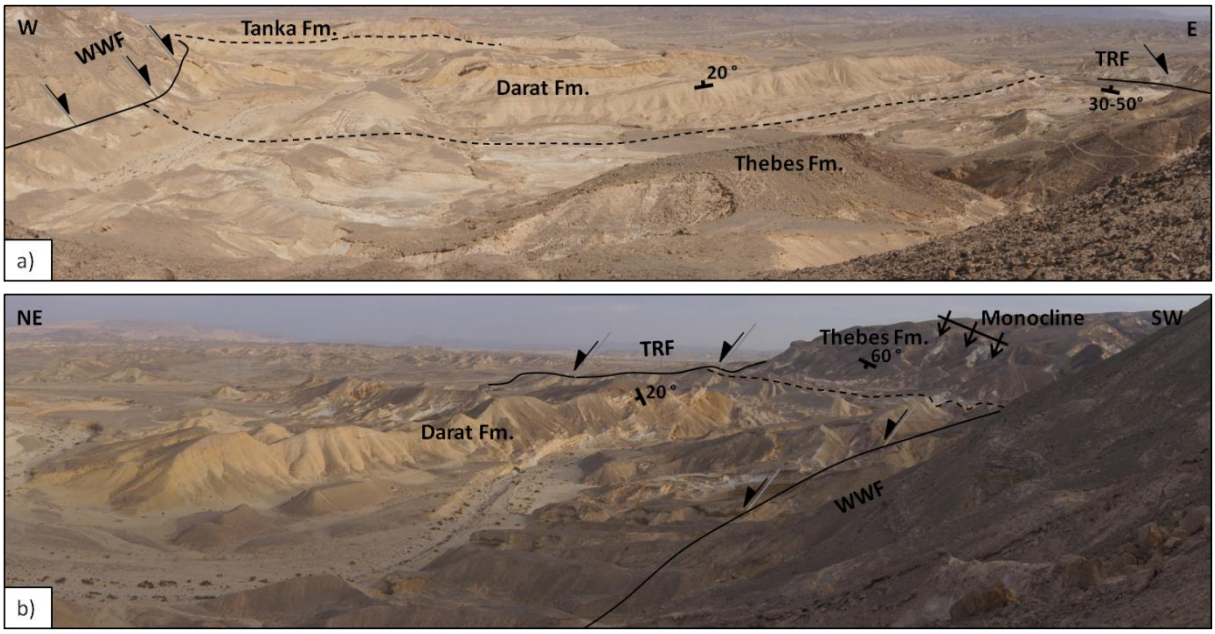

Figure 4.16: Overview of the ramp, looking down the ramp, towards north **(a)** and looking obliquely up the ramp, towards southeast **(b)**.

In order to assess the fracture systems in the relay ramp, a transect across the ramp, from WWF to TRF was made (Fig. 4.17). The transect consists of several scanlines measured in both the Thebes Fm. (Fig. 4.18a and b). and the Darat Fm. (Fig. 4.18c) across the ramp: 15 from the Thebes Fm., where two of them were taken in a N-S direction and eight from the Darat Fm., where three were taken in a N-S direction. The N-S scanlines are not included in the transect but were taken to assess the variability of fracture orientations in the ramp.

- The fracture frequencies in the Thebes Fm. are relatively stable, ranging from 1 to 30 fpm over a distance of 600 m. The same range is seen in the Darat Fm. over a distance of 350 m, with a peak of 46 fpm at the centre of the ramp. The mean fracture frequency ranges from 7,0 - 9,4 fpm and is therefore not notably elevated above the background fracturing levels.
- The fracture orientations in the western part of the Thebes Fm. show three trends: NW-SE (fault oblique), N-S (fault-parallel) and NE-SW (fault-oblique) (Fig. 4.17a), while the fractures in the central part of the Thebes Fm. are mainly oriented N-S (Fig. 4.17b). In the eastern part of the Thebes Fm. the fractures are mainly oriented E-W (fault-transverse) and N-S (Fig. 4.17c). The fractures in the western part of the Darat

Fm. are mainly oriented N-S with minor trends oriented NE-SW and NW-SE (Fig. 4.17d), while the fractures in the eastern part of the Darat Fm. are mainly oriented N-S with a minor trend oriented E-W (Fig. 4.17e).

- The fractures are in both formations characterized as hairline fractures and calcite-filled fractures. Cross-cutting relations of the studied factures in the ramp reveal that the N-S, NE-SW and NW-SE trending fractures are mutually cross-cutting, while the E-W trending fractures cross-cut and truncate all other fractures.

4.3.1 Ramp geometry calculations

Geometry parameters of the relay ramp can be used to calculate a linkage criterion (Soliva and Benedicto, 2004) and a preferred geometry value (Hus *et al.*, 2005). The parameters used are relay displacement (total displacement for the bounding faults), fault separation (distance between the bounding faults) and fault overlap (overlapping distance along the bounding faults).

Table 4.9: *Geometry parameters of the studied relay ramp*

Relay displacement	250 m
Fault separation	1200 m
Fault overlap	1000/2000 m (min/max)

Based on the data from Table 4.9 a linkage criterion can be calculated by dividing the relay displacement by the fault separation: $\frac{250\text{ m}}{1200\text{ m}} = 0.21$, and a preferred geometry value by dividing the fault overlap by the fault separation: maximum $\frac{2000\text{ m}}{1200\text{ m}} = 1.2$ or minimum $\frac{1000\text{ m}}{1200\text{ m}} = 0.8$. These values will be further addressed in the discussion.

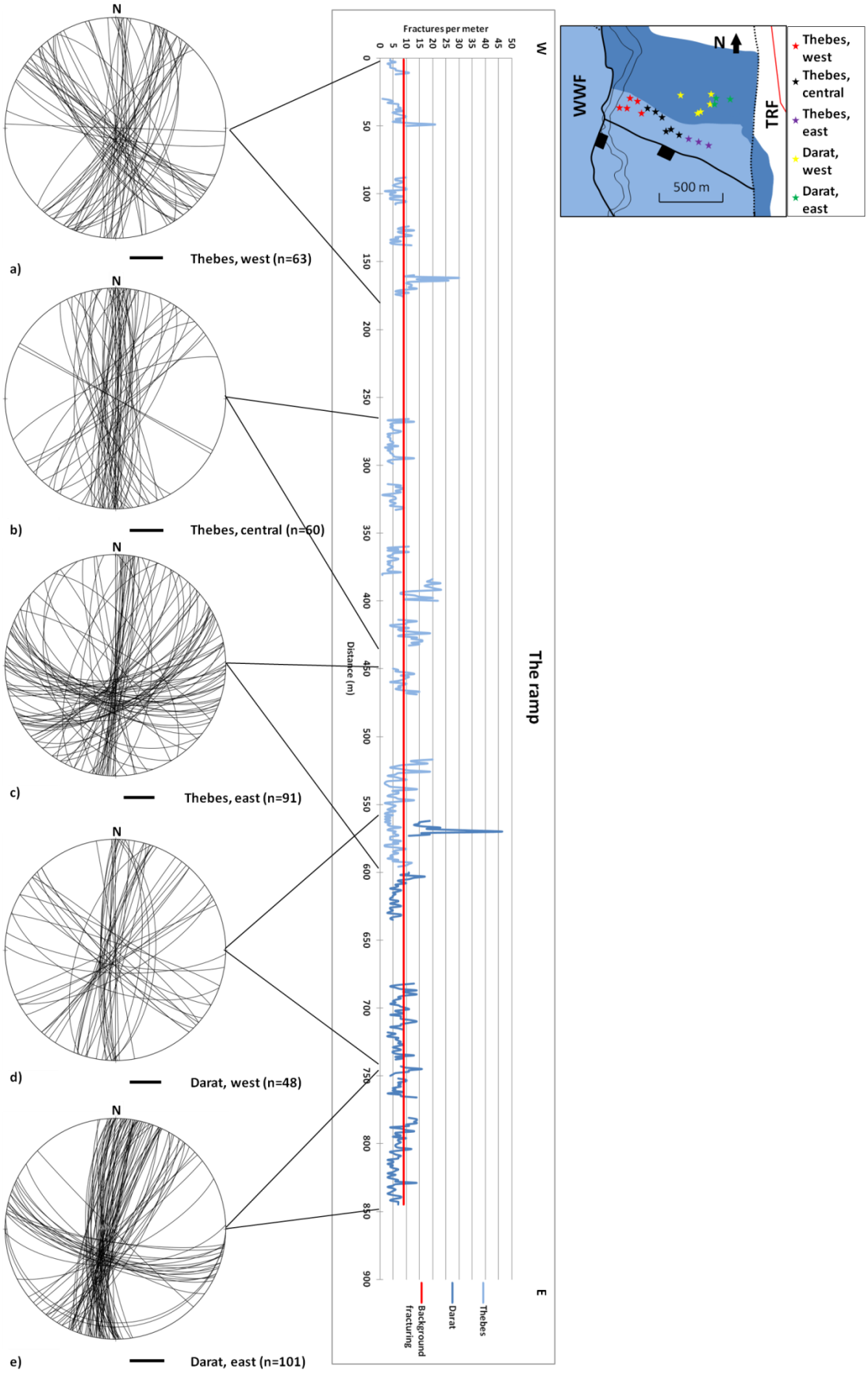

Figure 4.17: Fracture frequencies across the ramp bounded by the WWF to the west and TRF to the east. Fracture orientations are shown as equal area lower hemisphere stereonets. **(a)** The western part of Thebes, **(b)** the central part, **(c)** the eastern part, **(d)** the western part of Darat and **(e)** the eastern part.

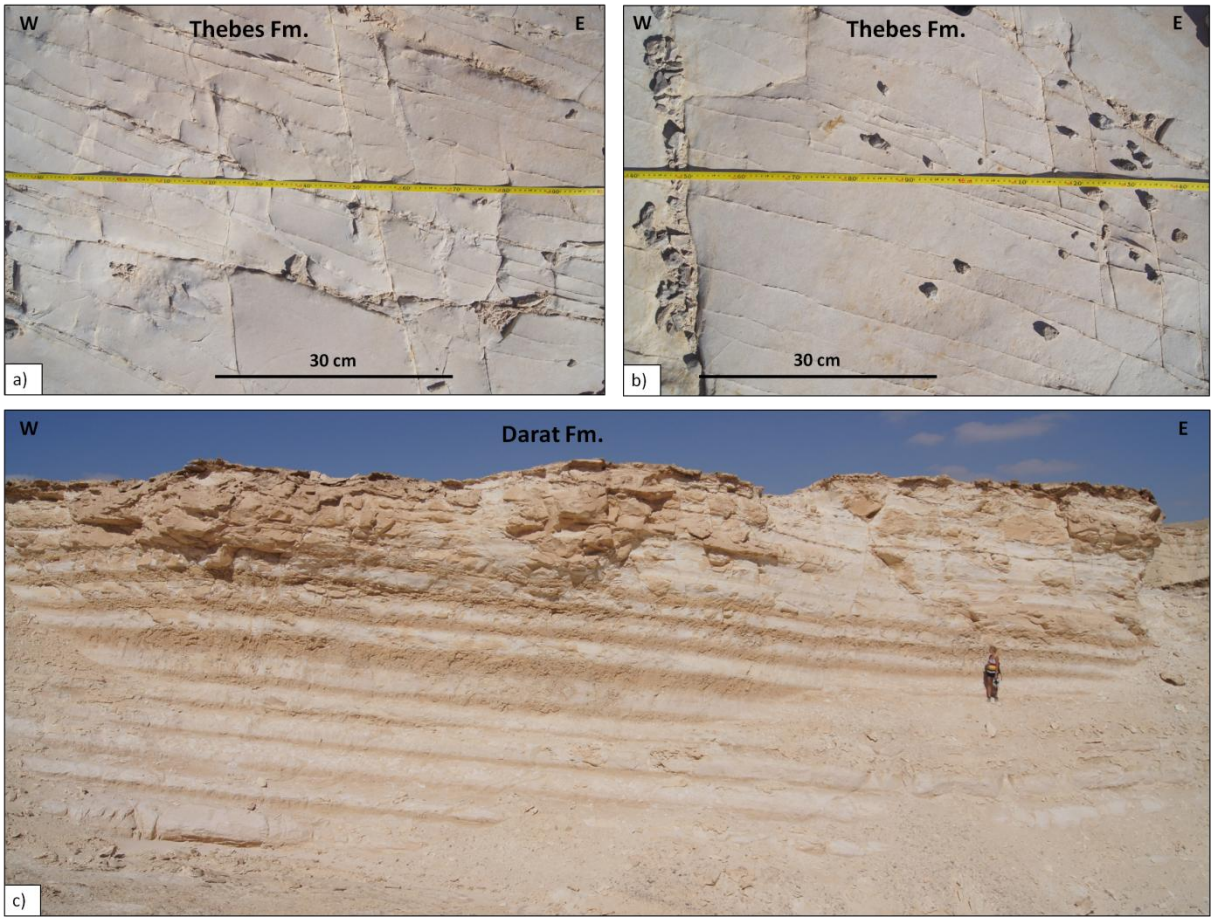

Figure 4.18: (a) and **(b)** Close-up of the Thebes Fm. showing fractures oriented mainly E-W and some N-S. Both represent the stereonet in Figure 4.16c. **(c)** Photo of one of the measured walls in the Darat Fm.

Table 4.10: *Key data from the ramp.*

Locality	Max fracture frequency	Min fracture frequency	Mean fracture frequency
Thebes, west	30	1	8,1
Thebes, central	23	1	8,1
Thebes, east	20	2	6,3
Darat, west	46	4	9,4
Darat, east	16	3	7,0

Table 4.10 shows that there are an even distribution of fractures along the ramp, both for the Thebes and Darat Fm.

Summary of the ramp

The ramp possesses a variety of fracture orientations where the fault-parallel trend is the most prominent, with subordinate fault-oblique and fault-transverse fractures. The fault-parallel and fault-oblique fractures are mutually cross-cutting, while the transverse-fractures cross-cut and

truncate all other fractures. Cross-cutting relationships will be further addressed in the discussion. There are no prominent differences in fracture frequencies for the Thebes Fm. and the Darat Fm, and the frequencies are also only slightly higher than the measured background fracturing levels.

4.4 Fault throw vs. fracture frequency

In Figure 4.19 fault throw is plotted against max number of fractures per locality for LWWF, WWF and TRF. All measurements are from the hanging wall.

The fracture distribution along the Little Wadi Wasit Fault (Fig. 4.19a) shows a decrease towards north that corresponds with a decrease in fault throw. All localities are in the Thebes Fm. At the southernmost locality the max fracture frequency is 78 fpm with a throw around 60 m. Further north at the next locality, the max fracture frequency is slightly decreased to 69 fpm as the throw has decreased to c. 40 m. The northernmost locality shows a further decrease in max fracture frequency (31 fpm) with a throw value of c. 30 m that is thought to lie close to the northern tip of the fault. The mean fracture frequencies follow the same pattern as the max fracture frequencies.

The Wadi Wasit Fault (Fig. 4.19b) shows a more complex fracture distribution. The northernmost locality is in the Tanka Fm. and has a relatively high max number of fractures (64 fpm) with a high throw (c. 250 m). Continuing southwards the throw is slightly decreasing and the hanging wall goes into the Darat Fm. The northernmost locality in the Darat Fm. has a very high max fracture frequency (> 100 fpm) and then drops rapidly southwards through three localities with max fracture frequencies below 60 fpm, as the throw value decreases below c. 200 m. Further south lays the Thebes Fm. where the northernmost locality has a relatively low fracture frequency (46 fpm) and the throw is still estimated to be just above 200 m. Further south the max fracture frequency rises rapidly for the two next localities (100 and 85 fpm). In this area the throw continues to decrease and is estimated to be below 150 m. The next locality to the south has a very max low fracture frequency (25 fpm), and further south the max fracture frequency is increasing to 49 fpm and 92 fpm as the throw is slightly decreasing below 20 m. The southernmost locality has a max fracture frequency of 39 fpm and is thought to be around the southern tip of the Wadi Wasit Fault. The mean fracture frequencies are more or less following the same pattern as the max fracture frequencies.

The Thal Ridge Fault (Fig. 4.19c) also shows an uneven distribution of fractures. At the southernmost locality the max fracture frequency is above 100 fpm with a mean of 70 fpm and the throw is assumed to be above 400 m, but there are no exact values from this part of the fault. Moving northwards the max fracture frequencies are decreasing rapidly over three localities with 36, 30 and 34 fpm, respectively. The mean fracture frequencies for these localities are ranging from 20-30 fpm. There are no throw values at this part as well, but it is assumed to be above 400 m. Further north the max fracture frequency is increasing to above 100 fpm over the two northernmost localities, while the mean fracture frequencies show a more even distribution of 40-60 fpm. At this part the throw begins to decrease and is estimated to be around 250 m at the northernmost locality.

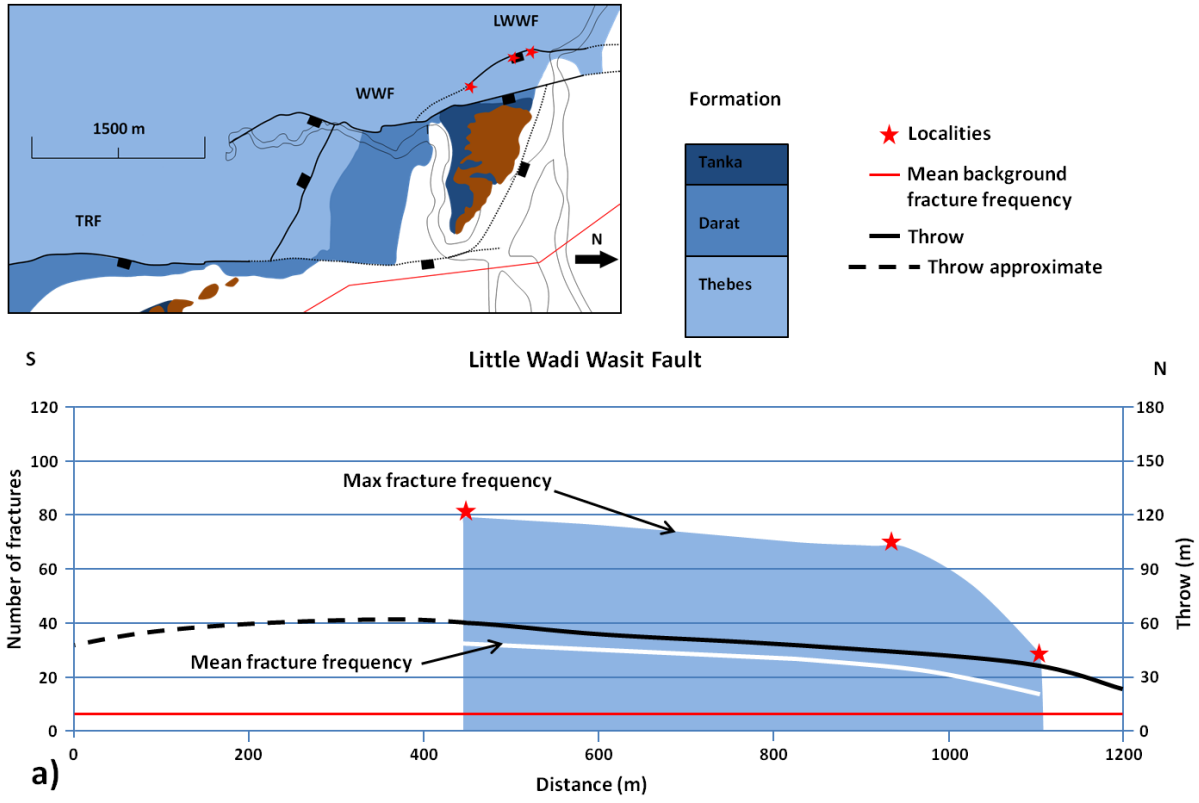

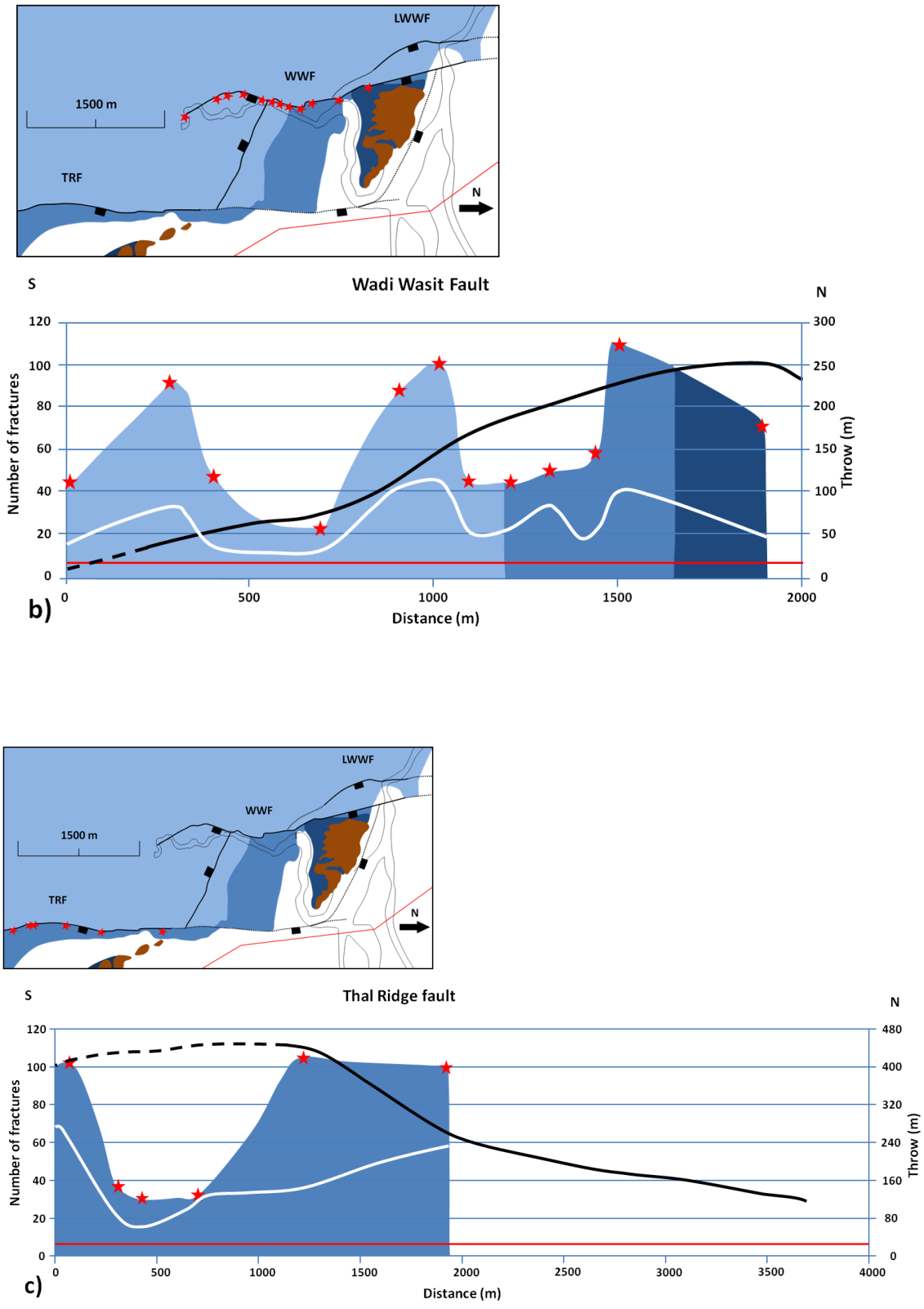

Figure 4.19: Max and mean fractures per locality plotted against fault throw for LWWF **(a)**, WWF **(b)** and TRF **(c)**. The red stars on the overview map show the localities and correspond with the stars on the graph. **(a)** Distance 0 m represents where the LWWF and WWF connect, **(b)** distance 0 m represents the approximate southern tip of WWF and **(c)** distance 4000 m represents a possible tip for TRF.

5. Discussion

5.1 Introduction

The aim of this chapter is to discuss the observed structural features along the studied faults and in the relay ramp. Part 5.2 discusses the variability of fracture systems along the individual faults with, with focus on single-tip fault interaction or bifurcation, double-tip fault interaction and tip zone processes. Part 5.3 deals with the fracture systems variability across the studied relay ramp with emphasis on the structural complexity. Part 5.4 discusses the potential effects of shale smear along the studied faults, while parts 5.5 and 5.6 deal with predictions of relative damage zone geometry, complexity in subsurface reservoirs, permeability structure and implications for fluid flow.

5.2 Fracture systems variability along the main faults

It is well known that faults are more complex, three-dimensional structures comprising zones of deformed rock (e.g. Caine *et al.*, 1996; Childs *et al.*, 2009). As presented herein (Chapter 4.2), the damage zone architecture varies along the studied faults. This part will begin with a discussion of damage zones related to individual faults, and then continue on the damage zone on single-fault tip interaction or bifurcation and lastly fault tips.

5.2.1 Damage zone width and geometry of the individual faults

The localities along the Thal Ridge Fault are all located south of the overlapping zone and the data presented can therefore be considered, in this context, to represent an isolated fault (although it is, *sensu stricto*, part of the larger overall large-scale relay structure studied herein). According to typical Andersonian fault theory Anderson (1951), fractures around normal faults should form perpendicular to the least compressive stress; i.e. form parallel to fault strike. Fault-parallel fractures are the main trend along the TRF and support this assumption (Fig. 5.1e). However, in addition to fault sub-parallel fractures, fault sub-perpendicular fractures are observed along the TRF. This is in accordance to Kattenhorn *et al.* (2000) who argue that stress perturbation induced by growing fault tips may form a more complex fracture pattern. The perturbation effect of propagating faults has also been documented (e.g. Barton and Zoback, 1994; Maerten *et al.*, 2002) to affect orientations of secondary structures such as minor faults and fractures. Kattenhorn *et al.* (2000) suggest that

fractures oriented at high angles to fault strike may have formed along laterally propagating fault tips, representing a halt in growth period before the fault tip propagated further.

Increased fracturing in the proximity of faults has been noted by several studies (e.g. Knott *et al.*, 1996; Beach *et al.*, 1999; Berg and Skar, 2005; Mitchell and Faulkner, 2009) and is related to the frictional resistance in the fault core as slip builds up (Kim *et al.*, 2004). Fracture mechanics models have shown that the decrease of fractures away from faults is linked to the decay of stress (Faulkner *et al.*, 2010). de Joussineau and Aydin (2007) describe the fault core as a highly fractured zone that develops through progressive slip. This trend is also observed along the LWWF, WWF and TRF which shows an overall high fracture frequency in the proximity to the principal slip surface. Localities with low frequencies close to the faults are most likely a result of measurement errors (see explanation in Chapter 4) and the overall trend is therefore interpreted to be higher.

An asymmetric deformation pattern along faults has been studied at a range of scales and in many different geological settings (e.g. Koestler and Ehrmann, 1991; Aarland and Skjerven, 1998; Berg and Skar, 2005; Ferrill *et al.*, 2011). Koestler and Ehrmann (1991), Aarland and Skjerven (1998) and Berg and Skar (2005) documented a wider hanging wall damage zone compared to the footwall, while Doughty (2003) and Ferrill *et al.* (2011) observed the opposite. Schueller *et al.* (in press) documented a wider hanging wall damage zone but similar fracture frequencies on both sides. Along the LWWF, WWF and TRF, the hanging wall is consistently more deformed than the footwall. Ferrill *et al.* (2011) studied damage zones in carbonates and argue that the width of damage zones is early established. Internal deformation is likely to continue within the established damage zone during accumulation of displacement. They further argue that a wide hanging wall damage zone may develop above an upward growing upper fault tip, while a more deformed footwall may develop below a downward growing lower fault tip. This argument is based on the concept of *trishear* deformation, which is a triangular zone of distributed shear stress concentration around vertically propagating fault tips (Pollard and Segall, 1987; Allmendinger, 1998). A highly deformed hanging wall, as observed in the present study, may therefore be associated with an upward propagating fault. Furthermore, on the contrary, Berg and Skar (2005) argue that a wider hanging wall is related to the asymmetric strain that develops during folding of the hanging wall, and that more deformation is therefore expected in the hanging wall contrary the footwall.

One factor that is not considered in these publications is the effects of mechanical contrasts in the faulted lithologies. Could the asymmetric damage zone deformation be a

result of lithological differences? Observations from the southern part of the WWF, where both the footwall and the hanging wall is comprised of the Thebes Fm., show an asymmetric damage zone deformation across the fault. In this area the fault throw is relatively low, assuming that internal lithological variations are no likely explanation of the variations. This is supported by the background fracturing levels which also show modest variations between the formations. There is therefore no obvious links between lithology and damage zone deformation.

Damage zones may also be affected by the magnitude of throw along faults. Several studies have shown that there is a positive correlation between damage zone deformation and fault throw (e.g. Knott *et al.*, 1996; Beach *et al.*, 1999; Fossen and Hesthammer, 2000; Shipton and Cowie, 2001). Shipton and Cowie (2003) and Schueller *et al.* (in press) suggest a model of fault evolution where the damage zone is progressively widened through time. Based on the data from this thesis, high deformation is observed both at high and low throw values. There are though some trends indicating a positive relationship (e.g. along the LWWF), but no obvious correlation between damage zone deformation and fault throw can be made. This may be a result of the different lithologies comprising the hanging wall; the fracture frequency in the Darat Fm. is expected to be a little lower than in the Thebes Fm. because it consists of more ductile beds, which tend to be less fractured (Ferrill and Morris, 2008), the Tanka Fm. is even more brittle than the Thebes Fm., but consists of thinner beds which tend to display more fractures (Ladeira and Price, 1981). It is no doubt that damage zones are affected by fault throw, but in this case it is difficult to discern any correlation when they comprise several different lithologies.

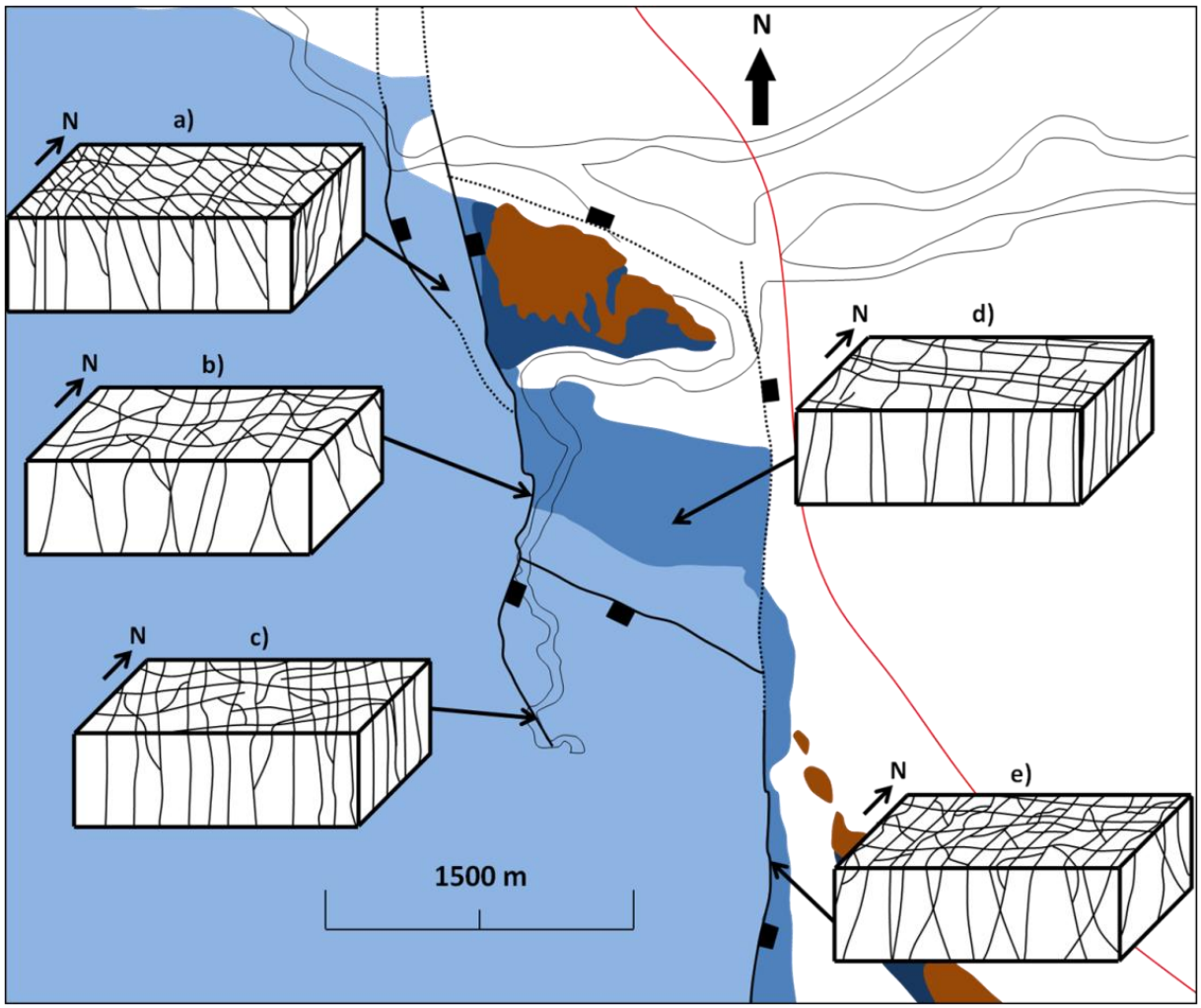

Figure 5.1: Model of fracture variability, represented by (main fracture orientation for each of the fracture boxes related to the main fault orientation) **(a)** fractures in single-tip fault interaction or bifurcation; fault-parallel, N-S and E-W oriented fractures, **(b)** double-tip fault interaction; fault-perpendicular and fault-parallel fractures, **(c)** tip zone; fault-parallel, fault-perpendicular and a variety of orientation fractures, **(d)** the ramp; low frequency fault-oblique, fault-parallel and fault-perpendicular fractures and **(e)** individual fault; fault-parallel and fault perpendicular fractures.

5.2.2 Single-tip fault interaction or bifurcation of the LWWF and the WWF

The LWWF connects with the WWF in a branch point, which may represent a point of fault segment bifurcation or the location of single-tip fault interaction (*sensu* Fossen *et al.*, 2005). Fossen *et al.* (2005) argue that single-tip fault interaction points may induce an anomalously high fracture frequency. Two localities (LWWF 3 and WWF 3) are located close to the branching point. However, both localities display an anomalously high fracture frequency and complexity compared to the other localities in the same formation and a wide range of fracture orientations (Fig. 5.1a). Could the LWWF have initiated as an individual fault and later propagated in the WWF? Or is it formed as a tip line bifurcation of the WWF?

Bifurcation is another possible explanation, and is generally observed near the end of long faults and is a result of propagation of a single fault that splays into different segments (Marchal *et al.*, 2003; Walsh *et al.*, 2003). Bifurcation can result from even small tip-line irregularities and form two sub-parallel slip surfaces (Huggins *et al.*, 1995), and eventually re-join to form a full lens of more or less deformed rock (Childs *et al.*, 1996). Martel *et al.* (1988) argue that bifurcation may form due to tensile stress concentrations at fault tips, while Cooke (1997) suggests that points of variable frictional properties along faults also may result in bifurcation.

Based on this information, it is still difficult to judge whether the LWWF may have initiated as an individual fault and later propagated into the WWF, or if the LWWF is a result of bifurcation of the WWF. The result is, however, anomalously high fracture frequencies and a high variability of fracture orientations.

5.2.3 Tip zone processes

Fault terminations are the transition from slip surfaces to unbroken rock in front of fault tips. Terminations are generally associated with zones of structural complexity (e.g. Shipton and Cowie, 2001; Kim and Sanderson, 2006) and can be classified as *tip damage zones* (*sensu* Kim *et al.*, 2004). Cowie and Scholz (1992) suggest that most stress is situated in the proximity of fault tips, and that this damage can be more severe than from slip on fault planes (Vermilye and Scholz, 1999). On the contrary, Martel (1997) postulate that the damage does not need to be high in the proximity of fault tips. Kim and Sanderson (2006) classified five types of tip damage zone structures: (1) wing cracks/normal faults, (2) horsetail splay fractures/faults, (3) synthetic branch faults, (4) antithetic faults and (5) solution surfaces/thrust faults. The tip damage zone observed at the southern extent of the WWF is characterized as a splay of both synthetic and antithetic normal faults (Fig. 5.1c). Similar, but larger, fault splay geometry at the tip of faults has been documented by Kirkpatrick *et al.* (2008).

5.3 Fracture systems variability across the relay ramp

Fault overlap zones or relay zones such as the one studied herein are known to have an anomalously wide *linking damage zone* (*sensu* Kim *et al.*, 2004). Overlapping and linking damage zones often feature elevated fracture frequencies and a wide range of fracture orientations. These features are induced by accumulated strain transferred between the ramp-bounding faults, which produce a zone of local stress as well as strain anomalies (Kattenhorn

et al., 2000). Linking damage zones in carbonate rocks have only been studied to some extent (e.g. Sharp *et al.*, 2000; Bonson *et al.*, 2007; Rotevatn and Bastesen, 2012). In siliciclastic rocks linking damage zones are well documented (e.g. Çiftçi and Bozkurt, 2007; Rotevatn *et al.*, 2007) and are shown to display temporal and spatial variations. The complexity of relay ramps is a result of spatially heterogeneous strain that occur in relay ramps (e.g. Soliva *et al.*, 2008). Other authors specify and argue that fault interaction overlap produce: (1) increased local shear stress in the relay ramp (Crider and Pollard, 1998) and (2) rotation of local stress field in the relay ramp as a function of the σ_1/ σ_2 principal stress ratio (Kattenhorn *et al.*, 2000). Trudgill and Cartwright (1994) and Dawers and Anders (1995) argue that fault linkage is more likely to happen if the separation between the ramp bounding faults is small compared to the length of the faults. Gupta and Scholz (2000) suggest that when a fault tip grows into a stress drop region produced by an interacting fault, a higher displacement anomaly near the growing tip will balance the stress drop. They further argue that once a fault tip grows into a region of critical stress, the fault tip will stop propagating or begin to link. In the case of the studied ramp-bounding faults it is unknown which fault that grew first and produced a stress drop region that affected the other fault.

The central part of the WWF comprises fracture orientations mainly oriented sub-perpendicular to the fault (Fig. 5.1b). This may be an effect of entering the overlap zone between WWF and TRF, where strain is transferred between fault strands by folding of relay beds and the formation of fault-perpendicular fractures. An overlap zone like this, where two faults with similar strike interact through the formation of a relay ramp, can be classified as *double-tip fault interaction* (*sensu* Fossen *et al.*, 2005).

How complex is the studied relay ramp really? To answer this question one need to look at the fracture frequency and orientation data. One could suspect that the fracture frequencies across the ramp are controlled by lithology. Observations indicate and as discussed above that there are no prominent differences in fracture frequencies in the Thebes Fm. and the Darat Fm. across the ramp. There are though some fracture frequency peaks, which most likely are a feature of local high strain accumulation and may represent fracture corridors (Ogata *et al.*, 2012; Rotevatn and Bastesen, 2012). The fracture frequencies are also only slightly elevated above the background fracturing levels, in contrast to other relay ramps studied in carbonates (e.g. Rotevatn and Bastesen, 2012). This may indicate that the deformation of the relay ramp is rather low.

A question arising from this is “Why is the relay ramp not more deformed?” A possible explanation can be found by looking at the geometry of the ramp. Fault separation,

which is the distance between two overlapping faults, is an important geometrical factor, related to stress reduction (Cowie and Roberts, 2001). Gupta and Scholz (2000) suggest that fault growth and propagation is retarded within the area of stress reduction around faults. Therefore, fault separation between two normal faults is an important parameter when evaluating fault interaction through their stress fields (e.g. Gupta and Scholz, 2000; Cowie and Roberts, 2001). Soliva and Benedicto (2004) made a linkage criterion based on three types of relay geometry: open, linked and fully breached. Calculations for the studied ramp indicate that it is, according to Soliva and Benedicto (2004), an open ramp, considerably far away from values indicating a breached ramp. This prediction is a result of the large spacing between the WWF and the TRF compared to the relay displacement. In addition to compare the fault separation with relay displacement, it is possible to compare it with the overlapping distance. Hus *et al.* (2005) studied relay ramp geometries including overlap/separation analysis, and suggested that relay ramps have a certain preferred geometry. They found a mean overlap/separation value of 3.12, while the overlap/separation value for the studied relay ramp is maximum 1.2 and minimum 0.8, depending on the northern extent of the TRF. However, compared, the studied relay ramp has a low overlap/separation value, which means that the separation distance between the WWF and TRF is large compared to the overlapping distance.

Based on the calculations from models from both Soliva and Benedicto (2004) and Hus *et al.* (2005); the separation between the WWF and TRF is too big compared to both the relay displacement and the overlapping distance. This is therefore a plausible explanation of why the deformation in the relay ramp is so low.

The cross-cutting relationships of the fractures in the relay ramp (Fig. 5.1d) reveal that the fault-parallel (N-S) and fault-oblique (NE-SW and NW-SE) fractures predate the fault-transverse (E-W) fractures. Kattenhorn *et al.* (2000) argue that oblique fractures (< 30° to fault strike) in relay ramps can be explained by rotation of the local stress field and interaction of remote fault-perpendicular stress. Rotevatn and Bastesen (2012) argue that in order to explain growth of fractures at great distances away from faults and at high angles to fault strike, an increase of the locally rotated fault-parallel stress and/or a relative relaxation of remote stresses perpendicular to the main fault trend must occur. They further state that there are no published evidence suggesting a relaxation or a rotation of remote stress during fault growth in the Suez Rift, but the fact that the Suez area where affected by continual and stable extension until c. 5 Ma (e.g. Lyberis, 1988; Patton *et al.*, 1994) is widely agreed. The studied faults are as a result of the extension likely to have been affected by stable remote stresses

during growth. The fault-transverse fractures may therefore reflect the latest stage of local stress field perturbation during fault propagation and overlap. At this point extreme local stress and rotation of the principal stress axes made it possible for fractures to grow at high angles to fault strike.

Armstrong (1997) and Sharp *et al.* (2000) have as mentioned earlier interpreted the studied ramp as a *hanging wall breached relay ramp* (*sensu* Trudgill and Cartwright, 1994; Cartwright *et al.*, 1996). Field observations from this thesis do, however, not support their interpretation. Firstly, there are no indications of any significant linking fault segment that cuts through the entire ramp and connects the overlapping faults. There are, however, some small cross-cutting faults in the southern part of the ramp, but they are too small to represent a relay ramp breaching. Rather, they are minor faults that locally accommodate strain enforced by the folding of the relay beds. Secondly, the fracture frequencies across the ramp are only slightly elevated above the background fracturing levels, which is an unlikely feature of a breached relay ramp. Thirdly, the aforementioned separation distance between WWF and TRF is too big compared to the total relay ramp displacement. The calculated value by following the linkage criterion from Soliva and Benedicto (2004) suggests, as mentioned, an open relay ramp geometry with a value considerably far away from values indicating a breached ramp. Fourthly, the separation distance is too big compared to the overlapping distance. Calculated separation/overlap value is, as mentioned, much lower than the preferred value for relay ramp geometry predicted by Hus *et al.* (2005).

The configuration of the studied relay ramp can therefore be interpreted to represent a transition between stage 2 and 3 in the relay ramp evolution scheme by Peacock and Sanderson (1994); a soft-linked relay ramp or, at the most, a soft-linked relay ramp with *incipient breaching and folding of relay beds*. Additional growth of the fault could have initiated progressive fracturing and faulting and eventually formed a connecting fault, breaching the relay ramp.

5.4 Potential effects of shale smear on fault damage zone

In carbonate-shale sequences, shale smear is an important feature of fault zones (e.g. Elvik, 2012). Shaly units does not tend to undergo brittle deformation, to a similar extent, as carbonate units when involved in faulting, but are rather smeared along the fault as a membrane of clay (Sperrevik *et al.*, 2000). One of the mechanisms that control the development of shale smear is the low shear strength of clay and the high fluid pressure, due

to low permeability, that allow the shale units to be ductile deformed (Lehner and Pilaar, 1997). It can also be related to the competency contrast between the shale units and surrounding mechanical stronger material; shale units have a lower competency than the surrounding rock, and will therefore fold/bend along a fault and develop as shale smear along the fault (Færseth, 2006).

In this study, shale smear is only observed in the northern part of the WWF (locality WWF 1 and 2), where the Khaboba Fm., consisting of ductile shale, are smeared along the fault (Fig. 5.2). Along the LWWF, TRF and the southern part of WWF the fault core is observed as relatively discrete slip surfaces and at some localities as fault rock lenses. Shale smear is not observed, because there are no shale present in the stratigraphy that are faulted.

Aydin and Eyal (2002) have studied the effects of shale smear and argue that the occurrence of shale smear can reduce the deformation in the hanging wall. The fracture frequencies in the hanging wall along the WWF are generally higher than the footwall, except for locality WWF 1 where shale smear is present. This is opposite to what other works suggest, which conclude that hanging wall should have more deformation (e.g. Aarland and Skjerven, 1998; Berg and Skar, 2005). An explanation of this feature may be that the hanging wall Tanka Fm. lies above the Khaboba Fm. and is protected by the shale smear against the fault. Elvik (2012) argues that shale smear may act as a "cushion", accommodating strain ductile. In contrast, the footwall will, during faulting, not be protected because the Thebes Fm. has been faulted against itself and the overlying Darat Fm, creating a high frictional deformation zone. In addition, the Tanka Fm. consists of thin beds and a low fracture frequency is therefore not expected (Ladeira and Price, 1981). Where shale smear is not present, slip between competent carbonate rocks will increase the friction and hence deformation may be increased in both footwall and hanging wall. One can therefore assume that shale smear may reduce the hanging wall deformation, but since there is only one studied locality where this was possible to observe, it is difficult to judge whether this is an isolated occurrence or a recurring pattern. However, the findings do agree well with other studies (e.g. Aydin and Eyal, 2002; Elvik, 2012).

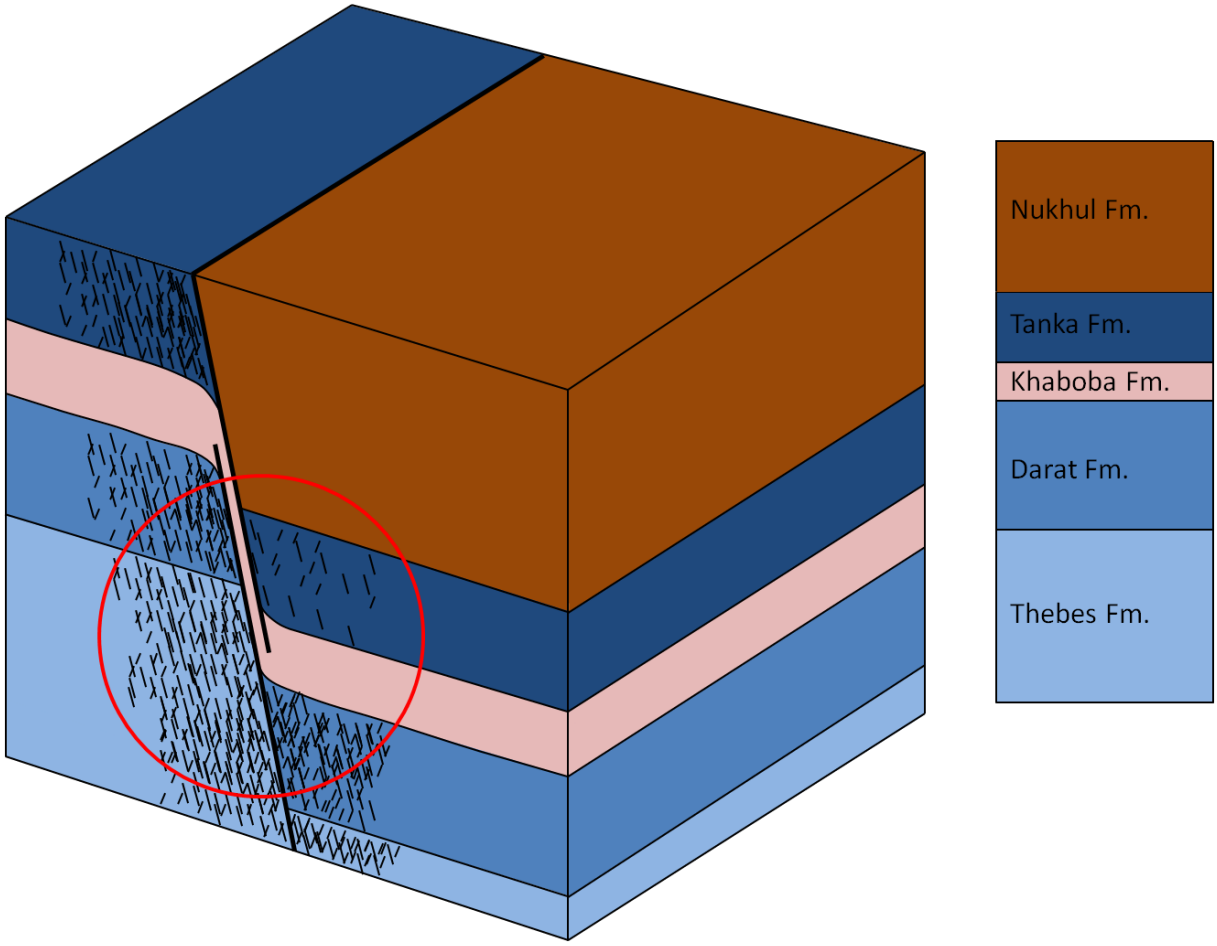

Figure 5.2: Conceptual model of shale smear where the Khaboba Fm. becomes entrained into the fault. Note a lower deformation in hanging wall Tanka Fm. Red ring indicates area of interest.

5.5 Subsurface carbonate reservoir predictions of damage zone geometry and complexity along normal faults and in relay ramps

Subsurface studies are limited to seismic resolution, outcrop studies are therefore of great importance in order to obtain details of subseismic scale features like faults and fractures. Some information, but very minimal and highly spatially restricted, may be achieved by wellbore data (e.g. Wu and Pollard, 2002) and from seismic anisotropy maps. Fracture characterization in the subsurface is therefore reliant on analogue models based on outcrop studies in order to understand the nature of subseismic structures.

The present study may elucidate some of the features related to fault linkage zones, and help determining damage zone geometries and fracture characteristics along normal faults and in relay ramp in carbonate reservoirs. Exact damage zone geometry may not be predictable but linkage zones are generally assumed to comprise a wider and more complex damage zone than individual faults. By studying geometrical parameters, if obtainable, like

fault separation, relay displacement and overlap distance one can make a prediction of the complexity of the linkage zone; it might not be as complex as first assumed, such as the example studied herein. However, some generic predictions of damage zones and fracture characteristics in subsurface linkage zones and faults can be made:

- Individual faults may feature an asymmetric deformation pattern. As presented in the current study, the hanging wall is generally more deformed than the footwall, except where shale smear is present; this is also, supported by previous work (e.g. Koestler and Ehrmann, 1991; Aarland and Skjerven, 1998; Berg and Skar, 2005). However, fractures along individual faults are suggested to be oriented mainly fault-parallel (Anderson, 1951) with subordinate fault-perpendicular fractures (Kattenhorn *et al.*, 2000).

- Single-tip fault interaction or bifurcation are associated with increased structural complexity that may induce an anomalously high fracture frequency (Fossen *et al.*, 2005) and a high variability of fracture orientations.

- Fault terminations and tip damage zones are generally associated with increased structural complexity (e.g. Shipton and Cowie, 2001; Kim and Sanderson, 2006). The studied tip damage zone features minor synthetic and antithetic faults, which also has been documented by other work (e.g. Kirkpatrick *et al.*, 2008).

- Damage zones geometry is variable and dependent on several factors, such as mechanical stratigraphy, fault throw and fault core morphology (e.g. Faulkner *et al.*, 2010). Studies (e.g. Knott *et al.*, 1996; Beach *et al.*, 1999; Fossen and Hesthammer, 2000; Shipton and Cowie, 2001) have shown a positive correlation between damage zone deformation and fault throw.

- Linkage zones are generally associated with a wider and more complex damage zone than along individual faults (e.g. Kim *et al.*, 2004; Çiftçi and Bozkurt, 2007; Rotevatn and Bastesen, 2012). However, the width of damage zones may not be as large as first expected. As presented in the current study, and supported by Soliva and Benedicto (2004) and Hus *et al.* (2005) the linking damage zone deformation is dependent on

geometrical parameters which control the stress field interaction; separation vs. relay displacement and separation vs. overlapping distance.

5.6 Permeability structure and implications for fluid flow in relay ramps

The permeability of naturally fractured, low permeable reservoirs, such as carbonates, is strongly controlled by fractures. Particularly, fracture frequency is important in the understanding of fluid flow, but is difficult to measure in the subsurface (Ortega *et al.*, 2010). Highly fractured zones are shown to induce increased permeability which consecutively induces local conduits for fluid flow (Matthäi and Belayneh, 2004). Fault linkage and fluid flow have been studied in siliciclastic rocks (e.g. Bense and Van Balen, 2004; Manzocchi *et al.*, 2008) with emphasis on cross-fault fluid conduits in soft-linked relay ramps. Bed continuity in folded relay ramp beds (Rotevatn *et al.*, 2009) is the main conduit, while juxtaposition of reservoir units at different stratigraphic levels (Manzocchi *et al.*, 2010) also is important. An unbreached ramp is therefore a possible pathway for fluids and is in an otherwise tight carbonate reservoir influenced by flow-inducing fractures.

Implications of the damage zone variability, studied herein, are important in order to predict permeability distribution of subsurface reservoirs. Individual faults generally feature fault-parallel fractures that induce fault-parallel flow, while fault-perpendicular fractures are not as common, limiting the cross-fault permeability. Relay ramps are, however, generally more complex and some permeability and fluid flow predictions, based on the current study, can be made:

- Relay ramps comprise an increased variability of fracture orientations, as presented herein, and normally increased fracture frequencies, compared to damage zones along individual faults. This leads to an increased matrix ratio and connectivity, which in turn lead to a higher permeability (e.g. Berkowitz, 1995).

- Lateral fault-parallel permeability in the linking damage zone is likely to increase. The effect is, however, limited since the lateral fault-parallel permeability already is enhanced by fault-parallel fractures outside the relay ramp.

- Vertical fault-parallel permeability is also assumed to increase. Sealing units may be breached by local stress field modification in the relay ramp (Gartrell *et al.*, 2004), increasing the permeability.

- Relay ramps are typically comprised of fractures oriented at high angles to fault strike, cross-cutting the ramp. These fractures are likely to increase the cross-fault permeability, which is usually low along individual faults. Breached or near-breached relay ramps may form transverse fractures dissecting the entire ramp (Rotevatn and Bastesen, 2012), which probably will significantly increase the cross-fault permeability. The increased permeability may, in a reservoir, connect two otherwise separate reservoir units.

6. Conclusions

The current study presents fracture systems variability along normal faults and across a relay ramp, with emphasis on damage zone geometry and fracture characterization. In addition, potential effects of shale smear, predictions of damage zone geometry and complexity in subsurface reservoirs, and permeability structure and implications for fluid flow have been addressed. The following conclusions are drawn:

- The studied faults display an asymmetric damage zone deformation pattern, where the hanging wall is generally more deformed than the footwall. This may be a result of upward propagation of the faults and/or because most of the fault movement is represented by downward movement of the hanging wall. It is also concluded that there are no obvious links between lithology and the observed deformation pattern.

- The studied faults also display increased fracture frequencies in the proximity to the fault core. This is related to build up of frictional resistance in the fault core, during slip events. Decay of stress away from the faults then leads to decreased fracture frequencies.

- Single-tip fault interaction or bifurcation point proved to feature an anomalously high fracture frequency. This may be a result of the perturbed stress fields (c.f. Kattenhorn *et al.*, 2000) and enhanced normal stresses (c.f. Crider and Pollard, 1998) between the faults involved.

- The tip zone of one of the studied faults is featured by a variety of fracture orientations and is characterized as a splay of both synthetic and antithetic normal faults.

- Occurrence of shale smear is observed to reduce hanging wall deformation, but it is difficult to judge whether this is an isolated occurrence or a recurring pattern. As shale smear was only present at one locality. However, the findings do agree well with other studies (e.g. Aydin and Eyal, 2002; Elvik, 2012).

- Cross-cutting relations of fractures in the relay ramp reveal that the fault-parallel and fault-oblique fractures predate the fault-transverse fractures. The fault-transverse fractures are interpreted to reflect the latest stage of local stress field perturbation during fault propagation and overlap. At this point extreme local stress and rotation of the principal stress axes made it possible for fractures to grow at high angles to fault strike. These fractures are also likely to increase the cross-fault permeability, which is usually low along individual faults.

- The linking damage zone enveloping the relay ramp studied herein is characterized by a relatively low complexity, with fracture frequencies only slightly elevated above background fracturing levels, compared to other studies of relay ramps in carbonates (e.g. Rotevatn and Bastesen, 2012). The low complexity is interpreted to be a result of: (1) large separation distance between the Wadi Wasit Fault and the Thal Ridge Fault compared to relay displacement and (2) large separation distance compared to overlapping distance. The studied relay ramp is therefore interpreted to represent a transition between stage 2 and 3 in the relay ramp evolution scheme by Peacock and Sanderson (1994): a soft-linked relay ramp or, at the most, a soft-linked relay ramp with incipient breaching.

7. References

Aarland, R., and Skjerven, J., 1998. Fault and fracture characteristics of a major fault zone in the northern North Sea: analysis of 3D seismic and oriented cores in the Brage Field (Block 31/4). *In*: Coward, M.P., Daltaban, T.S., Johnson, H. (eds.). *Structural Geology in Reservoir Characterization*. Geological Society, London, Special Publications. v. 127. p. 209-229.

Abdine, A., 1981. Egypt's petroleum geology: good grounds for optimism. World Oil. v. 193. no. 7. p. 99-112.

Abul-Nasr, R. A., and Thunell, R. C., 1987. Eocene eustatic sea level changes, evidence from Western Sinai, Egypt. Palaeogeography, Palaeoclimatology, Palaeoecology. v. 58. no. 1–2. p. 1-9.

Agosta, F., and Aydin, A., 2006. Architecture and deformation mechanism of a basin-bounding normal fault in Mesozoic platform carbonates, central Italy. Journal of Structural Geology. v. 28. no. 8. p. 1445-1467.

Allmendinger, R. W., 1998. Inverse and forward numerical modeling of trishear fault-propagation folds. Tectonics. v. 17. no. 4. p. 640-656.

Anders, M. H., and Schlische, R. W., 1994. Overlapping Faults, Intrabasin Highs, and the Growth of Normal Faults. The Journal of Geology. v. 102. p. 165-180.

Anderson, E. M., 1951. The Dynamics of Faulting. Oliver & Boyd, Edinburgh.

Angelier, J., 1985. Extension and rifting: the Zeit region, Gulf of Suez. Journal of Structural Geology. v. 7. no. 5. p. 605-612.

Armstrong, B., 1997. The temporal and spatial evolution of clastic syn-tectonic sedimentation on and adjacent to a developing relay ramp: an example from the Suez Rift [Masters: The University of Edinburgh.

Aydin, A., and Eyal, Y., 2002. Anatomy of a normal fault with shale smear: Implications for fault seal. AAPG Bulletin. v. 86. no. 8. p. 1367-1381.

Bahat, D., 1999. Single-layer burial joints vs single-layer uplift joints in Eocene chalk from the Beer Sheva syncline in Israel. Journal of Structural Geology. v. 21. no. 3. p. 293-303.

Barnett, J. A. M., Mortimer, J., Rippon, J. H., Walsh, J. J., and Watterson, J., 1987. Displacement Geometry in the Volume Containing a Single Normal Fault. AAPG Bulletin. v. 71. no. 8. p. 925-937.

Barton, C. A., and Zoback, M. D., 1994. Stress perturbations associated with active faults penetrated by boreholes: Possible evidence for near-complete stress drop and a new technique for stress magnitude measurement. Journal of Geophysical Research. v. 99. no. B5. p. 9373-9390.

Bastesen, E., and Braathen, A., 2010. Extensional faults in fine grained carbonates–analysis of fault core lithology and thickness–displacement relationships. Journal of Structural Geology. v. 32. no. 11. p. 1609-1628.

Bastesen, E., Braathen, A., Nøttveit, H., Gabrielsen, R. H., and Skar, T., 2009. Extensional fault cores in micritic carbonate – Case studies from the Gulf of Corinth, Greece. Journal of Structural Geology. v. 31. no. 4. p. 403-420.

Bastesen, E., and Rotevatn, A., 2012. Evolution and structural style of relay zones in layered limestone-shale sequences: insights from the Hammam Faraun Fault Block, Suez rift, Egypt. Journal of the Geological Society. v. 169. no. 4. p. 477-488.

Bayer, H.-J., Hötzl, H., Jado, A. R., Roscher, B., and Voggenreiter, W., 1988. Sedimentary and structural evolution of the northwest Arabian Red Sea margin. Tectonophysics. v. 153. no. 1-4. p. 137-151.

Beach, A., Welbon, A. I., Brockbank, P. J., and McCallum, J. E., 1999. Reservoir damage around faults; outcrop examples from the Suez Rift. Petroleum Geoscience. v. 5. no. 2. p. 109-116.

Bense, V. F., and Van Balen, R., 2004. The effect of fault relay and clay smearing on groundwater flow patterns in the Lower Rhine Embayment. Basin Research. v. 16. no. 3. p. 397-411.

Berg, S. S., and Skar, T., 2005. Controls on damage zone asymmetry of a normal fault zone: outcrop analyses of a segment of the Moab fault, SE Utah. Journal of Structural Geology. v. 27. no. 10. p. 1803-1822.

Berkowitz, B., 1995. Analysis of Fracture Network Connectivity Using Percolation Theory. Mathematical Geology. v. 27. no. 4. p. 467-483.

Billi, A., Salvini, F., and Storti, F., 2003. The damage zone-fault core transition in carbonate rocks: implications for fault growth, structure and permeability. Journal of Structural Geology. v. 25. no. 11. p. 1779-1794.

Bonson, C. G., Childs, C., Walsh, J. J., Schöpfer, M. P., and Carboni, V., 2007. Geometric and kinematic controls on the internal structure of a large normal fault in massive limestones: The Maghlaq Fault, Malta. Journal of structural geology. v. 29. no. 2. p. 336-354.

Bosworth, W., 1995. A high-strain rift model for the southern Gulf of Suez (Egypt). *In*: Lambiase, J. J. (eds.). *Hydrocarbon Habitat in Rift Basins*. Geological Society, London, Special Publications. v. 80. p. 75-102.

Bosworth, W., Huchon, P., and McClay, K. R., 2005. The Red Sea and Gulf of Aden Basins. Journal of African Earth Sciences. v. 43. no. 1-3. p. 334-378.

Bosworth, W., Khalil, S., Clare, A., Comisky, J., Abdelal, H., Reed, T., and Kokkoros, G., 2012. Integration of outcrop and subsurface data during the development of a naturally fractured Eocene carbonate reservoir at the East Ras Budran concession, Gulf of Suez, Egypt. *In*: Spence, G. H., Redfern, J., Aguilera, R., Bevan, T. G., Cosgrove, J. W., Couples, G. D.&Daniel, J.-M. (eds.) 2012. *Advances in the Study of Fractured Reservoirs*. Geological Society, London, Special Publications. v. 374.

Caine, J. S., Evans, J. P., and Forster, C. B., 1996. Fault zone architecture and permeability structure. Geology. v. 24. no. 11. p. 1025-1028.

Cartwright, J. A., Mansfield, C., and Trudgill, B., 1996. The growth of normal faults by segment linkage. *In*: From Buchanan, R G. & Nieuwland, D. A. (eds). *Modern Developments in Structural Interpretation, Validation and Modelling*. Geological Society, London, Special Publications. v. 99. p. 163-177.

Cartwright, J. A., Trudgill, B. D., and Mansfield, C. S., 1995. Fault growth by segment linkage: an explanation for scatter in maximum displacement and trace length data

from the Canyonlands Grabens of SE Utah. Journal of Structural Geology. v. 17. no. 9. p. 1319-1326.

Casey, M., and Butler, R. W. H., 2004. Modelling approaches to understanding fold development: implications for hydrocarbon reservoirs. Marine and Petroleum Geology. v. 21. no. 7. p. 933-946.

Childs, C., Manzocchi, T., Walsh, J. J., Bonson, C. G., Nicol, A., and Schöpfer, M. P., 2009. A geometric model of fault zone and fault rock thickness variations. Journal of Structural Geology. v. 31. no. 2. p. 117-127.

Childs, C., Watterson, J., and Walsh, J. J., 1995. Fault overlap zones within developing normal fault systems. Journal of the Geological Society. v. 152. no. 3. p. 535-549.

Childs, C., Watterson, J., and Walsh, J. J., 1996. A model for the structure and development of fault zones. Journal of the Geological Society. v. 153. no. 3. p. 337-340.

Çiftçi, N. B., and Bozkurt, E., 2007. Anomalous stress field and active breaching at relay ramps: a field example from Gediz Graben, SW Turkey. Geological Magazine. v. 144. no. 4. p. 687-699.

Cochran, J. R., 1983. A model for development of the Red Sea. AAPG Bulletin. v. 67. no. 1. p. 41-69.

Colletta, B., Le Quellec, P., Letouzey, J., and Moretti, I., 1988. Longitudinal evolution of the Suez rift structure (Egypt). Tectonophysics. v. 153. no. 1–4. p. 221-233.

Cooke, M. L., 1997. Fracture localization along faults with spatially varying friction. Journal of Geophysical Research. v. 102. no. B10. p. 22425-22434.

Cowie, P. A., and Roberts, G. P., 2001. Constraining slip rates and spacings for active normal faults. Journal of Structural Geology. v. 23. no. 12. p. 1901-1915.

Cowie, P. A., and Scholz, C. H., 1992a. Growth of Faults by Accumulation of Seismic Slip. Journal of Geophysical Research. v. 97. no. B7. p. 11085-11095.

Cowie, P. A., and Scholz, C. H., 1992b. Physical explanation for the displacement-length relationship of faults using a post-yield fracture mechanics model. Journal of Structural Geology. v. 14. no. 10. p. 1133-1148.

Crider, J. G., and Pollard, D. D., 1998. Fault linkage: Three-dimensional mechanical interaction between echelon normal faults. Journal of Geophysical Research. v. 103. no. B10. p. 24373-24391.

Dawers, N. H., and Anders, M. H., 1995. Displacement-length scaling and fault linkage. Journal of Structural Geology. v. 17. no. 5. p. 607-614.

Dawers, N. H., Anders, M. H., and Scholz, C. H., 1993. Growth of Normal Faults: Displacement-length scaling. Geology. v. 21. no. 12. p. 1107-1110.

de Joussineau, G., and Aydin, A., 2007. The evolution of the damage zone with fault growth in sandstone and its multiscale characteristics. Journal of Geophysical Research. v. 112. no. B12.

Doughty, P. T., 2003. Clay smear seals and fault sealing potential of an exhumed growth fault, Rio Grande rift, New Mexico. AAPG Bulletin. v. 87. no. 3. p. 427-444.

Elvik, L., 2012. Characterisation of extensional faults in carbonate rocks (Suez Rift, Egypt); with particular focus on the role of shale smear [Masters: University of Bergen.

Evans, A. L., 1988. Neogene tectonic and stratigraphic events in the Gulf of Suez rift area, Egypt. Tectonophysics. v. 153. no. 1-4. p. 235-247.

Evans, A. L., 1990. Miocene sandstone provenance relations in the Gulf of Suez: insights into synrift unroofing and uplift history. AAPG Bulletin. v. 74. no. 9. p. 1386-1400.

Eyal, Y., Gross, M. R., Engelder, T., and Becker, A., 2001. Joint development during fluctuation of the regional stress field in southern Israel. Journal of Structural Geology. v. 23. no. 2. p. 279-296.

Faulkner, D. R., Jackson, C. A. L., Lunn, R. J., Schlische, R. W., Shipton, Z. K., Wibberley, C. A. J., and Withjack, M. O., 2010. A review of recent developments concerning the structure, mechanics and fluid flow properties of fault zones. Journal of Structural Geology. v. 32. no. 11. p. 1557-1575.

Ferrill, D. A., and Morris, A. P., 2008. Fault zone deformation controlled by carbonate mechanical stratigraphy, Balcones fault system, Texas. AAPG Bulletin. v. 92. no. 3. p. 359-380.

Ferrill, D. A., Morris, A. P., McGinnis, R. N., Smart, K. J., and Ward, W. C., 2011. Fault zone deformation and displacement partitioning in mechanically layered carbonates: The Hidden Valley fault, central Texas. AAPG Bulletin. v. 95. no. 8. p. 1383-1397.

Finn, M. D., Gross, M. R., Eyal, Y., and Draper, G., 2003. Kinematics of throughgoing fractures in jointed rocks. Tectonophysics. v. 376. no. 3-4. p. 151-166.

Fossen, H., 2010. Structural Geology. Cambridge University Press.

Fossen, H., and Hesthammer, J., 2000. Possible absence of small faults in the Gullfaks Field, northern North Sea: implications for downscaling of faults in some porous sandstones. Journal of Structural Geology. v. 22. no. 7. p. 851-863.

Fossen, H., Johansen, T. E. S., Hesthammer, J., and Rotevatn, A., 2005. Fault interaction in porous sandstone and implications for reservoir management; examples from southern Utah. AAPG Bulletin. v. 89. no. 12. p. 1593-1606.

Færseth, R. B., 2006. Shale smear along large faults: continuity of smear and the fault seal capacity. Journal of the Geological Society. v. 163. no. 5. p. 741-751.

Garfunkel, Z., 1981. Internal structure of the Dead Sea leaky transform (rift) in relation to plate kinematics. Tectonophysics. v. 80. no. 1-4. p. 81-108.

Gartrell, A., Zhang, Y., Lisk, M., and Dewhurst, D., 2004. Fault intersections as critical hydrocarbon leakage zones: integrated field study and numerical modelling of an example from the Timor Sea, Australia. Marine and petroleum geology. v. 21. no. 9. p. 1165-1179.

Gawthorpe, R. L., Jackson, C. A. L., Young, M. J., Sharp, I. R., Moustafa, A. R., and Leppard, C. W., 2003. Normal fault growth, displacement localisation and the evolution of normal fault populations: the Hammam Faraun fault block, Suez rift, Egypt. Journal of Structural Geology. v. 25. no. 6. p. 883-895.

Gibson, R. G., 1994. Fault-zone seals in siliciclastic strata of the Columbus Basin, offshore Trinidad. AAPG Bulletin. v. 78. no. 9. p. 1372-1385.

Goguel, J., 1965. Traité de Tectonique. Masson Paris.

Gross, M. R., Fischer, M. P., Engelder, T., and Greenfield, R. J., 1995. Factors controlling joint spacing in interbedded sedimentary rocks: integrating numerical models with field observations from the Monterey Formation, USA. *In*: Ameen, M. S. (eds.). *Fractography: fracture topography as a tool in fracture mechanics and stress analysis*. Geological Society, London, Special Publications. v. 92. p. 215-233.

Gupta, A., and Scholz, C. H., 2000. A model of normal fault interaction based on observations and theory. Journal of Structural Geology. v. 22. no. 7. p. 865-879.

Gupta, S., Underhill, J. R., Sharp, I. R., and Gawthorpe, R. L., 1999. Role of fault interactions in controlling synrift sediment dispersal patterns: Miocene, Abu Alaqa Group, Suez Rift, Sinai, Egypt. Basin Research. v. 11. no. 2. p. 167-189.

Helgeson, D. E., and Aydin, A., 1991. Characteristics of joint propagation across layer interfaces in sedimentary rocks. Journal of Structural Geology. v. 13. no. 8. p. 897-911.

Huggins, P., Watterson, J., Walsh, J., and Childs, C., 1995. Relay zone geometry and displacement transfer between normal faults recorded in coal-mine plans. Journal of Structural Geology. v. 17. no. 12. p. 1741-1755.

Hus, R., Acocella, V., Funiciello, R., and De Batist, M., 2005. Sandbox models of relay ramp structure and evolution. Journal of Structural Geology. v. 27. no. 3. p. 459-473.

Imber, J., Tuckwell, G. W., Childs, C., Walsh, J. J., Manzocchi, T., Heath, A. E., Bonson, C. G., and Strand, J., 2004. Three-dimensional distinct element modelling of relay growth and breaching along normal faults. Journal of Structural Geology. v. 26. no. 10. p. 1897-1911.

Jackson, C. A. L., Gawthorpe, R. L., Leppard, C. W., and Sharp, I. R., 2006. Rift-initiation development of normal fault blocks: insights from the Hammam Faraun fault block, Suez Rift, Egypt. Journal of the Geological Society. v. 163. no. 1. p. 165-183.

Jackson, C. A. L., and Rotevatn, A., in press. Structure and evolution of a polyphase salt-influenced normal fault system: implications for models of normal fault growth.

Jackson, J., and McKenzie, D., 1983. The geometrical evolution of normal fault systems. Journal of Structural Geology. v. 5. no. 5. p. 471-482.

Jackson, J., White, N. J., Garfunkel, Z., and Anderson, H., 1988. Relations between normal-fault geometry, tilting and vertical motions in extensional terrains: an example from the southern Gulf of Suez. Journal of Structural Geology. v. 10. no. 2. p. 155-170.

Kattenhorn, S. A., Aydin, A., and Pollard, D. D., 2000. Joints at high angles to normal fault strike: an explanation using 3-D numerical models of fault-perturbed stress fields. Journal of Structural Geology. v. 22. no. 1. p. 1-23.

Khalil, S. M., and McClay, K. R., 2001. Tectonic evolution of the NW Red Sea - Gulf of Suez rift system. *In*: Wilson, R. C. L., Whitmarsh, R. B., Taylor, B. & Froitzheim, N. (eds.). *Non-Volcanic Rifting of ContinentalMargins: A Comparison of Evidence from Land and Sea.* Geological Society, London, Special Publications. v. 187. p. 453-473.

Kim, Y.-S., Peacock, D. C. P., and Sanderson, D. J., 2004. Fault damage zones. Journal of Structural Geology. v. 26. no. 3. p. 503-517.

Kim, Y.-S., and Sanderson, D. J., 2006. Structural similarity and variety at the tips in a wide range of strike–slip faults: a review. Terra Nova. v. 18. no. 5. p. 330-344.

Kirkpatrick, J., Shipton, Z., Evans, J. P., Micklethwaite, S., Lim, S., and McKillop, P., 2008. Strike-slip fault terminations at seismogenic depths: The structure and kinematics of the Glacier Lakes fault, Sierra Nevada United States. Journal of Geophysical Research. v. 113. no. B4.

Knott, S. D., Beach, A., Brockbank, P. J., Lawson Brown, J., McCallum, J. E., and Welbon, A. I., 1996. Spatial and mechanical controls on normal fault populations. Journal of Structural Geology. v. 18. no. 2. p. 359-372.

Koestler, A. G., and Ehrmann, W. U., 1991. Description of brittle extensional features in chalk on the crest of a salt ridge (NW Germany). *In*: Roberts, A.M., Yielding, G., Freeman, B. (eds.). *The Geometry of Normal Faults*. Geological Society, London, Special Publications. v. 56. p. 113-123.

Kuss, J., Scheibner, C., and Gietl, R., 2000. Carbonate Platform to Basin Transition along an Upper Cretaceous to Lower Tertiary Syrian Arc Uplift, Galala Plateaus, Eastern Desert of Egypt. GeoArabia. v. 5. no. 3. p. 405-424.

Ladeira, F. L., and Price, N. J., 1981. Relationship between fracture spacing and bed thickness. Journal of Structural Geology. v. 3. no. 2. p. 179-183.

Larsen, P. H., 1988. Relay structures in a Lower Permian basement-involved extension system, East Greenland. Journal of Structural Geology. v. 10. no. 1. p. 3-8.

Laubach, S. E., 1988. Subsurface fractures and their relationship to stress history in East Texas basin sandstone. Tectonophysics. v. 156. no. 1-2. p. 37-49.

Lehner, F. K., and Pilaar, W. F., 1997. The emplacement of clay smears in synsedimentary normal faults: inferences from field observations near Frechen, Germany. Norwegian Petroleum Society Special Publications. v. 7. p. 39-50.

Lindsay, N., Murphy, F., Walsh, J., and Watterson, J., 1993. Outcrop studies of shale smears on fault surfaces. *In*: Flint, S.S. & Bryant, I.D. (eds.). *The Geological Modelling of Hydrocarbon Reservoirs and Outcrop Analogues*. Special Publications, International Association of Sedimentologists. v. 15. p. 113-123.

Lyberis, N., 1988. Tectonic evolution of the Gulf of Suez and the Gulf of Aqaba. Tectonophysics. v. 153. no. 1-4. p. 209-220.

Maerten, L., Gillespie, P., and Pollard, D. D., 2002. Effects of local stress perturbation on secondary fault development. Journal of Structural Geology. v. 24. no. 1. p. 145-153.

Manzocchi, T., Childs, C., and Walsh, J. J., 2010. Faults and fault properties in hydrocarbon flow models. Geofluids. v. 10. no. 1-2. p. 94-113.

Manzocchi, T., Heath, A. E., Palananthakumar, B., Childs, C., and Walsh, J. J., 2008. Faults in conventional flow simulation models: a consideration of representational assumptions and geological uncertainties. Petroleum Geoscience. v. 14. no. 1. p. 91-110.

Marchal, D., Guiraud, M., and Rives, T., 2003. Geometric and morphologic evolution of normal fault planes and traces from 2D to 4D data. Journal of Structural Geology. v. 25. no. 1. p. 135-158.

Martel, S. J., 1997. Effects of cohesive zones on small faults and implications for secondary fracturing and fault trace geometry. Journal of Structural Geology. v. 19. no. 6. p. 835-847.

Martel, S. J., and Boger, W. A., 1998. Geometry and mechanics of secondary fracturing around small three-dimensional faults in granitic rock. Journal of Geophysical Research. v. 103. no. B9. p. 21299-21314.

Martel, S. J., Pollard, D. D., and Segall, P., 1988. Development of simple strike-slip fault zones, Mount Abbot quadrangle, Sierra Nevada, California. Geological Society of America Bulletin. v. 100. no. 9. p. 1451-1465.

Matthäi, S. K., and Belayneh, M., 2004. Fluid flow partitioning between fractures and a permeable rock matrix. Geophysical Research Letters. v. 31. no. 7. p. L07602.

McConaughy, D. T., and Engelder, T., 1999. Joint interaction with embedded concretions: joint loading configurations inferred from propagation paths. Journal of Structural Geology. v. 21. no. 11. p. 1637-1652.

McGrath, A. G., and Davison, I., 1995. Damage zone geometry around fault tips. Journal of Structural Geology. v. 17. no. 7. p. 1011-1024.

McKenzie, D., and Jackson, J., 1986. A block model of distributed deformation by faulting. Journal of the Geological Society. v. 143. no. 2. p. 349-353.

Micarelli, L., Moretti, I., and Daniel, J., 2003. Structural properties of rift-related normal faults: the case study of the Gulf of Corinth, Greece. Journal of Geodynamics. v. 36. no. 1-2. p. 275-303.

Micarelli, L., Moretti, I., Jaubert, M., and Moulouel, H., 2006. Fracture analysis in the south-western Corinth rift (Greece) and implications on fault hydraulic behavior. Tectonophysics. v. 426. no. 1–2. p. 31-59.

Mitchell, T., and Faulkner, D., 2009. The nature and origin of off-fault damage surrounding strike-slip fault zones with a wide range of displacements: a field study from the Atacama fault system, northern Chile. Journal of Structural Geology. v. 31. no. 8. p. 802-816.

Montenat, C., Ott D'Estevou, P., Purser, B., Burollet, P.-F., Jarrige, J.-J., Orszag-Sperber, F., Philobbos, E., Plaziat, J.-C., Prat, P., Richert, J.-P., Roussel, N., and Thiriet, J.-P., 1988. Tectonic and sedimentary evolution of the Gulf of Suez and the northwestern Red Sea. Tectonophysics. v. 153. no. 1–4. p. 161-177.

Moretti, I., and Colletta, B., 1987. Spatial and temporal evolution of the Suez rift subsidence. Journal of Geodynamics. v. 7. no. 1-2. p. 151-168.

Morley, C. K., Nelson, R. A., Patton, T. L., and Munn, S. G., 1990. Transfer zones in the East African rift system and their relevance to hydrocarbon exploration in rifts. AAPG Bulletin. v. 74. no. 1. p. 1234-1253.

Moustafa, A. R., 1993. Structural characteristics and tectonic evolution of the east-margin blocks of the Suez rift. Tectonophysics. v. 223. no. 3-4. p. 381-399.

Moustafa, A. R., 1996. Internal structure and deformation of an accommodation zone in the northern part of the Suez rift. Journal of Structural Geology. v. 18. no. 1. p. 93-107.

Moustafa, A. R., 2003. Explanatory notes for the geologic maps of the eastern side of the Suez Rift (western Sinai Peninsula). Egypt, AAPG/Datapages GIS Series. p. 34.

Moustafa, A. R., and Abdeen, M., 1992. Structural setting of the Hammam Faraun block, eastern side of the Suez rift. Journal of the Faculty of Science, University of Kuwait. v. 19. p. 291-310.

Moustafa, A. R., and El Shaarawy, D. A., 1987. Tectonic setting of the northern Gulf of Suez: Proceedings of the 5th Annual Meeting. Egyptian Geophysical Society. p. 339-368.

Narr, W., and Suppe, J., 1991. Joint spacing in sedimenlary rocks. Journal of Structural Geology. v. 11. no. 9. p. 1037-1048.

Ogata, K., Senger, K., Braathen, A., Tveranger, J., and Olaussen, S., 2012. The importance of natural fractures in a tight reservoir for potential CO2 storage: a case study of the upper Triassic–middle Jurassic Kapp Toscana Group (Spitsbergen, Arctic Norway). *In*: Spence, G. H., Redfern, J., Aguilera, R., Bevan, T. G., Cosgrove, J. W., Couples, G. D. & Daniel, J.-M. (eds.). *Advances in the Study of Fractured Reservoirs*. Geological Society, London, Special Publications. v. 374.

Ortega, O. J., Gale, J. F., and Marrett, R., 2010. Quantifying diagenetic and stratigraphic controls on fracture intensity in platform carbonates: An example from the Sierra Madre Oriental, northeast Mexico. Journal of Structural Geology. v. 32. no. 12. p. 1943-1959.

Patton, T. L., Moustafa, A. R., Nelson, R. A., and Abdine, S. A., 1994. Tectonic Evolution and Structural Setting of the Suez Rift. *In*: Landon, S. M. (eds.). *Interior Rift Basins.* AAPG Memoirs. v. 59. p. 7-55.

Peacock, D. C. P., 2001. The temporal relationship between joints and faults. Journal of Structural Geology. v. 23. no. 2. p. 329-341.

Peacock, D. C. P., and Mann, A., 2005. Evaluation of the Controls on Fracturing in Reservoir Rocks. Journal of Petroleum Geology. v. 28. no. 4. p. 385-396.

Peacock, D. C. P., and Sanderson, D. J., 1991. Displacements, segment linkage and relay ramps in normal fault zones. Journal of Structural Geology. v. 13. no. 6. p. 721-733.

Peacock, D. C. P., and Sanderson, D. J., 1994. Geometry and development of relay ramps in normal fault systems. AAPG Bulletin. v. 78. no. 2. p. 147-165.

Petit, J.-P., and Mattauer, M., 1995. Palaeostress superimposition deduced from mesoscale structures in limestone: the Matelles exposure, Languedoc, France. Journal of Structural Geology. v. 17. no. 2. p. 245-256.

Pohn, H. A., 1981. Joint spacing as a method of locating faults. Geology. v. 9. no. 6. p. 258-261.

Pollard, D., and Segall, P., 1987. Theoretical displacements and stresses near fractures in rock: with applications to faults, joints, veins, dikes, and solution surfaces. Fracture mechanics of rock. v. 277. no. 349. p. 277-349.

Pollard, D. D., and Aydin, A., 1988. Progress in understanding jointing over the past century. Geological Society of America Bulletin. v. 100. no. 8. p. 1181-1204.

Rawnsley, K. D., Peacock, D. C. P., Rives, T., and Petit, J.-P., 1998. Joints in the Mesozoic sediments around the Bristol Channel Basin. Journal of Structural Geology. v. 20. no. 12. p. 1641-1661.

Renshaw, C. E., and Pollard, D. D., 1995. An Experimentally Verified Criterion for Propagation Across Unbounded Frictional Interfaces in Brittle, Linear Elastic Materials. International journal of rock mechanics and mining sciences & geomechanics abstracts. v. 32. no. 3. p. 237-249.

Richardson, M., and Arthur, M. A., 1988. The Gulf of Suez-northern Red Sea Neogene rift: a quantitive basin analysis. Marine and Petroleum Geology. v. 5. no. 3. p. 247-270.

Rippon, J. H., 1984. Contoured patterns of the throw and hade of normal faults in the Coal Measures (Westphalian) of north-east Derbyshire. Proceedings of the Yorkshire Geological Society. v. 45. no. 3. p. 147-161.

Rives, T., Razak, M., Petit, J.-P., and Rawnsley, K. D., 1992. Joint spacing: analogue and numerical simulations. Journal of Structural Geology. v. 14. no. 8-9. p. 925-937.

Robson, D. A., 1971. The structure of the Gulf of Suez (Clysmic) rift, with special reference to the eastern side. Journal of the Geological Society. v. 127. no. 3. p. 247-271.

Rotevatn, A., and Bastesen, E., 2012. Fault linkage and damage zone architecture in tight carbonate rocks in the Suez Rift (Egypt): implications for permeability structure along segmented normal faults. *In*: Spence, G. H., Redfern, J., Aguilera, R., Bevan, T. G., Cosgrove, J. W., Couples, G. D. & Daniel, J.-M. (eds.). *Advances in the Study of Fractured Reservoirs*. Geological Society, London, Special Publications. v. 374.

Rotevatn, A., Buckley, S. J., Howell, J. A., and Fossen, H., 2009. Overlapping faults and their effect on fluid flow in different reservoir types: a LIDAR-based outcrop modeling and flow simulation study. AAPG Bulletin. v. 93. no. 3. p. 407-427.

Rotevatn, A., Fossen, H., Hesthammer, J., Aas, T. E., and Howell, J. A., 2007. Are relay ramps conduits for fluid flow? Structural analysis of a relay ramp in Arches National Park, Utah. *In*: Lonergan, L., Jolly, R. J. H., Sanderson, D. J. & Rawnsley, K. (eds). *Fractured Reservoirs*. Geological Society, London, Special Publications. v. 270. p. 55-71.

Salah, M. G., and Alsharhan, A. S., 1997. The Miocene Kareem Formation in the southern Gulf of Suez, Egypt: A review of stratigraphy and petroleum geology. Journal of Petroleum Geology. v. 20. no. 3. p. 327-346.

Samuel, M. D., Ismail, A. A., Akarish, A. I. M., and Zaky, A. H., 2009. Upper Cretaceous stratigraphy of the Gebel Somar area, north-central Sinai, Egypt. Cretaceous Research. v. 30. no. 1. p. 22-34.

Schlische, R. W., and Anders, M. H., 1996. Stratigraphic effects and tectonic implications of the growth of normal faults and extensional basins. *In*: Beratan, K.K., (eds.). *Reconstructing the History of Basin and Range Extension Using Sedimentology and Stratigraphy.* Geological Society of America, Special Publication. v. 303. p. 183-203.

Scholz, C. H., Dawers, N. H., Yu, J. Z., Anders, M. H., and Cowie, P. A., 1993. Fault Growth and Fault Scaling Laws: Preliminary Results. Journal of Geophysical Research. v. 98. no. B12. p. 21951-21961.

Schueller, S., Braathen, A., Fossen, H., and Tveranger, J., in press. Spatial distribution of deformation bands in damage zones of extensional faults in porous sandstones: Statistical analysis of field data. Journal of Structural Geology.

Schütz, K. I., 1994. Structure and Stratigraphy of the Gulf of Suez, Egypt. *In*: Landon, S. M. (eds.). *Interior Rift Basins.* AAPG Memoirs. v. 59. p. 57-96.

Scott, R. W., and Govean, F. M., 1985. Early depositional history of a rift basin: Miocene in Western Sinai. Palaeogeography, Palaeoclimatology, Palaeoecology. v. 52. no. 1–2. p. 143-158.

Secor, D. T. J., 1965. Role of fluid pressure in jointing. American Journal of Science. v. 263. no. 8. p. 633-646.

Sepúlvda, N., and Zack, A. L., 1991. The effects of overburden stress on the specific storage and hydraulic conductivity of artesian aquifers. Journal of Hydrology. v. 128. no. 1-4. p. 305-321.

Shaocheng, J., Zheming, Z., and Zichao, W., 1998. Relationship between joint spacing and bed thickness in sedimentary rocks: effects of interbed slip. Geological Magazine. v. 135. no. 5. p. 637-655.

Sharp, I. R., Gawthorpe, R. L., Armstrong, B., and Underhill, J. R., 2000a. Propagation history and passive rotation of mesoscale normal faults: implications for synrift stratigraphic development. Basin Research. v. 12. no. 3-4. p. 285-305.

Sharp, I. R., Gawthrope, R. L., Underhill, J. R., and Gupta, S., 2000b. Fault-propagation folding in extensional settings: Examples of structural style and synrift sedimentary response from the Suez rift, Sinai, Egypt. Geological Society of America Bulletin. v. 112. no. 12. p. 1877-1899.

Shipton, Z., and Cowie, P., 2001. Damage zone and slip-surface evolution over μm to km scales in high-porosity Navajo sandstone, Utah. Journal of Structural Geology. v. 23. no. 12. p. 1825-1844.

Shipton, Z., and Cowie, P., 2003. A conceptual model for the origin of fault damage zone structures in high-porosity sandstone. Journal of Structural Geology. v. 25. no. 3. p. 333-344.

Sibson, R. H., 1996. Structural permeability of fluid-driven fault-fracture meshes. Journal of Structural Geology. v. 18. no. 8. p. 1031-1042.

Soliva, R., and Benedicto, A., 2004. A linkage criterion for segmented normal faults. Journal of Structural Geology. v. 26. no. 12. p. 2251-2267.

Soliva, R., Benedicto, A., Schultz, R., Maerten, L., and Micarelli, L., 2008. Displacement and interaction of normal fault segments branched at depth: implications for fault growth and potential earthquake rupture size. Journal of Structural Geology. v. 30. no. 10. p. 1288-1299.

Sperrevik, S., Færseth, R. B., and Gabrielsen, R. H., 2000. Experiments on clay smear formation along faults. Petroleum Geoscience. v. 6. no. 2. p. 113-123.

Trudgill, B., and Cartwright, J. A., 1994. Relay-ramp forms and normal-fault linkages, Canyonlands National Park, Utah. Geological Society of America Bulletin. v. 106. no. 9. p. 1143-1157.

van der Pluijm, B. A., and Marshak, S., 2004. Earth Structure: An Introduction to Structural Geology and Tectonics. W. W. Norton & Company.

Vermilye, J. M., and Scholz, C. H., 1998. The process zone: A microstructural view of fault growth. Journal of Geophysical Research. v. 103. no. B6. p. 12223-12237.

Vermilye, J. M., and Scholz, C. H., 1999. Fault propagation and segmentation: insight from the microstructural examination of a small fault. Journal of Structural Geology. v. 21. no. 11. p. 1623-1636.

Walsh, J. J., Bailey, W. R., Childs, C., Nicol, A., and Bonson, C. G., 2003. Formation of segmented normal faults: a 3-D perspective. Journal of Structural Geology. v. 25. no. 8. p. 1251-1262.

Walsh, J. J., Nicol, A., and Childs, C., 2002. An alternative model for the growth of faults. Journal of Structural Geology. v. 24. no. 11. p. 1669-1675.

Walsh, J. J., and Watterson, J., 1988. Analysis of the relationship between displacements and dimensions of faults. Journal of Structural Geology. v. 10. no. 3. p. 239 - 247.

Watterson, J., 1986. Fault Dimensions, Displacements and Growth. Pure and Applied Geophysics. v. 124. no. 1/2. p. 365-373.

Wu, H., and Pollard, D. D., 2002. Imaging 3-D fracture networks around boreholes. AAPG Bulletin. v. 86. no. 4. p. 593-604.

Yielding, G., Freeman, B., and Needham, D. T., 1997. Quantitative fault seal prediction. AAPG Bulletin. v. 81. no. 6. p. 897-917.

Young, M. J., Gawthorpe, R. L., and Sharp, I. R., 2003. Normal fault growth and early syn-rift sedimentology and sequence stratigraphy: Thal Fault, Suez Rift, Egypt. Basin Research. v. 15. no. 4. p. 479-502.

Background fractures Wadi Dolly 1

Thebes Fm.
Profile: 160°
Start: 36R 0498679 3229915

Distance (m)	Fractures	Orientation	Lithology	Comments
1	5	220/89, 164/70, 182/85	Grainstone ↓	
2	2	191/85		
3	8	200/86		
4	3	200/70		
5	6	215/80		
6	4	214/84, 196/89		
7	4	213/87		
8	4	200/87, 130/86		
9	4			
10	15	250/70, 240/90,	Mudstone ↓	
11	11	200/90		
12	7			
13	11	280/85		
14	9	242/87		
15	3	204/78		
16	13	220/88, 288/87		
17	7			
18	7			
19	8	215/72, 260/88		
20	10			
21	11	160/40, 210/89		
22	13	218/85		
23	8			
24	10	226/85, 230/90, 191/69		
25	14	180/82		
26	12			
27	7			
28	11			
29	7	243/60		
30	8	226/85		
31	6			
32	7			
33	10			
34	8			
35	7			
36	6			
37	7			
38	4			

Background fractures Wadi Dolly 2

Thebes Fm.
Profile: 160°
Start: 36R 0498679 3229915

Distance (m)	Fractures	Orientation	Lithology	Comments
1	5	039/75, 238/82	Grainstone ↓	
2	10			
3	6			
4	7	201/83		
5	7	200/89		
6	4			
7	4			
8	3	204/80		
9	3			
10	5			
11	5	190/87		
12	6			
13	3			
14	4			
15	3			
16	3	291/89		
17	4			
18	3			
19	2			
20	3	262/50		
21	2			
22	4			
23	2			
24	6	134/80		
25	6			
26	3			
27	6			
28	8			
29	2	200/84		
30	3			
31	3			
32	5	190/72		
33	2			
34	3			
35	3			
36	2			
37	3			
38	2			

APPENDIX: Scanlines

Background fractures Wadi Dolly 3

Thebes Fm.
Profile (240° (10m) -> 300°)
36R 0498640 3229781

Distance (m)	Fractures	Orientation	Lithology	Comments
1	3	330/50	Packstone ↓	
2	6			
3	6			
4	5	358/80		
5	5			
6	4	110/78		
7	8			
8	6			
9	6			
10	14			10-15 m: fracture corridor
11	12	190/82		
12	x			
13	x			
14	9	154/79		
15	12	230/78		
16	8			
17	7	145/85		
18	6	213/88		
19	11	205/90		
20	8			
21	8			
22	5	206/30		
23	6			
24	7	209/63		
25	8			
26	12			

APPENDIX: Scanlines

Background fractures Wadi Tayeba

Thebes Fm.
Profile: 80°
Start: 36R 0497322 03233056

Distance (m)	Fractures grainstone	Fractures mudstone	Orientations
1	3	10	356/80
2	4	6	346/78
3	4	8	350/89
4	6	8	328/84
5	3	3	
6	4	10	184/78
7	4	6	
8	4	6	112/88
9	2	5	010/85
10	3	6	
11	4	10	
12	5	11	198/75
13	4	14	
14	3	10	356/87
15	2	10	178/85
16	2	10	356/89
17	3	5	
18	3	7	308/80
19	3	7	
20	1	9	
21	3	12	
22	3	10	
23	4	14	170/71
24	4	4	
25	5	4	002/90
26	x	6	014/89
27	x	7	
28	x	10	
29	x	10	
30	x	8	

LWWF 1 fw

Footwall
Thebes Fm. Wacke/packstone
Start: 36R 499808 3232083

Distance (m)	Fractures	Orientations	Comments
1	19	338/86	
2	16	336/90	
3	24	342/80	
4	16	152/88	
5	16	150/88	
6	17		
7	16		

APPENDIX: Scanlines

LWWF 1 hw

Hanging wall
Thebes Fm. Wacke/packstone
Start: 36R 499808 3232083

Distance (m)	Fractures	Orientations	Comments
0-7	x	325/79	Hairlines
8	16	332/74	One fracture: 1 cm wide with calcite fill
9	19	202/70	
10	15	340/80	
11	14	342/86	
12	9	350/86	
13	11	332/85	
14	13		
15	19		
16	16		
17	18		
18	17		
19	18		
20	14		
21	12		
22	8		
23	10		
24	25		
25	31		
26	18		
27	12		
28	10		
29	10		
30	11		
31	12		

LWWF 2 fw

Footwall
Thebes Fm. Wacke/packstone
Start: 36R 499839 3231958

Distance (m)	Fractures	Orientations	Comments
1	25	146/88	Hairlines
2	26	142/89	
3	10	162/90	
4	15	150/90	
5	20	150/90	

APPENDIX: Scanlines

LWWF 2 hw

Hanging wall
Thebes Fm. Wacke/packstone
Start: 36R 499839 3231958

Distance (m)	Fractures	Orientations	Comments
1	40	338/74	Hairlines
2	69	329/82	Two fractures (1 cm width) with calcite
3	34	332/90	fill.
4	27	328/89	Sub-parallel fractures to the fault are
5	32		more than 10 meters long.
6	36		
7	45		
8	23		
9	31		
10	31		
11	20		
12	26		
13	32		
13-18	x		
19	33		
20	24		
21	20		
22	14		
23	7		
24	12		
25	8		
26	13		
27	10		
28	7		
29	13		
30	3		

APPENDIX: Scanlines

LWWF 3 hw

Hanging wall
Thebes Fm. Wacke/packstone
Start: 36R 500144 3231458

Distance (m)	Fractures	Orientations	Comments
0-30	x	348/60	Generally hairlines
31	46	316/85	
32	36	320/80	
33	13	318/76	One calcite fracture, 1 cm width
34	22	330/80	
35	21	340/88	
36	18	338/77	
37	19	335/80	
38	18	333/77	
39	11	001/86	
40	7	010/80	
41	8	008/78	
42	6	005/88	
43	17	358/90	
44	78	090/80	44-50 meter = stockwork fractures
45	69	275/88	
46	46		
47	48		
48	57		
49	63		
50	59		

APPENDIX: Scanlines

WWF 1 fw

Footwall
Thebes Fm. Wacke/packstone
Start: 36R 0500312 3231404
Stop: 36R 0500277 3231387

Distance (m)	Fractures	Orientation	Comments
1	44	045/23	
2	58	325/09	
3	86	338/06	Bedding: 335/50
4	99		
5	131		
6	62		
7	94	244/50	
8	108	167/00	Horizontal fracture: 40 mm gap
9	136		
10	51	124/54	
11	31	170/30	Fe minerals.
12	60	315/69	
13	39	125/88	
14	52	122/68	Vertical fractures, fracture with 10 mm
15	36	147/57	calcite cement
16	23		
17	21	140/70	
18	40	291/88	Chert lenses, two calcite fractures (10 and 55 mm)
19	45	108/87	
20	36	138/65	
21	48	152/72	
22	49	305/60	
23	44	307/70	Fe minerals
24	36	141/68	
25	58		
26	55	151/58	
27	54	143/70	
28	x		
29	x		
30	x		
31	x		
32	x		
33	x		
34	x		
35	x		
36	22		
37	24	160/80	
38	26	160/80	
39	38	160/78	Bedding: 290/29
40	31	150/71	
41	32		
42	x		
43	x		
44	x		
45	x		
46	15	340/80	
47	17		
48	23		

49	21	225/80	
50	14		Generally: Hairlines, calcite cement.
51	20		Biggest fractures are horizontal when
52	20		counting on the top, while the biggest
53	24		are vertical when counting on the side.
54	21		
55	27		

APPENDIX: Scanlines

WWF 1 hw

Hanging wall
Tanka Fm.
Start: 36R 0500324 3231408
Stop: 36R 0500353 3231450

Distance (m)	Fractures	Orientation	Comments
1	34	160/90	
2	30	120/85	
3	60	140/90	
4	42	310/60	
5	64		
6	33	120/80	
7	52		
8	59	340/85	
9	26	095/70, 090/80	
10	22		
11	41		
12	23	120/80, 140/70	
13	16	135/70, 210/85	
14	36	155/67	
15	23	021/52, 325/61	
16	24	124/82, 012/83	
17	18	143/76, 124/79	
18	22	073/87, 131/79	
19	17	151/74	
20	19	058/53	
21	24	104/71, 124/69	
22	15	062/82, 132/87	
23	17	067/78, 324/82	
24	17	142/87, 192/89	
25	10	316/85, 165/88	
26	17	340/87	
27	18	122/88	
28	14	074/86	
29	19		
30	16		
31	19		
32	23		
33	16	041/88, 082/84	
34	23	148/81	
35	15	180/80, 070/90	
36	15	090/69, 080/65	2 fractures with 10 mm gap
37	21	140/70, 120/70	1 fracture with 70 mm gap, calcite
38	20	060/75, 080/70	1 fracture with 10 mm gap
39	20	075/70, 135/70	Calcite
40	24	120/75, 095/75	1 fracture with 60 mm gap
41	18	180/70	
42	14	000/20	
43	11	050/90	
44	8	265/70	
45	21	108/82	
46	24	100/88	
47	14	165/76	
48	18	152/83, 090/84	
49	19	160/67, 005/70	

50	18	253/88	
51	15	162/82	
52	15	077/88	Generally: Bigger fractures and more hematite near the fault core. Most of the fractures were bed bound, only some of the biggest crossed other beds. The biggest fractures were vertical and had an N/S orientation.
53	10	061/88	
54	22	074/83	
55	17	240/85	
56	11	130/75	
57	9	145/80	
58	14	14/80	

APPENDIX: Scanlines

WWF 2 fw

Footwall
Thebes Fm. Wacke/packstone
Start: 36R 0500315 3231368
Stop: 36R 0500296 3231350

Distance (m)	Fractures	Orientation	Comments
1	12		
2	32		
3	29		
4	89		Stockwork fractures
5	39	160/67	
6	39		
7	x		
8	41		
9	29	131/73	
10	18	302/88	
11	24		
12	17		
13	14		
14	29		One fracture: 16 mm gap
15	31		
16	20		
17	21		
18	27		
19	37		Generally: Hairlines and calcite cement.
20	18		

WWF 3 hw

Hanging wall
Darat Fm. Wacke/mudstone
Start: 36R 0500485 3230990
Stop: 36R 0500494 3230982
Fault: 350/60

Distance (m)	Fractures	Orientations	Comments
1	111		
2	65		
3	54		
4	42		
5	46		
6	35		
7	34		
8	36		
9	x		
10	x		
11	29		
12	29		
13	22		
14	53		Stockwork fractures
15	33		
16	31		
17	30		
18	23		

APPENDIX: Scanlines

WWF 4 hw

Hanging wall
Profile 080° (14 m) -> 124°
Darat Fm. Wacke/mudstone
Start: 36R 0500512 3230755
Stop: 36R 0500527 3230748
Fault: 336/62

Distance (m)	Fractures	Orientations	Comments
1	52		Weathered surface, making it difficult to measure. May be more fractures
2	48	158/68	
3	45		
4	38		
5-13	x		
14	23	245/58, 252/60	
15	11	242/45	
16	14	238/43	
17	10	044/32	
18	11		
19	10		
20	13	227/66	
21	11		
22	9	235/62	
23	13		
24	15		
25	12	230/74	

WWF 5 hw

Hanging wall
Darat Fm. Wacke/mudstone
Start: 36R 0500556 3230645
Stop: 36R 0500570 3230629
Fault: 011/66

Distance (m)	Fractures	Orientations	Comments
0-6	x		
7	49		
8	38		
9	30		
10	33		
11	29		
12	54	220/68	
13	43	080/90, 260/72, 255/68	
14	35	262/80	
15	24		
16	21	184/75	

APPENDIX: Scanlines

WWF 6 hw

Hanging wall
Darat Fm. Wacke/mudstone
Start: 36R 0500555 3230556
Stop: 36R 0500568 3230533
Fault: 004/65

Distance (m)	Fractures	Orientations	Comments
0-4	x		
5	44		
6	29		
7	28		
8	26	190/70	
9	24	210/81	
10	29		
11	21	263/88	
12	31	020/90, 023/89	
13	16	036/80	
14	25		
15	30	202/70	
16	20	047/78, 041/85	
17	14		
18	17	018/78	
19	26	038/80	

WWF 7 hw

Hanging wall
Thebes Fm. Wacke/packstone
Start: 36R 0500520 3230458
Stop: 36R 0500545 3230453

Distance (m)	Fractures	Orientations	Comments
0-11	x		
12	20		
13	14	012/90, 003/90	
14	16	009/85	
15	18		
16	21		
17	13	069/70	
18	14		
19	11	114/70, 310/73	
20	17	152/69	
21	9	311/82	
22	7	348/82	
23	6	162/90	
24	7		
25	9	120/70	
26	7	140/70	
27	10	319/79	
28	11	024/68	
29	7	154/90	
30	9	139/78	
31	7	014/58	

WWF 8 hw

Hanging wall
Thebes Fm. Wacke/packstone
Profile: 093°
Start: 36R 0500531 3230455
Stop: 36R 0500553 3230459

Distance (m)	Fractures	Orientation	Comments
1	33		
2	44		
3	43		
4	46		
5	38		
6	32	151/62	
7	33		
8	24		
9	22		
10	23	339/82	
11	14		
12	18		
13	19	032/58 – 133/72	
14	20	027/82	
15	18	016/59	
16	16	023/63	
17	13		
18	15	020/60	
19	13		
20	17		Generally: Hairlines and calcite cement.
21	8		

WWF 9 hw

Hanging wall
Thebes Fm. Wacke/packstone
Profile: 035°
Start: 36R 0500484 3230353
Stop: 36R 0500503 3230352

Distance (m)	Fractures	Orientation	Comments
1	100+	006/60	
2	100+		
3	100+		
4	55	000/82	
5	50	028/83	
6	61	176/82	
7	47		
8	63		
9	x		
10	54		
11	44		
12	36		
13	53		
14	41	048/79	
15	46	032/87	
16	57	223/76	
17	49	223/89	
18	40	320/67	
19	49	228/73	
20	31	050/64	
21	29	228/85	
22	30	032/83	
23	41		
24	32		
25	24	259/79	
26	22		
27	27		Generally: Hairlines and calcite cement.
28	29		

WWF 10 fw

Footwall
Thebes Fm. Wacke/packstone
Profile: 214°
Start: 36R 0500489 3230304
Stop: 36R 0500467 3230292

Distance (m)	Fractures	Orientation	Comments
1	72		
2	35		
3	32		
4	44		Weathered
5	45		Weathered
6	47		Weathered
7	44		
8	37		
9	44		
10	43		
11	31		
12	34		
13	37		
14	35		Weathered
15	x		
16	31		
17	36		
18	35		
19	38	130/69	
20	36		
21	25		
22	42		
23	33	152/62	
24	29		
25	26		
26	21		
27	22		
28	20		Generally: Hairlines and calcite cement.
29	20	090/67	
30	19		

WWF 10 hw

Hanging wall
Thebes Fm. Wacke/packstone
Profile: 214°
Start: 36R 0500489 3230304
Stop: 36R 0500520 3230320 (+- 13 m)

Distance (m)	Fractures	Orientation	Comments
1	85		
2	68		
3	63		
4	44		Weathered
5	49		
6	58		
7	58		
8	51		
9	39		
10	36		
11	46		
12	45		
13	57		
14	36		
15	38		
16	42		
17	35		
18	38		
19	34	214/81	
20	37		
21	42		
22	43		
23	37		
24	33		
25	45		
26	36		
27	38		
28	24		Generally: Hairlines and calcite cement.
29	34		Chert nodules.
30	33		

APPENDIX: Scanlines

WWF 11 hw

Profile 050°
Thebes Fm. Wacke/packstone
Start: 36R 0500448 3230065 (3230088)
Stop: 36R 0500448 3230093

Distance (m)	Fractures	Orientations	Comments
0-27	x		
28	18	204/80, 180/82	
29	13	191/68	
30	15		
31	13	351/87	
32	14		
33	17		
34	17	176/78, 183/72	
35	13	172/78	
36	14	342/77	
37	13	170/88	
38	15	016/90	
39	19	147/87	
40	25	190/88	

WWF 12 hw

Profile 070° (12 m) -> 090°
Thebes Fm. Wacke/packstone
Start: 36R 0500438 3229734
Stop: 36R 0500464 3229725
Fault: 307/60

Distance (m)	Fractures	Orientations	Comments
1	49	188/79, 194/84	
2	31	158/85	
3	24	301/80	
4	12	010/90, 050/80	
5	10	122/82	
6	10	126/60	
7	7	020/71	
8	8	043/86	
9	13	108/82, 037/80	
10	11		
11	13	041/89, 125/70	
12	23	028/82, 024/84	
13	16	298/71, 010/79	
14	19	010/80, 126/76	
15	14	306/72	
16	16	292/66	
17	13	292/75, 294/75	
18	14	304/74, 306/72	
19	6	186/90, 196/90	

WWF 13 hw

Profile 040°
Thebes Fm. Wacke/packstone
Start: 36R 0500501 3229622
Stop: 36R 0500512 3229633
Fault: 322/70

Distance (m)	Fractures	Orientations	Comments
1	x		
2	x		
3	x		
4	92	291/82, 190/85, 304/81	
5	63	137/90, 142/90	
6	34	307/84, 320/63, 215/84, 039/80	
7			
8	46	037/78, 038/80, 059/80	
9	47	040/72, 240/90, 045/88	
10	31	042/71, 148/90	
11	18	196/82, 165/72	
12	32	170/75	
13	23		
14	19	182/82, 029/89	
15	24		
16	15	180/90, 190/90	
17	16	345/84	

APPENDIX: Scanlines

WWF 14 fw

Profile 257° (10 m) -> 300°
Thebes Fm. Grainstone
Start: 36R 0500672 3229333
Stop: 36R 0500641 3229351
Fault: 328/65

Distance (m)	Fractures	Orientations	Comments
1	35		
2	14	131/71, 129/73, 182/81	
3	22	290/85	
4	20	123/80, 178/79	
5	9		
6	8	114/60	
7	15	320/72, 130/70	
8	10		
9	8	344/62	
10	19		
11	9	038/80	
12	22	319/89	
13	34	300/75	Fault or fracture corridor oriented
14	44		228/80
15	14		
16	18	198/78	
17	16		
18	20		
19	17	298/80	
20	15	178/86	
21	11	151/62	
22	17		
23	10	052/87	
24	22	118/79	
25	14	213/76	
26	5	052/80	
27	13		
28	10	218/78	
29	7	234/62	
30	2		
31	9	184/70	
32	8		
33	7		
34	7	238/65	
35	11		
36	6	184/63	
37	7		
38	6	185/62	
39	7		
40	6	143/86	

APPENDIX: Scanlines

WWF 14 hw

Profile 060°
Thebes Fm. Grainstone
Start: 36R 0500672 3229333
Stop: 36R 0500686 3229348
Fault: 328/65

Distance (m)	Fractures	Orientations	Comments
1	39	121/68	
2	24		
3	19	308/60	
4	29	141/21	
5	32		
6	x		Fault?
7	18	134/80, 138/80, 138/69	
8	12	130/80	
9	19	115/88	
10	9	128/82	
11	12		
12	14		
13	16		
14	13		
15	18		
16	10	108/78	
17	15		
18	11		
19	15	120/82	
20	12		

TRF 1 hw

Hanging wall
Profile 040°
Darat Fm. Wacke/packstone
Start: 36R 0501734 3229260
Stop: 36R 0501737 3229267
Fault: 346/85

Distance (m)	Fractures	Orientations	Comments
1	100+		
2	82		
3	67	105/80, 310/80	Anastomosing fractures
4	48	140/73	
5	65	142/70	
6	49		Weathered surface
7	35		
8	38	332/80	
9	46	154/82	

APPENDIX: Scanlines

TRF 2 fw

Footwall
Profile 266°
Thebes Fm. Wackestone
Start: 36R 0501843 3228576
Stop: 36R 0501815 03228577

Distance (m)	Fractures	Orientations	Comments
1	45	030/87	Anastomosing fractures ↓
2	51	200/75	
3	45	352/79	
4	29	230/80	Conjugate fracture network ↓
5	23	239/89	
6	20	214/75	
7	22	315/60	
8	24	022/70	
9	15	200/58	
10	22	159/55	
11	25	191/60	
12	x	359/56	
13	12	348/66	
14	11		
15	13	140/75	
16	x	156/82	
17	x		
18	19	058/85	
19	13		
20	7		
21	10	016/80	
22	10	260/85	
23	13	040/85	
24	12	042/88	
25	15	390/75	Distributed fracture network ↓
26	22		
27	12	140/55	
28	12		
29	13		
30	9		
31	6		
32	13		

TRF 2 hw

Hanging wall
Profile (108° (24m) -> 020° (51m) -> 070°)
Start: 36R 0501758 3228609

Distance (m)	Fractures	Orientations	Comments	Lithology
1	x		Fault: 002/58	
2	x		Fault rock lenses	
3	106	218/78, 204/71, 088/75, 054/86		Wacke/packstone↓
4	61			
5	55			
6	54			
7	51	247/62, 021/69		
8	x			
9	x			
10	x			
11	42			Mudstone ↓
12	73			
13	45	203/68		
14	59			
15	48	204/19		
16	54			
17	46	205/60		
18	x			
19	x			
20	x			
21	x			
22	x			
23	x			
24	x			
25	x			
26	x			
27	x		Fault: 001/60	
28	x			
29	x			
30	x			
31	77		Stockwork network	Mud/wackestone ↓
32	46	282/70		
33	50	287/89		
34	33	025/52, 042/78		
35	30	033/62, 022/70		
36	47			
37	31			
38	x			
39	x			
40	x			
41	x			
42	x			
43	x			
44	x			
45	x			
46	x			
47	x			
48	x			
49	x			

50	x			
51	42			Pack/wackestone ↓
52	38			
53	45			
54	38			
55	28			
56	25			
57	25	216/70	Large fracture or fault: 004/90	
58	16	222/78, 250/60		
59	20			
60	20	204/70		
61	36			
62	32	190/70, 196/70		
63	23			
64	26	220/69	Fracture corridor: 40 cm wide with	
65	18		calcite cement	
66	25	090/90, 192/82		
67	29	220/70, 200/78, 118/90, 210/73		
68	28			
69	30			
70	26			
71	11			
72	11			
73	10			
74	18			
75	16			

TRF 3 hw

Hanging wall
Profile 130°
Thebes Fm. Wacke/packstone
Start: 36R 0501662 3228078
Fault: 006/83

Distance (m)	Fractures	Orientations	Comments
1	34	208/75, 212/58	Weathered surface, may be more
2	33	049/38, 209/58	fractures than measured
3	31	175/78, 185/90	Anastomosing fractures
4	29	158/90, 024/79	
5	26	030/55	

APPENDIX: Scanlines

TRF 4 hw

Hanging wall
Profile 060°
Thebes Fm. Wacke/packstone
Start: 36R 0501675 3227721
Stop: 36R 0501679 3227719

Distance (m)	Fractures	Orientations	Comments
1	30	178/70, 178/80, 160/82	Scanline may not start at the fault core
2	19	124/62	
3	13	168/82	
4	19	158/76, 163/72	
5	12	290/76	
6	13	290/78	
7	12	280/85	
8	9	194/82	
9	22	294/85	
10	15	332/42	

TRF 5 hw

Hanging wall
Profile 110°
Thebes Fm. Wacke/packstone
Start: 36R 0501676 3227694
Stop: 36R 0501701 3227692
Fault: 340/82

Distance (m)	Fractures	Orientations	Comments
1	36	154/78, 095/56	Anastomosing fractures
2	34	338/80, 158/90, 158/80	
3	17	156/63	
4	21	333/82, 060/84	
5	9	156/78	
6	18	086/78, 075/88	
7	28	155/80	
8	15	156/76	
9	18	252/70, 150/90	
10	11	272/59, 260/88, 067/89	

APPENDIX: Scanlines

TRF 6 fw

Profile 260°
Thebes Fm. Wacke/packstone
Start: 36R 0501755 3227449
Stop: 36R 0501747 3227448
Fault: 358/68

Distance (m)	Fractures	Orientations	Comments
1	42		
2	30		
3	30	190/63	
4	21	210/78	Anastomosing fractures
5	26	109/80	
6	24		
7	22	199/66, 200/71	Weathered surface, difficult to measure
8	20		
9	20	202/76	
10	18	090/90, 227/80	
11	13		
12	15	217/85	
13	17		
14	13	192/82	

TRF 6 hw

Profile 040°
Thebes Fm. Wacke/packstone
Start: 36R 0501755 3227449
Stop: 36R 0501762 3227450
Fault: 358/68

Distance (m)	Fractures	Orientations	Comments
1	x		Lineation: 70 -> 270
2	100+	158/72, 196/80	Anastomosing fractures
3	100+	317/87	
4	77	095/90	
5	63		
6	63	212/78, 201/80	
7	42	132/80	
8	38		

APPENDIX: Scanlines

The ramp, Darat transect 1

Profile 260°
Darat Fm. Mud/wackestone
Start: 36R 0501185 3230398
Stop: 36R 0501175 3230399

Distance (m)	Fractures	Orientations	Comments
1	19	202/82	
2	15		
3	15	181/86, 200/80	
4	13		
5	16	195/83	
6	23		
7	18	015/90	
8	33	311/82	
9	46	185/84, 300/80, 099/79	
10	16	007/86, 010/90	
11	19	005/71	
12	11	016/82, 018/89	

The ramp, Darat transect 2

Profile 270°
Darat Fm. Mud/wackestone
Start: 36R 0501250 3230258
Stop: 36R 0501211 3230261

Distance (m)	Fractures	Orientations	Comments
1	11	036/86	
2	11	039/87	
3	8		
4	17	052/84	
5	13		
6	11		
7	7		
8	8		
9	10		
10	6		
11	7		
12	6	186/75	
13	4	048/90	
14	8		
15	7		
16	5	180/78	
17	6	181/84	
18	5		
19	5		
20	4		
21	4	038/82, 186/82	
22	7		
23	6		
24	4	185/79	
25	7		
26	8	195/85	
27	4		
28	4	180/80, 191/81	
29	5	180/79	

30	4	
31	3	184/81, 171/82
32	8	
33	8	205/80
34	5	
35	4	192/75
36	5	

APPENDIX: Scanlines

The ramp, Darat transect 3

Profile 270°
Darat Fm. Mud/wackestone
Start: 36R 0501332 3230310
Stop: 36R 0501297 3230313

Distance (m)	Fractures	Orientations	Comments
1	13		
2	7		
3	4		
4	6		
5	8		
6	14		
7	9	138/82	
8	11		
9	14		
10	9	066/90	
11	7		
12	8		
13	6	063/82	
14	5		
15	6		
16	4		
17	7		
18	8		
19	10		
20	11	060/83	
21	6	061/71, 054/81	
22	7		
23	9		
24	4		
25	8		
26	8		
27	8		
28	12	135/75	
29	14	133/90	
30	11	128/76	
31	8	037/90, 120/80	
32	8		
33	4		
34	7		
35	9	131/85, 138/82, 001/65	

APPENDIX: Scanlines

The ramp, Darat transect 4

Profile 280°
Darat Fm. Mud/wackestone
Start: 36R 0501351 3230420
Stop: 36R 0501323 3230427

Distance (m)	Fractures	Orientations	Comments
1	3	194/88	Bedding: 298/20
2	6	204/86, 204/87	
3	4	203/84	
4	3		
5	7	204/87	
6	6	046/87	
7	7	032/80, 024/82	
8	8	204/89	
9	7	176/80, 198/85	
10	9	031/79	
11	7	063/72	
12	5	035/74	
13	7	196/87	
14	8	193/82	
15	5		
16	5	135/88	
17	7	190/89	
18	13	029/82	
19	6	199/87, 020/87	
20	9		
21	6	025/90	
22	x		
23	x		
24	x		
25	x		
26	8	179/81	
27	10	192/83	
28	16	190/84	
29	11		
30	11	029/70	
31	6		
32	5	190/87	
33	4	023/78	

APPENDIX: Scanlines

The ramp, Darat transect 5

Profile 264°
Darat Fm. Mud/wackestone
Start: 36R 0501359 3230315
Stop: 36R 0501344 3230317

Distance (m)	Fractures	Orientations	Comments
1	7	110/60	
2	10	180/79	
3	10	170/90	
4	7	180/90	
5	8		
6	7	178/90	
7	8		
8	5	092/73	
9	6		
10	5		
11	9		
12	3	002/60	
13	8	184/79	
14	8		
15	14		

The ramp, Darat transect 6

Profile 270°
Darat Fm. Mud/wackestone
Start: 36R 0501436 3230337
Stop: 36R 0501373 3230352

Distance (m)	Fractures	Orientations	Comments
1	11	180/70	
2	14	177/70	
3	14	178/68	
4	13	009/89	
5	14		
6	10	180/72	
7	11	184/80	
8	4	186/70	
9	8		
10	10	186/82	
11	13		
12	6		
13	6	183/72	
14	8	188/80	
15	5	178/72	
16	10	188/90	
17	7	190/85	
18	7	198/70	
19	8		
20	7		
21	6	187/78	
22	6		
23	7	178/77	
24	12		
25	8		
26	4		
27	5		
28	6		
29	8		
30	7	193/82	
31	7		
32	3		
33	5	172/76	
34	5		
35	3		
36	5	023/90	
37	4		
38	5	185/69	
39	7	200/70	
40	6		
41	5		
42	3	183/86	
43	6		
44	4		
45	3	042/78	
46	5	039/73	
47	7		
48	6	020/90	
49	14		

APPENDIX: Scanlines

50	6	
51	5	
52	3	
53	5	
54	6	180/88
55	5	192/70
56	4	
57	3	
58	5	
59	8	
60	8	
61	5	194/83
62	4	
63	7	
64	7	
65	7	

APPENDIX: Scanlines

The ramp, Darat N-S 1

Profile 210°
Darat Fm. Mud/wackestone
Start: 36R 0501263 3230273
Stop: 36R 0501250 3230258

Distance (m)	Fractures	Orientations	Comments
1	10		Fault: 148/62
2	12	199/63	1,5 m displacement
3	12		
4	7		
5	11	180/86	
6	5		
7	10		
8	8		
9	10	200/83	
10	7		
11	10	182/82	
12	12	182/79	
13	7		
14	10		
15	17		
16	13	213/88	
17	10		
18	19		
19	9	042/85	
20	16		
21	5	289/85, 179/80	
22	13	040/90, 200/82	
23	12	042/87	

The ramp, Darat N-S 2

Profile 340°
Darat Fm. Mud/wackestone
Start: 36R 0501342 3230365
Stop: 36R 0501339 3230378
Picture: 2804

Distance (m)	Fractures	Orientations	Comments
1	13	102/73, 099/70, 096/16	
2	10		
3	12	098/80	
4	15	092/12, 008/90	
5	9	114/62, 188/80	
6	15	104/65	
7	14	103/62, 191/88	
8	13	009/90	
9	14	100/80	
10	12	115/66, 188/82	

APPENDIX: Scanlines

The ramp, Darat N-S 3

Profile 180°
Darat Fm. Mud/wackestone
Start: 36R 0501372 3230342
Stop: 36R 0501360 3230323

Distance (m)	Fractures	Orientations	Comments
1	12	126/70	
2	11	108/70	Fractures oriented 90-100° are most
3	10	104/68	thoroughgoing
4	8		
5	7		
6	11	098/65	
7	13		
8	8		
9	10	088/63	
10	8		
11	8	110/68	
12	7		
13	6	116/70	
14	4		
15	12	180/76	
16	9		
17	8		
18	9		
19	12	111/66	
20	5	178/80	
21	9	108/63	
22	8		
23	8	118/68	
24	9		

The ramp, Thebes transect 1

Profile 110°
Thebes Fm. Wacke/packstone
Start: 36R 0500660 3230344
Stop: 36R 0500672 3230334
Picture: 2895

Distance (m)	Fractures	Orientations	Comments
1	4	018/72, 129/89	Fractures oriented 080-100° are most
2	4	040/84, 125/89	thoroughgoing
3	6	041/78, 127/88	
4	3	034/85, 028/82	
5	4	026/80, 344/82	
6	4	035/60	
7	4	028/77, 123/86	
8	6	225/78	
9	6	024/50	
10	9	130/78	
11	11	023/72	
12	6		

The ramp, Thebes transect 2

Profile 130°
Thebes Fm. Wacke/packstone
Start: 36R 0500690 3230337
Stop: 36R 0500707 3230361

Distance (m)	Fractures	Orientations	Comments
1	1	023/72	Thoroughgoing fractures oriented 270-285°
2	4		
3	5	021/80	
4	3	037/75	
5	7	021/63, 146/68	
6	7	138/72, 142/80	
7	7	150/86, 142/83	
8	8	148/78, 026/60	
9	6		
10	9		
11	5		
12	6		
13	8	021/86, 136/83	
14	10		
15	9	136/70	
16	6	136/74	
17	8		
18	5		
19	12	328/64, 026/82	
20	21		
21	10	138/90	

APPENDIX: Scanlines

The ramp, Thebes transect 3

Profile 130°
Thebes Fm. Wacke/packstone
Start: 36R 0500745 3230414
Stop: 36R 0500765 3230402

Distance (m)	Fractures	Orientations	Comments
1	10	001/76	
2	6		
3	6		
4	9		
5	8	184/82	
6	6		
7	5		
8	7	000/82	
9	10	176/90	
10	10	006/89, 346/88	
11	2		
12	6	034/90	
13	4		
14	4	346/85	
15	9	152/89	
16	4		
17	4		
18	9		
19	10	358/75	
20	6		
21	6		

The ramp, Thebes transect 4

Profile 110°
Thebes Fm. Wacke/packstone
Start: 36R 0500781 3230402
Stop: 36R 0500795 3230399

Distance (m)	Fractures	Orientations	Comments
1	11	182/90	
2	8	188/90, 004/84	
3	7	092/90	
4	13	006/65	
5	7	001/80	
6	8		
7	10		
8	12		
9	6	022/90	
10	7		
11	4	003/86	
12	8		
13	4	115/76	
14	5		
15	12		

APPENDIX: Scanlines

The ramp, Thebes transect 5

Profile 110°
Thebes Fm. Wacke/packstone
Start: 36R 0500825 3230304
Stop: 36R 0500818 3230298

Distance (m)	Fractures	Orientations	Comments
1	13		Fractures trending 80-90° are most
2	10	055/84	thoroughgoing
3	30	186/60, 173/60	
4	14	048/90, 004/80	
5	26	162/70, 157/75	
6	11	150/72	
7	10		
8	12		
9	12	016/87, 008/90	
10	11		
11	14	002/88	
12	8		
13	6		
14	11	018/82, 012/84	
15	6		
16	8	010/82	
17	9		

The ramp, Thebes transect 6

Profile 110°
Thebes Fm. Wacke/packstone
Start: 36R 0500915 3230330
Stop: 36R 0500947 3230323

Distance (m)	Fractures	Orientations	Comments
1	11		Bedding: 296/19
2	3	210/80, 248/76	
3	13	226/70, 214/75	
4	5	217/82	
5	4		
6	5	042/76	
7	4	180/90	
8	5		
9	5		
10	8	007/80	
11	7	001/74	
12	3		
13	4	001/86	
14	3		
15	4	001/82	
16	4	179/88	
17	4		
18	5	187/89	
19	5		
20	3	191/84	
21	7	188/82	
22	2	006/87	
23	5	001/88	
24	3		
25	4		
26	4		
27	5	348/78	
28	5	180/80	
29	6		
30	13	120/90, 118/90	
31	5		
32	3		
33	4		
34	5		

The ramp, Thebes transect 7

Profile 110°
Thebes Fm. Wacke/packstone
Start: 36R 0500962 3230327
Stop: 36R 0500978 3230315

Distance (m)	Fractures	Orientations	Comments
1	3	186/80, 185/82	
2	8	358/72, 357/88	
3	6		
4	9	178/82	
5	8	356/78	
6	6		
7	8		
8	5	154/88	
9	1		
10	5		
11	6	162/85	
12	6	359/88	
13	4		
14	4		
15	6		
16	5	168/78	
17	4	338/80	
18	9		
19	9		
20	6	172/72	

APPENDIX: Scanlines

The ramp, Thebes transect 8

Profile 110°
Thebes Fm. Wacke/packstone
Start: 36R 0501005 3230282
Stop: 36R 0501021 3230264

Distance (m)	Fractures	Orientations	Comments
1	11	192/80	
2	3		
3	7	171/76	
4	3		
5	11	164/81, 004/89	
6	5		
7	5	176/82	
8	3		
9	4		
10	7	024/70	
11	6	033/65	
12	3		
13	4		
14	3		
15	4	000/86	
16	5	183/83	
17	4		
18	3	180/84	
19	3		
20	8	053/82, 032/81, 003/78	
21	1		
22	1		

The ramp, Thebes transect 9

Profile 080°
Thebes Fm. Wacke/packstone
Start: 36R 0501023 3230166
Stop: 36R 0501041 3230166
Picture: 2924

Distance (m)	Fractures	Orientations	Comments
1	20	006/90	
2	19	009/88	
3	18	003/89	
4	23	012/89	
5	19	004/90	
6	17	010/84	
7	19	018/90	
8	21	022/89	
9	23	312/90	
10	12		
11	8	008/87, 012/81	
12	8	300/80	
13	13	108/70	
14	15		
15	20	190/88	
16	9	184/87	
17	22	163/78	

APPENDIX: Scanlines

The ramp, Thebes transect 10

Profile 110°
Thebes Fm. Wacke/packstone
Start: 36R 0501054 3230185
Stop: 36R 0501083 3230173

Distance (m)	Fractures	Orientations	Comments
1	7	212/78	
2	14	190/66	
3	10	058/74	
4	10	002/85, 004/88	
5	4	000/90	
6	5	060/70	
7	11		
8	7	062/76	
9	8		
10	13	330/87	
11	19	170/90	
12	9	014/68	
13	7	035/55	
14	14		
15	12		
16	16	064/62	
17	16	058/60, 065/58	
18	12	001/90, 059/60, 007/90	
19	15	055/62	
20	11	063/71	

The ramp, Thebes transect 11

Profile 120°
Thebes Fm. Wacke/packstone
Start: 36R 0501099 3230170
Stop: 36R 0501113 3230161

Distance (m)	Fractures	Orientations	Comments
1	5	022/84	
2	7		
3	6	030/55	
4	11	108/62, 100/68	
5	13	111/66, 113/68	
6	8		
7	11		
8	10	203/60	
9	9		
10	7		
11	4		
12	10	100/62	
13	9	100/70	
14	7		
15	8		
16	6		
17	9		
18	15	174/72	
19	10		
20	14	068/62	

The ramp, Thebes transect 12

Profile 120°
Thebes Fm. Wacke/packstone
Start: 36R 0501159 3230156
Stop: 36R 0501181 3230134

Distance (m)	Fractures	Orientations	Comments
1	20	009/82	Zaiem took notes
2	12		
3	14		
4	18	048/80	
5	9		
6	6	078/70	
7	4		
8	8		
9	11	080/80	
10	19		
11	7		
12	6		
13	3	001/63	
14	6		
15	8		
16	10	079/72	
17	3		
18	2		
19	2		
20	3	074/80	
21	4		
22	10		
23	14	050/80	
24	5	059/62	
25	7		
26	7	169/85	
27	4	078/50	
28	3		
29	6		
30	7		
31	13		
32	7		
33	2		
34	4		
35	6		
36	5		
37	4	042/58	
38	3		
39	6		
40	3		
41	2		
42	5	062/58	
43	2		
44	4		
45	2		
46	4	041/87	
47	2		
48	4	035/81	
49	3	047/52	

50	4

The ramp, Thebes transect 13

Profile 120°
Thebes Fm. Wacke/packstone
Start: 36R 0501181 3230134
Stop: 36R 0501206 3230119

Distance (m)	Fractures	Orientations	Comments
1	8	050/81	
2	4		
3	3		
4	6		
5	5	030/74	
6	6	027/83	
7	7		
8	4		
9	4	046/82	
10	4		
11	8	007/80	
12	5		
13	7		
14	2	326/63	
15	2		
16	7	118/57	
17	10		
18	6	094/73	
19	5		
20	7		
21	5		
22	4		
23	5		
24	3		
25	7		
26	5		
27	12	092/78, 090/74	
28	11	097/64	
29	10		
30	7	110/60, 007/90	

APPENDIX: Scanlines

The ramp, Thebes N-S 1

Profile 040°
Thebes Fm. Wacke/packstone
Start: 36R 0500661 3230350
Stop: 36R 0500670 3230357

Distance (m)	Fractures	Orientations	Comments
1	10	116/82, 125/82	Bedding: 288/18
2	11	042/85, 040/82	
3	12	304/89	
4	8	312/83	
5	7		
6	9		
7	11		
8	8	099/82	
9	6		
10	4	022/48	
11	6		
12	3		
13	3		
14	7		
15	5		
16	3	147/70	

The ramp, Thebes N-S 2

Profile 030°
Thebes Fm. Wacke/packstone
Start: 36R 0501233 3230097
Stop: 36R 0501243 3230119

Distance (m)	Fractures	Orientations	Comments
1	16	094/62	
2	15	107/70	
3	18		
4	14	114/62	
5	8	005/88	
6	10	160/38	
7	17	149/45, 140/74	
8	13		
9	19	130/38	
10	23		
11	24	121/58	
12	8	088/70	
13	14		
14	8	092/60, 090/67	
15	14		
16	16		
17	8		
18	7	128/63	
19	10	082/63, 078/78	
20	22		
21	6		
22	6		
23	8		
24	5		
25	3		